ARCHIVES OF ACOUSTICS
20, 2, 115–138(1995)

LINEAR AND JUMP FREQUENCY CHANGES OF A SIGNAL IN A ROOM

L. RUTKOWSKI and E. OZIMEK

Institute of Acoustics
Adam Mickiewicz University
(60–769 Poznań, ul. Matejki 48/49)

The paper discusses the deformation of the instantaneous frequency of signals with linear and jump frequency changes propagating in a room. The instantaneous frequency deformation in a room has been compared on the basis of theoretical and experimental data. It was found out that deformation of the instantaneous frequency for linear and jump frequency changes reached extreme value at the minima of the amplitude of the resultant signal. For linear frequency changes the deformation is proportional to the rate of frequency changes, and to the delay time of the reflected wave. In turn, for jump frequency changes, the deformation increase with an increase in the jump value. The instantaneous frequency reaches final value after a time equal to the reverbation time of a room.

1. Introduction

An acoustic signal propagating in a room is deformed both in the amplitude and frequency domains. Sound deformations in a room in the amplitude domain has been discussed in the literature [2, 3, 4, 6]. Results of the investigations led to the development of an objective method of speech intelligibility in a room, called the RASTI method [4]. This method is based on the concept of the Modulation Transfer Function (MTF) adopted to the room acoustics [3]. The (MTF) represents the modulation depth reduction as a function of modulation frequency. So far much less attention has been devoted to signal distortion by the acoustical parameters of a room in the frequency domain. The problem is important with reference to the propagation in a room of real sounds such as speech and music which are characterized by a considerable variability in the frequency domain. Our first approach to the problem [8, 9, 10, 12, 14] indicated the existence of a number of interesing effects. The basic issue when evaluating effects connected with sound deformation in a room is to get quantitative relations between the transmitted sound and the sound received in a certain points of a room. A preliminary analysis of the problem has been discussed in paper [7]. In the theoretical part of the paper general dependencies between the transmitted and received sound in the aspect of a spectral-correlational analysis were

given. In the experimental part, changes in the spectral structure of complex sounds, propagating in selected rooms (models), with different spatial configuration and different reverberation times were determined. It has been found out that the value of changes is different in growth, steady state and decay process of a signal and depends on the location of the measurement point and the type of analysed sounds.

Sound deformation in a room was also discussed in the aspect of the multi-dimensional space theory [8, 9]. Assuming that the space of acoustic states of a room affects the signal space, producing as a result its deformation, relations between elements of these spaces were analyzed. We were also considering the possibilities of determining acoustic states of a room on the basis of the classification of sound deformation states.

Another interesting aspect of the frequency sound structure deformation in a room is the problem of changes in the so-called sound instantaneous frequency in the process of the growth and decay of signal [10, 14]. Generally, the resultant acoustic pressure in the sound growth or decay in a room can be treated as the signal of an amplitude and phase changeable time, which approximately can be expressed as follows:

$$p(t)=p_0(t)\ cos\ \varphi(t), \tag{1.1}$$

where: $p_0(t)$ — acoustic pressure amplitude, $\varphi(t)$ — instantaneous phase of acoustic pressure.
The instantaneous phase $\varphi(t)$ of the resultant signal can be expressed as:

$$\varphi(t)=\omega_0 t+f(t), \tag{1.2}$$

where: ω_0 — frequency of the signal transmitted into the room, $f(t)$ — the function „modulating" the phase of the signal transmitted into the room.
Function $f(t)$ represents jump changes of the phase of the resultant signal, resulting from the summation of the direct sound and successive reflections with different phase shifts. These jump phase changes cause a change in the time interval between successive zero crossings of the resultant signal.

On setting the instantaneous phase derivative in relation to time we get a value which characterizes the rate of changes of that phase, this being called instantaneous frequency:

$$\omega(t)=\frac{d\varphi(t)}{dt}=\frac{d}{dt}[\omega_0 t+f(t)]=\omega_0+\frac{df(t)}{dt}, \tag{1.3}$$

or otherwise

$$f(t)=\frac{1}{2\pi}\frac{d\varphi(t)}{dt}.$$

More details on the instantaneous frequency and its measurability are given in papers [1, 10]. It is interesting to note that in the literature [13] one may also find another definition of instantaneous frequency, based on the analysis of the number of

zero crossings of the real signal investigated. In this case instantaneous frequency is defined as the ratio of the number of zero crossings of this signal, determined over some time interval $\Delta\tau$, and the value of this interval. This ratio corresponds to the mean density of zeros of the signal over this interval and is sometimes called Rice frequency (f_R):

$$f_R = \lim_{T\to\infty} \frac{N}{\Delta\tau},$$

where N is the number of „positive" or „negative" zero crossings of the signal and $\Delta\tau$ is the averaging time interval.

According to (1.3), the sound instantaneous frequency, measured in the growth or decay process, is not equal to the frequency generated into the room but varies (fluctuates) around that value in agreement with the derivative of $df(t)/dt$. Quantity $\omega(t)$ as defined by expression (1.3) is thus a theoretical one, as it determines the value of the instantaneous frequency at a given time t, which cannot be implementend in experimental conditions. In these conditions, in expression (1.3) the differential quantities were replaced by the difference ones, i.e.

$$\omega(\Delta t) = \frac{\Delta\varphi}{\Delta t}. \tag{1.4}$$

In keeping with expression (1.4), the measure of the instantaneous frequency of the signal is the ratio of its phase change $\Delta\varphi$, occurring in the time interval Δt, over the duration of this interval. It has been generally stated that observed changes in the instantaneous frequency in a room have a random character and are within the range of several Hz. In a few special cases they can reach much greater values [10, 14].

2. Signal with linearly changing frequency

Let us consider a case when a sinusoidal signal, whose frequency is increasing linearly, is transmitted into the room, i.e.

$$\omega(t) = \omega_0 + \alpha t, \tag{2.5}$$

where: ω_0 — initial frequency, α — rate of frequency changes.

Let us assume that at a measuring point of the room there is a superposition of the direct wave and the first reflected wave which will reach the measuring point with a certain delay Δt (Fig.1).

Let us notice that as soon as the reflected wave reaches the measuring point, at any time t (e.g. 500 or 800 ms cf. Fig.1) there is a constant frequency difference between the direct and reflected waves, equal $\Delta f = 10$ Hz. In this case an effect similar to beating will occur. However, the effect is more complex because that frequency

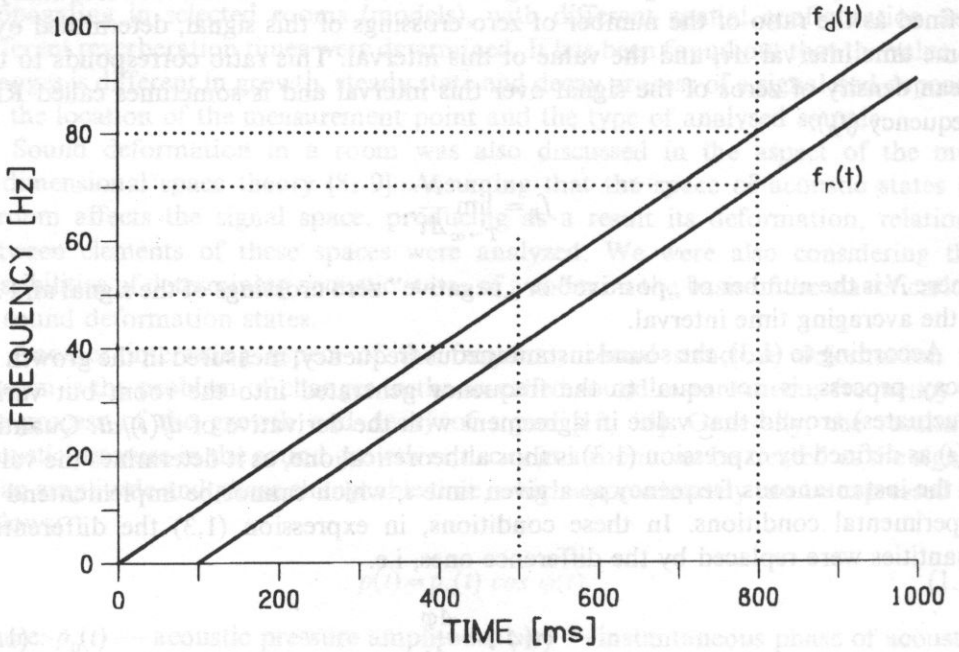

Fig. 1. Changes in instantaneous frequency in time for a direct wave $f_d(t)$ and reflected wave $f_r(t)$ (for clarity, time delay of the reflected wave equals $\Delta t = 100$ ms).

variations in time are continuous. For the assumed character of frequency changes the signal can be written as follows:

$$x(t) = x_0 \sin(\omega_0 t + \varphi_0 + \frac{\alpha t^2}{2}). \tag{2.6}$$

In the case of the direct wave and the reflected wave, the linear frequency change can be expressed as follows:

- direct wave: $\omega_d(t) = \omega_0 + \alpha t$,
- reflected wave: $\omega_r(t) = \omega_0 + \alpha(t - \Delta t)$.

The resultant signal at the measuring point in the room is equal:

$$x_{res}(t) = x_{0d} \sin(\varphi_d(t)) + x_{0r} \sin(\varphi_r(t)),$$

where: x_{0d}, x_{0r} — amplitudes of the direct and reflected waves, $\varphi_d(t), \varphi_r(t)$ — phases of the direct and reflected waves.

Phases of the direct and reflected waves, given that the initial phase $\varphi_0 = 0$, can be expressed as follows:

$$\varphi_d(t) = \omega_0 t + \frac{\alpha t^2}{2}, \tag{2.7}$$

$$\varphi_r(t)=\omega_0 t+\frac{\alpha t^2}{2}-\alpha\Delta t\ t. \tag{2.8}$$

The output signal resulting from the superposition of the direct and reflected waves can be written in the following form:

$$x_{\text{res}}(t)=A(t)\sin(\omega_0 t-\Phi(t)), \tag{2.9}$$

where: $\omega_0 t-\Phi(t)=\Phi_{\text{res}}(t)$ — phase of the resultant signal.

Considering the amplitudes and phases for the direct and reflected waves, following trigonometric transformations, we find formulae describing temporal changes of the instantaneous frequency and amplitude envelope. Changes in the frequency of the resultant signal:

$$\omega_{\text{res}}(t)=\frac{d\Phi_{\text{res}}(t)}{dt}=\omega_0+\alpha t-\frac{\alpha\Delta t(\delta^2+\delta\cos(\alpha\Delta tt))}{1+\delta^2+2\delta\cos(\alpha\Delta tt)}. \tag{2.10}$$

Changes in the amplitude envelope:

$$A(t)=x_{0d}\sqrt{1+\delta^2+2\delta\cos(\alpha\Delta tt)}, \tag{2.11}$$

where δ — the ratio of amplitudes of the reflected and the direct waves.

It can be seen in expression (2.10) that changes in the instantaneous frequency of the resultant signal occuring as a result of the superposition of two signals with linearly growing frequency have a more complex character than in the case with the elementary effect of beating. The amplitude envelope variation of the resultant signal is like the beating of two sinusoidal signals with a constant frequency difference.

3. Signal with jump changes of frequency

Let ut consider a case of a sinusiodal signal propagation in a room for which at a certain time a frequency jump appears. Such a change can be obtained by means of frequency modulation of the signal by a rectangular wave. The modulated signal $x(t)$ has the form:

$$x(t)=x_0\sin\left[\int_{-T/2}^{T/2}(\omega_1+\Delta\omega 1(t))dt\right]=x_0\sin\left[\int_{-T/2}^{T/2}\omega(t)dt\right], \tag{3.1}$$

where:

$$\omega(t)=\omega_1+\Delta\omega 1(t),$$

$$1(t)=\begin{cases}1 \text{ for } -T/2<t<0\\ 0 \text{ for } 0<t<T/2\end{cases},$$

$$\Delta\omega=\omega_2-\omega_1,$$

$$T=\frac{1}{f_m},$$

and ω_1 — the initial frequency value (i.e. before the jump), ω_2 — the final frequency value (after the jump), f_m — frequency of the rectangular modulation wave, $\Delta\omega/2$ — frequency deviation.
The conventional value of the carrier frequency of FM signal will be equal to:

$$\omega_0 = \omega_1 + \frac{\Delta\omega}{2}.$$

For relatively low frequency values of the rectangular signal ($f_m \to 0$) in the spectrum of the frequency modulated signal only two components with frequencies $\omega_1 + \Delta\omega/2$ and $\omega_2 - \Delta\omega/2$ can be distinguished. If a sinusoidal signal with a constant amplitude A and phase φ is transmitted into the room, then this signal, in a steady state, for frequency ω_1 can be represented in the following form:

$$x(t) = A \mid H(j\omega_1) \mid \sin(\omega_1 t), \tag{3.2}$$

Similary for frequency ω_2 one can write:

$$y(t) = A \mid H(j\omega_2) \mid \sin(\omega_2 t), \tag{3.3}$$

where: $\mid H(j\omega) \mid$ — the value of amplitude frequency response for frequency ω.
Let us further assume that at time $t = 0$ a signal frequency jump from value ω_1 to value ω_2 occurs. After the frequency jump, given the assumption of an exponential sound decay, signal amplitude, for frequency ω_1 will decrease in accordance with function:

$$x(t) = A \mid H(j\omega_1) \mid \exp(-kt)\sin(\omega_1 t). \tag{3.4}$$

In turn, signal amplitude, for frequency ω_2 will increase according to the form:

$$y(t) = A \mid H(j\omega_2) \mid [1 - \exp(-kt)]\sin(\omega_2 t), \tag{3.5}$$

where $k = 13.8/T_{60}$, T_{60} — room reverberation time for 60 dB decay. Let us assume that in the frequency range in question, in which the jump occurs, the dependence of the reverberation time on frequency is a slow-changing function.

At a certain time after the frequency jump, there will be a superposition of the decaying signal of frequency ω_1 and the growing signal of frequency ω_2. The resultant signal will be

$$z(t) = X_0 \exp(-kt)\sin(\omega_1 t) + Y_0[1 - \exp(-kt)]\sin(\omega_2 t). \tag{3.7}$$

where $X_0 = A \mid H(j\omega_1) \mid$, $Y_0 = A \mid H(j\omega_2) \mid$.

Next, we transform equation (3.7) to the following form:

$$z(t) = R(t)\sin(\varphi_r(t)),$$

where $R(t)$ — amplitude envelope of the resultant signal, $\varphi_r(t)$ — phase of the resultant signal.

After trigonometric transformations we get the following formula describing changes in instantaneous frequency after the frequency jump:

$$\omega(t)=\frac{d\varphi_r(t)}{dt}=\omega_1+\left\{Y_0^2\Delta\omega(1-\exp(-kt))^2+X_0Y_0\exp(-kt)\right.$$
$$\left.\times[k\sin(\Delta\omega t)+\Delta\omega(1-\exp(-kt))\cos(\Delta\omega t)]\right\}\cdot\frac{1}{R^2(t)} \tag{3.8}$$

where

$$R(t)=\sqrt{X_0^2\exp(-2kt)+Y_0^2(1-\exp(-kt))^2+2X_0Y_0\exp(-kt)(1-\exp(-kt))\cos(\Delta\omega t)}$$

— amplitude envelope after frequency jump.

On the basis of expression (3.8), calculations of changes of instantaneous frequency and the amplitude envelope of the signal after the frequency jump were made. The results of calculations allow to analyze these changes in detail with respect to such parameters as: the range of frequency jump Δf, room reverberation time T and quantity $\delta = |H(j\omega_2)| / |H(j\omega_1)|$.

4. Results of calculations and experiment for linear frequency changes

In order to check the machanism of the instantaneous frequency changes for linear FM, computer calculations were performed. For clarity of interpretation we took into account the superposition of direct and reflected waves. The aim of the calculations was to show how the rate of frequency changes, amplitude and time relations influence the resultant signal of instantaneous frequency changes.

Figures 2 and 3 show changes in frequency and the amplitude envelope for the ratio of amplitudes of the reflected wave to the direct wave $\delta=0.85$, delay of the reflected wave $\Delta t=20$ms and the rate of frequency changes α, respectively 250Hz/s and — 250Hz/s.

Characteristic deflections of instantaneous frequency from the linear dependence, indicated in Fig.2 and 3 by a dotted line, can be observed. Minima of the amplitude envelope correspond to extreme frequency deflections, irrespective of their direction.

It was interesting to find out to what extent the instantaneous frequency changes depend on such parameters: α — rate of frequency changes, δ — the ratio of the amplitudes of the reflected wave to the direct wave, Δt — time delay of the reflected wave. For this purpose, computer calculations were made whose results are shown in Fig. 4—6. The results, for clarity of the drawings, only refer to the deformation introduced as a result of the superposition which in reality occurs at the background of the linear frequency (cf. Fig. 2—3).

Analyzing the data shown in Fig. 2, 3 and 8 one can generally say that the minima of the amplitude envelope correspond to considerable deflections of the signal instantaneous frequency. The value of the deflection (Fig. 4—8) depends on the rate

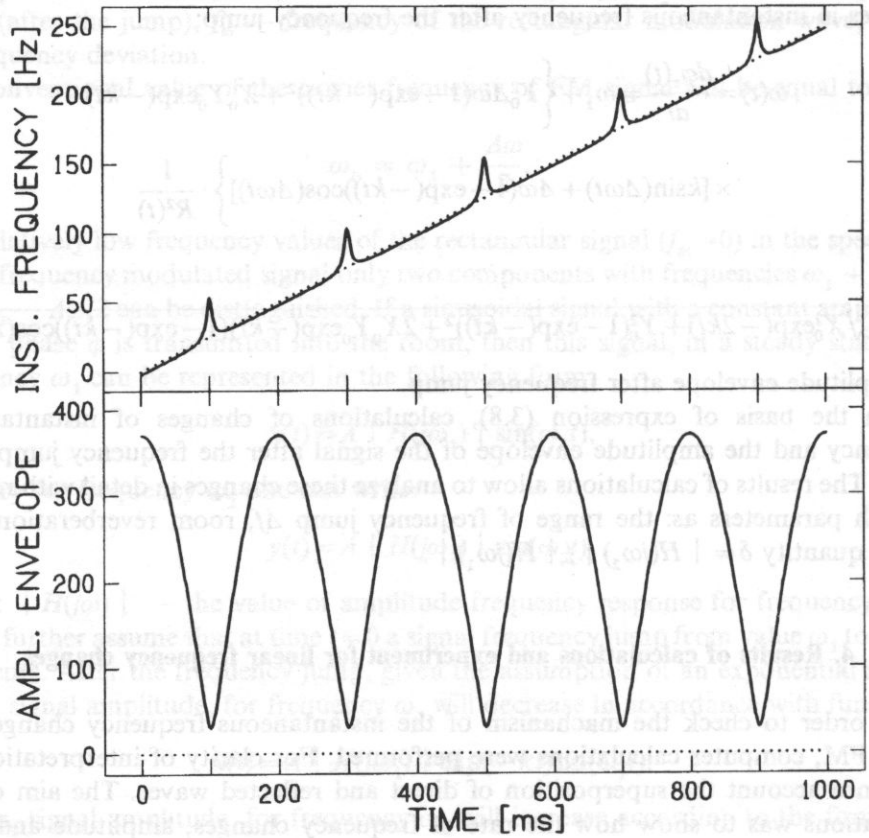

Fig. 2. Computer calculations of changes in instantaneous frequency and amplitude for a signal with a linearly growing frequency, for $\alpha = 250$ Hz/s, $\delta = 0.85$ and $\Delta t = 20$ ms.

of frequency changes, delay time of the reflected wave and the ratio of the amplitudes of the reflected wave to the directed wave. The frequency for which extreme deflection of frequency occurs depends linearly on the product of the rate of frequency changes α and time dealy Δt; this frequency corresponds to the frequency of changes in the amplitude envelope (Fig. 2 – 3). Furthermore, one can notice that with the increase in the amplitude ratio δ (Fig.5), deflections of instantaneous frequency lose their quasi-sinusoidal character and for large values of δ assume the form of short, one-sided deflections of high value. The direction of extreme frequency changes depends on the direction of frequency changes in the direct signal (sign at α) and whether coefficient δ is smaller or greater than 1. The time interval in which single frequency deflection occurs is inversely proportional to the rate of frequency changes, echo delay time, and the amplitude ratio δ.

The above results pertaining to instantaneous frequency changes refer to a relatively simple case of the superposition of a direct wave with one reflected wave.

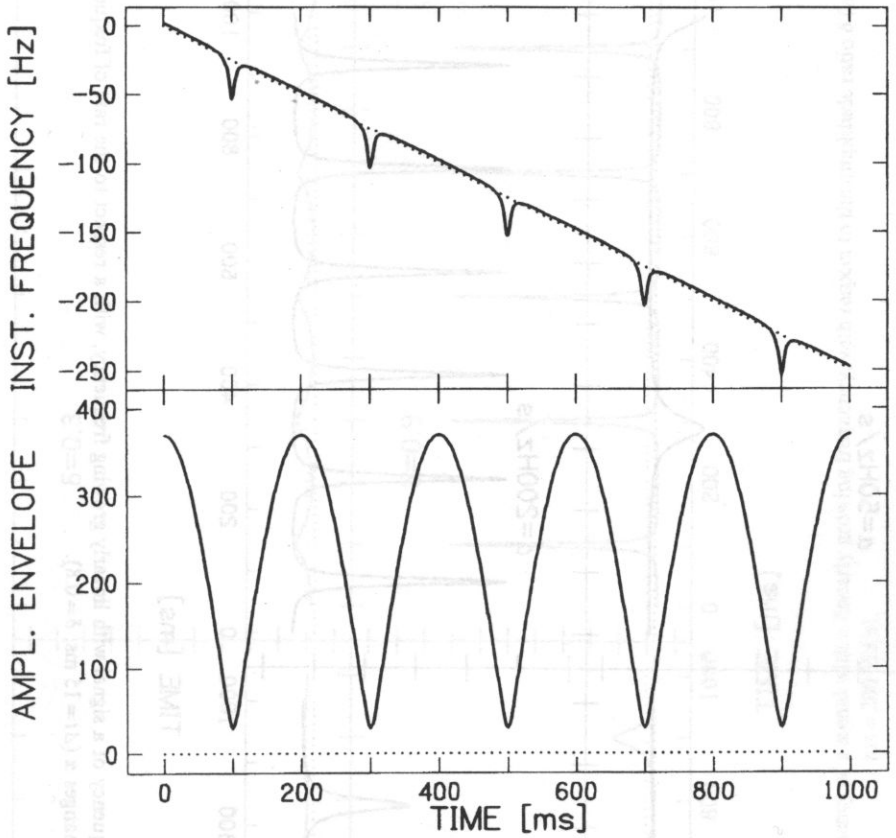

Fig. 3. Computer calculations of changes in instantaneous frequency and amplitude for a signal with a linearly growing frequency, for $\alpha = -250$ Hz/s, $\delta = 0.85$ and $\Delta t = 20$ ms.

Nevertheless, they permit an initial qualitative and quantitative analysis of deformation in the signal in the frequency domain. Computer analysis of frequency changes for a larger number of reflections is much more complex and does not permit a clear interpretation of these changes due to the growing number of signal parameters.

At the next stage of investigations, measurements of instantaneous frequency changes for a real room, i.e. under conditions in which a large number of reflections exist, were performed.

The measuring setup used in the investigations consisted of two sets — the transmitting set and the receiving set. The transmitting set consisted of computer (IBM PC486) which generated FM signals (linear or jump frequency changes) through 16 bit digital to analog converter, at sampling rate of 48.1 kHz and low pass filter at 8 kHz cut-off frequency. The signals were next supplied to the power amplifier and loudspeaker. The receiving set which consisted of two microphones with preamplifiers was connected to frequency demodulators and 16 bit analog to

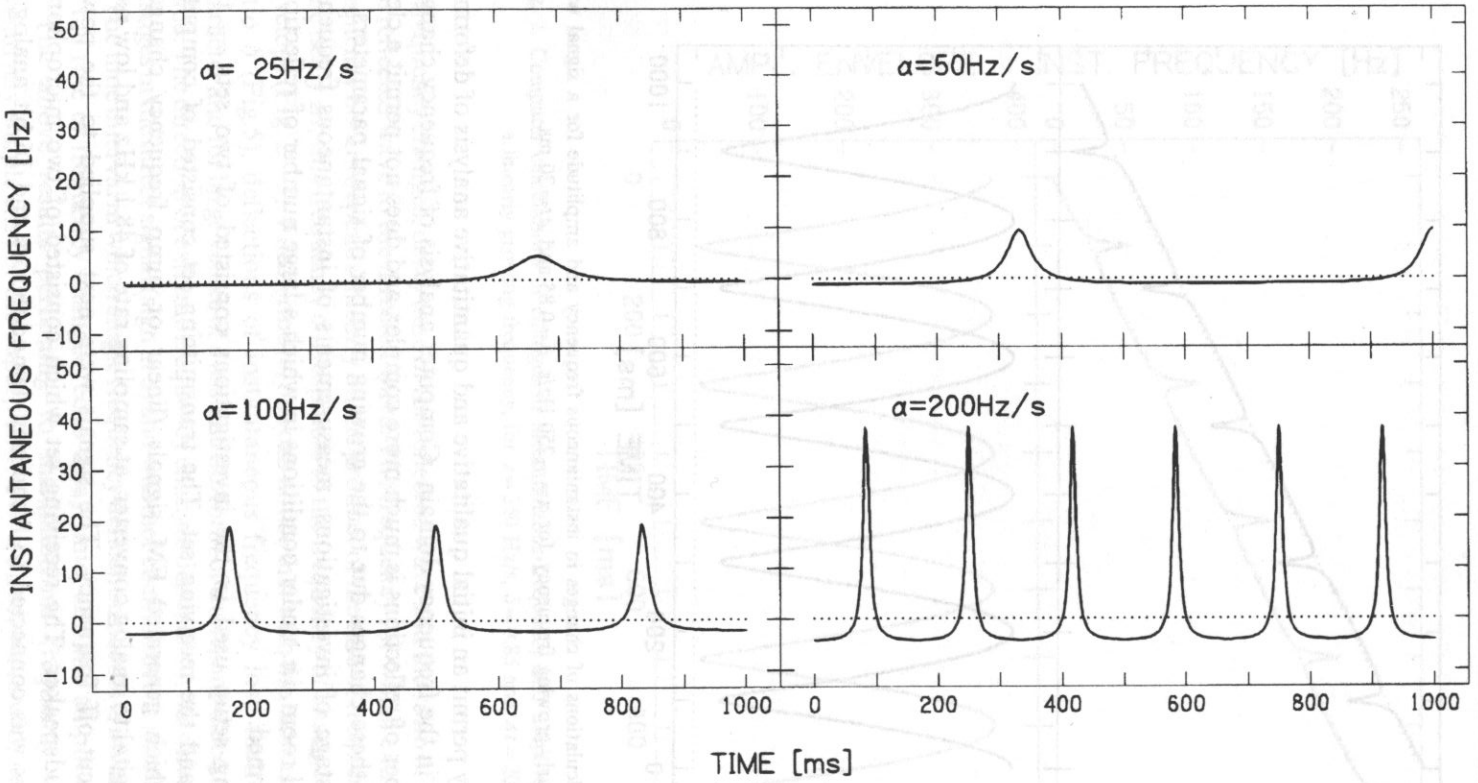

Fig. 4. Computer calculations of changes in instantaneous frequency of a signal with linearly growing frequency, with a respect to the rate of frequency changes α ($\Delta t = 15$ ms, $\delta = 0.8$).

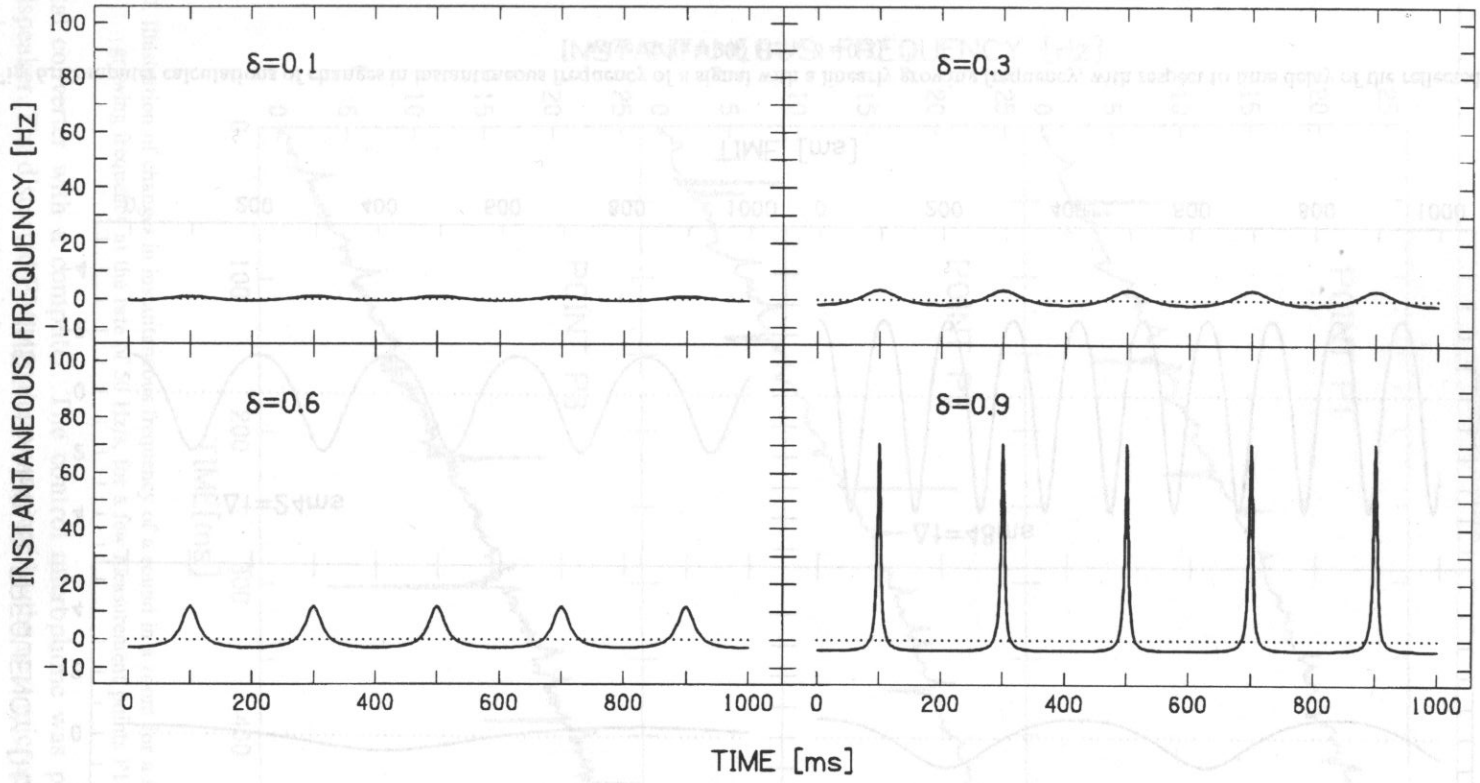

Fig. 5. Computer calculations of changes in instantaneous frequency of a signal with a linearly growing frequency, with respect to the amplitude ratio δ ($\Delta t = 25$ ms = 200 Hz/s).

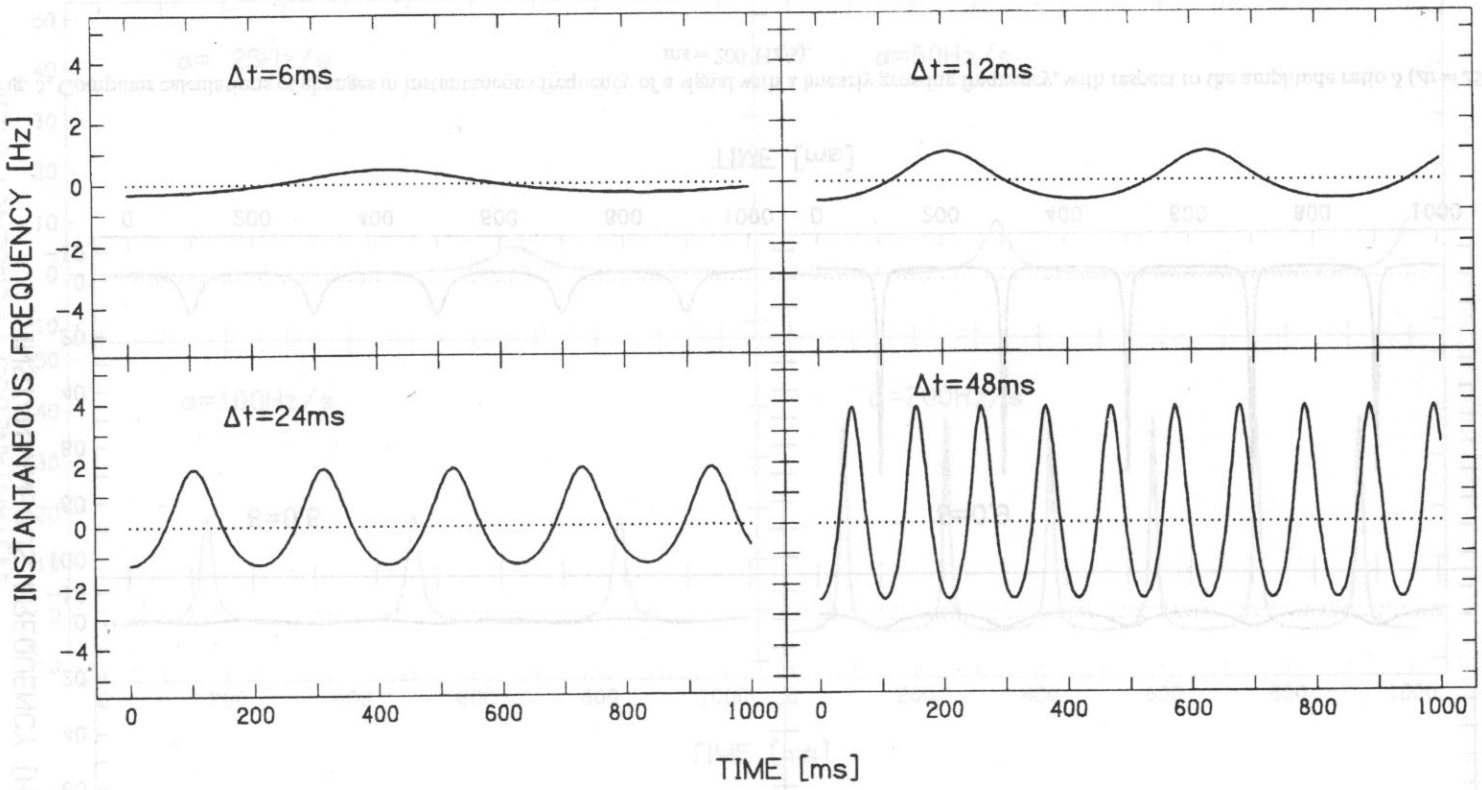

Fig. 6. Computer calculations of changes in instantaneous frequency of a signal with a linearly growing frequency, with respect to time delay of the reflected wave Δt ($\alpha = 200$ Hz/s, $\delta = 0.2$).

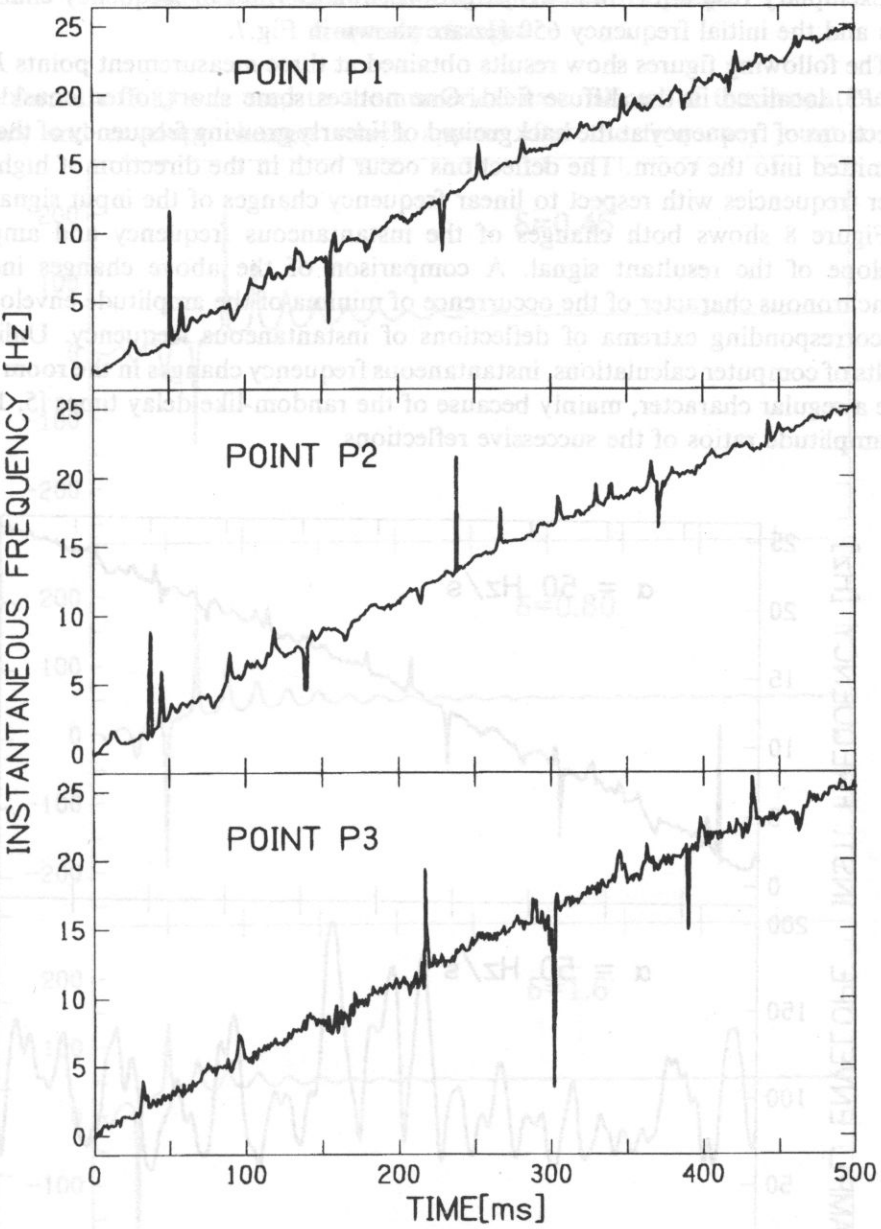

Fig. 7. Illustration of changes in instantaneous frequency of a sound in a room for a signal with linearly growing frequency at the rate of 50 Hz/s, for a few measurement points P1, P2, P3.

digital converter with a computer. The control microphone was placed near the loudspeaker. The distorted FM signal was received by the next microphone placed in the selected measurement point.

Exemplary results of these investigations, for the rate of frequency changes 50 Hz/s and the initial frequency 650 Hz are shown in Fig.7.

The following figures show results obtained at three measurement points $P1$, $P2$, and $P3$, localized in the diffuse field. One notices some short, often considerable, deflections of frequency at the background of linearly growing frequency of the signal trasmitted into the room. The deflections occur both in the direction of higher and lower frequencies with respect to linear frequency changes of the input signal.

Figure 8 shows both changes of the instantaneous frequency and amplitude envelope of the resultant signal. A comparison of the above changes indicates a synchronous character of the occurrence of minima of the amplitude envelope and the corresponding extrema of deflections of instantaneous frequency. Unlike the results of computer calculations, instantaneous frequency changes in the room do not have a regular character, mainly because of the random-like delay times [5, 15] and the amplitude ratios of the successive reflections.

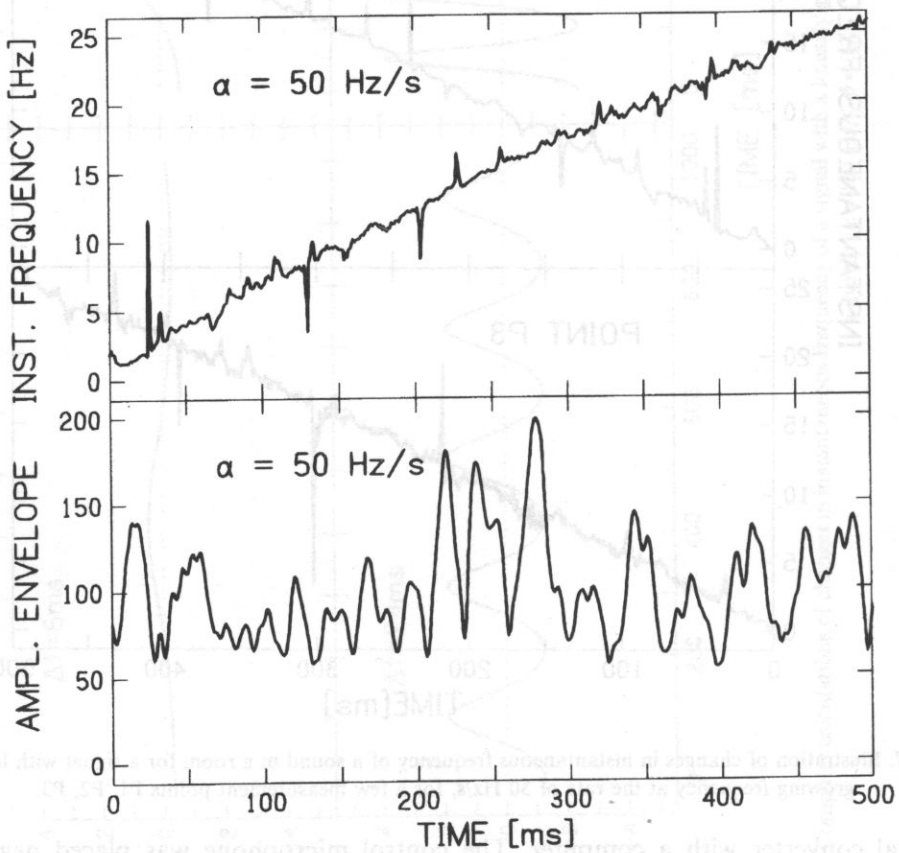

Fig. 8. Illustration of changes in instantaneous frequency and amplitude envelope recorded in a room for $\alpha = 50$ Hz/s.

5. Results of calculations and experiment for jump frequency changes

The formula (3.8) was used to the numerical calculations of the instantaneous frequency and envelope changes which appear after the frequency jump in the

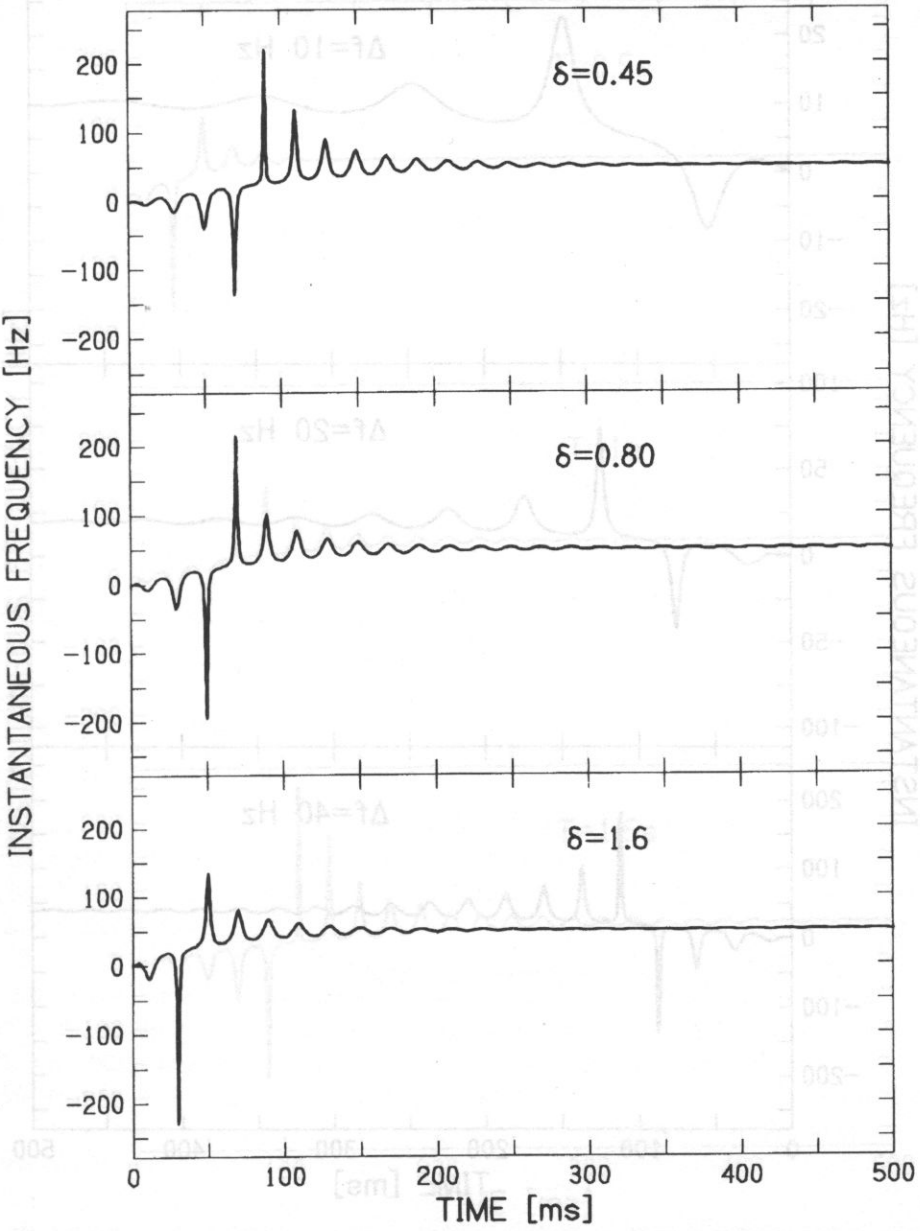

Fig. 9. Computer calculations of changes in instantaneous frequency of a signal, due to a frequency jump, for selected values of coefficient δ.($\Delta f = 50$ Hz; $T = 1$s).

room. The only difference between presented calculations and results for the real room is an assumption that the room decay process is an exponential one. Calculations were performed for selected signal parameters (range and direction of frequency jump) and room dependent parameters (amplitude ratio and reverberation time).

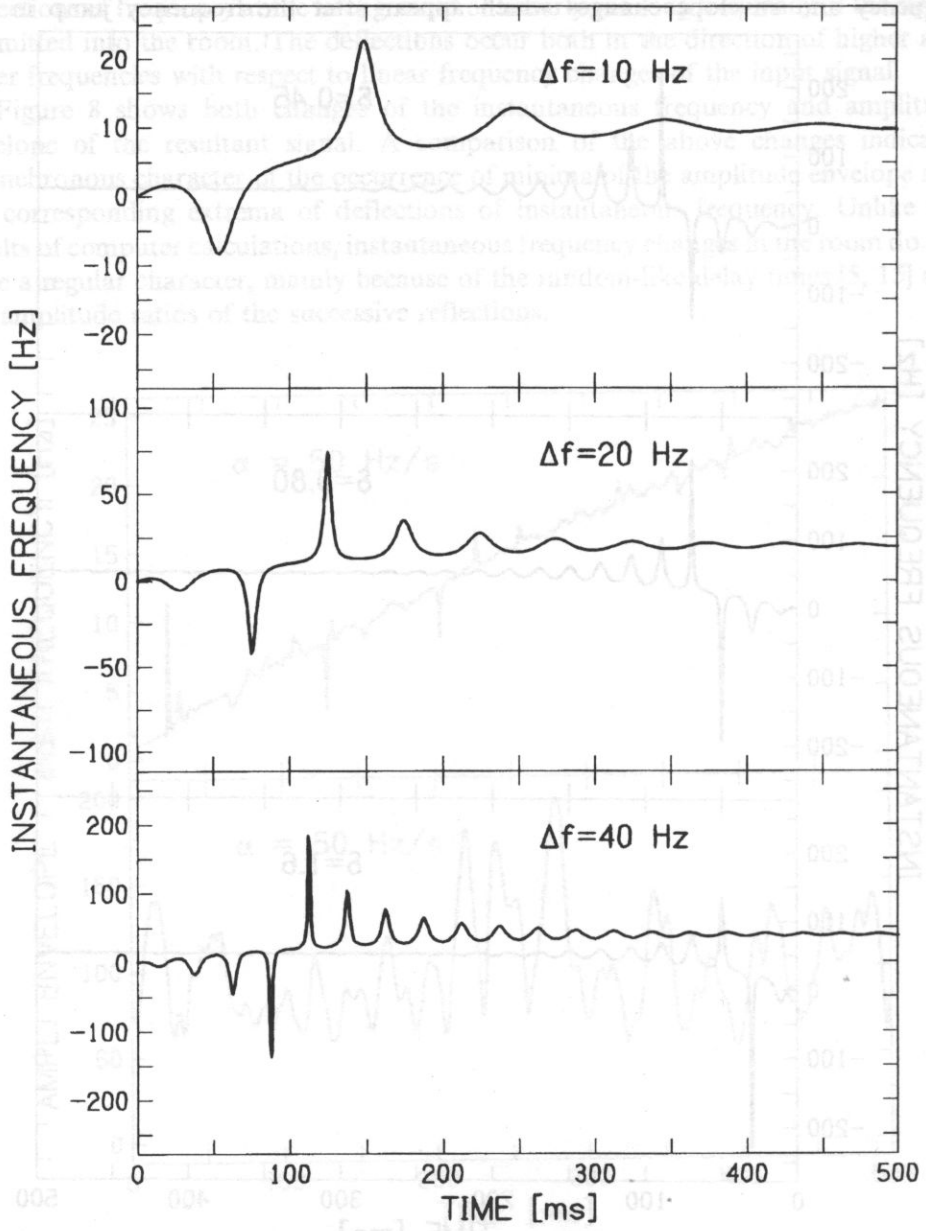

Fig. 10. Computer calculations of changes in instantaneous frequency of a signal, due to a frequency jump, for selected values of frequency jump Δf.($\delta = 0.1$; $T = 2$s).

Exemplary results of the calculations are shown in Figs. 9–12.

The moment at which signal frequency jump occurs corresponds to the zero value on the time axis. At successive time moments we observe characteristic fluctuations of instantaneous frequency nad then a fixed frequency value which corresponds to the

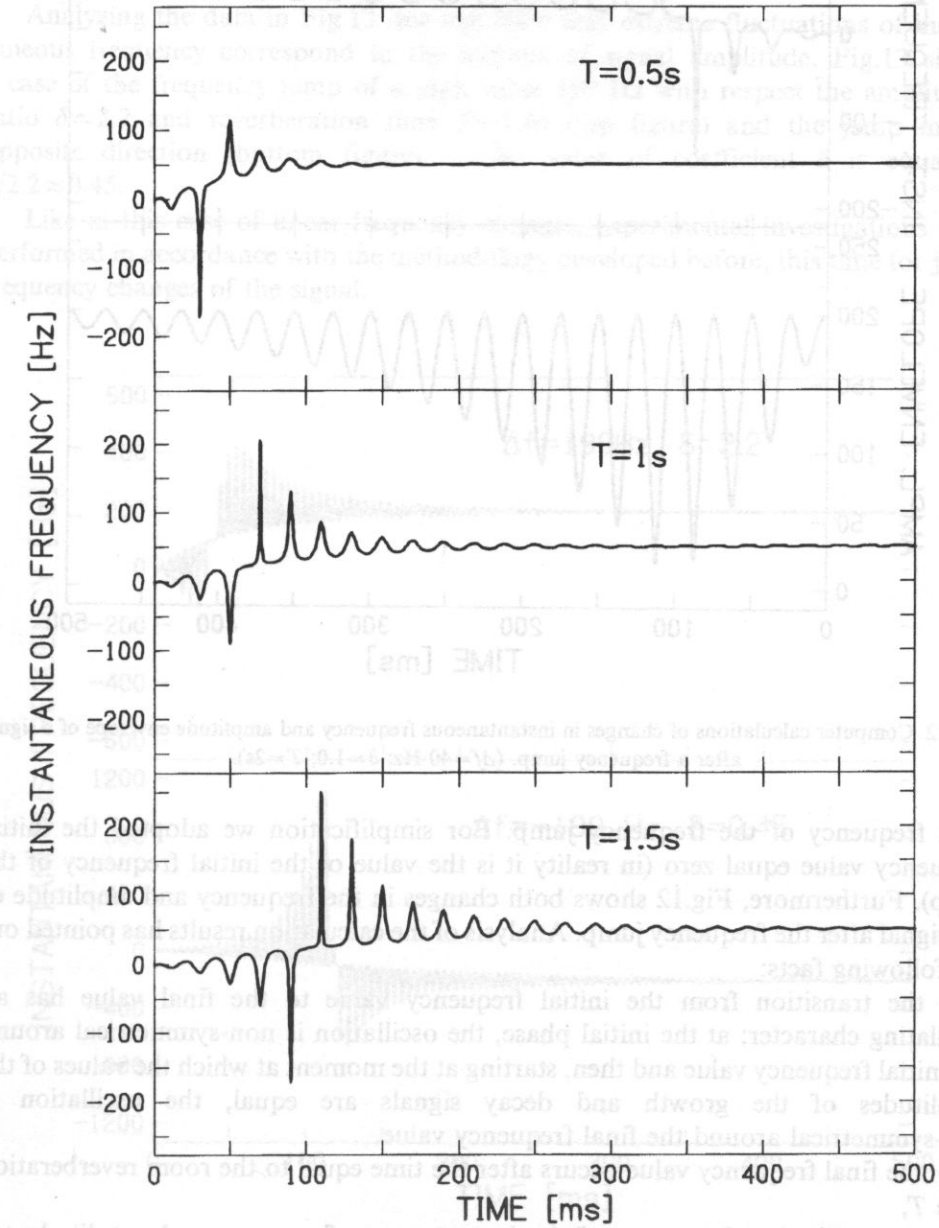

Fig. 11. Computer calculations of changes in instantaneous frequency of a signal, due to a frequency jump, for selected values of reverbation time T.($\Delta f = 50$ Hz; $\delta = 0.6$).

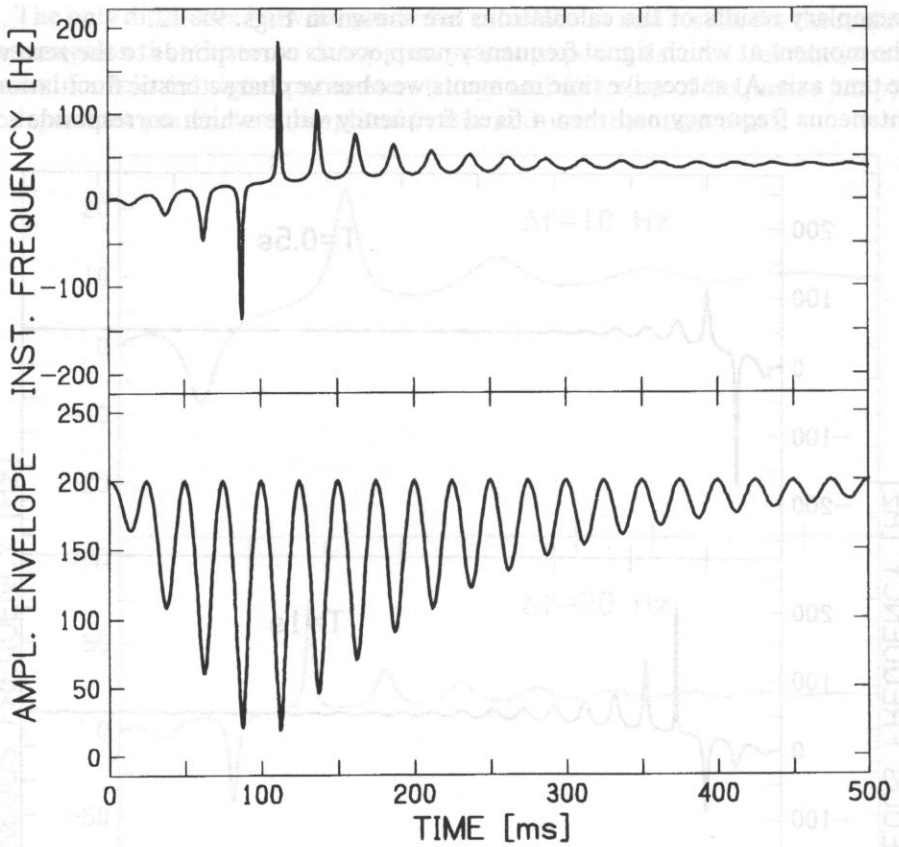

Fig. 12. Computer calculations of changes in instantaneous frequency and amplitude envelope of a signal after a frequency jump. ($\Delta f = 40$ Hz; $\delta = 1.0$; $T = 2$s).

final frequency of the frequency jump. For simplification we adopted the initial frequency value equal zero (in reality it is the value of the initial frequency of the jump). Furthermore, Fig.12 shows both changes in the frequency and amplitude of the signal after the frequency jump. Analysis of the calculation results has pointed out the following facts:

- the transition from the initial frequency value to the final value has an oscillating character; at the initial phase, the oscillation is non-symmetrical around the initial frequency value and then, starting at the moment at which the values of the amplitudes of the growth and decay signals are equal, the oscillation is non-symmetrical around the final frequency value,
- the final frequency value occurs after the time equal to the room reverberation time T,
- the oscillation frequency of the instantaneous frequency and amplitude envelope is equal to the value of the frequency jump,

• for the value of coefficient $\delta > 1$ the oscillation time around the initial frequency value is shortened,

• changes in time of the amplitude envelope have an oscillatory character, however without the change in the oscillation direction, which is characteristic of changes in instantaneous frequency.

Analyzing the data in Fig.12 one can state that extreme fluctuations of instantaneous frequency correspond to the minima of signal amplitude. Fig.13 shows a case of the frequency jump of a high value 199 Hz with respect the amplitudes ratio $\delta = 2.2$ and reverberation time $T = 1.4$s (top figure) and the jump in the opposite direction (bottom figure) — the value of coefficient δ is equal to $1/2.2 \approx 0.45$.

Like in this case of linear frequency changes, experimental investigations were performed in accordance with the methodology developed before, this time for jump frequency changes of the signal.

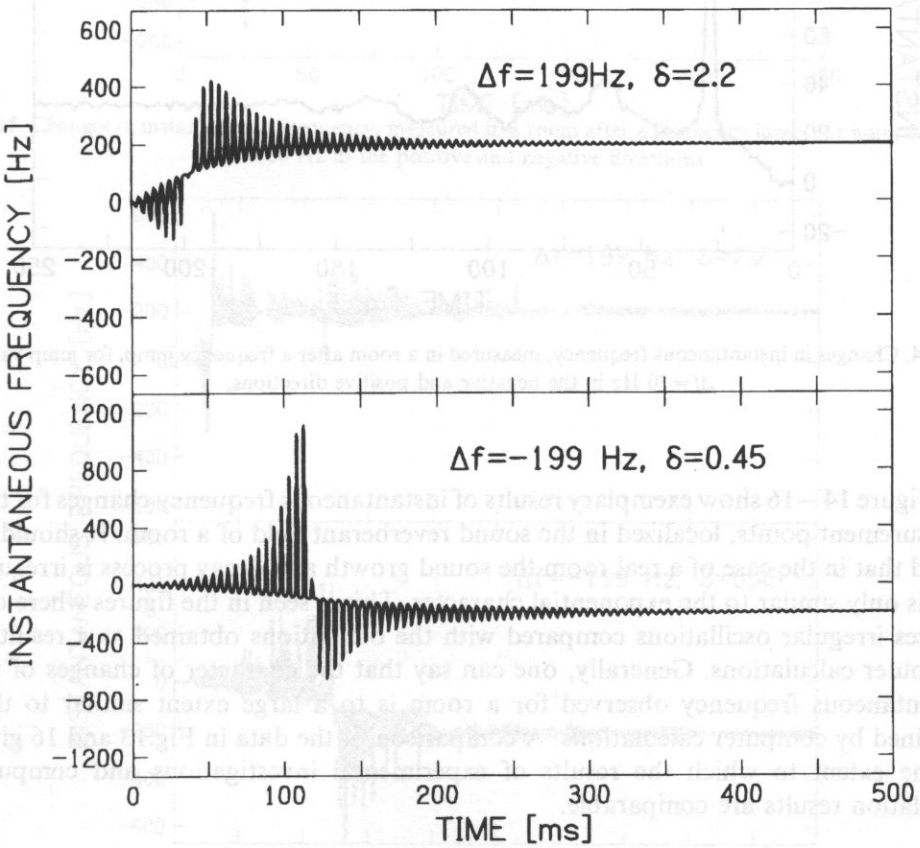

Fig. 13. Computer calculations of changes in instantaneous frequency of a signal after a frequency jump, for jump values $\Delta f = 199$ Hz in the positive and negative directions. ($T = 1.4$ s).

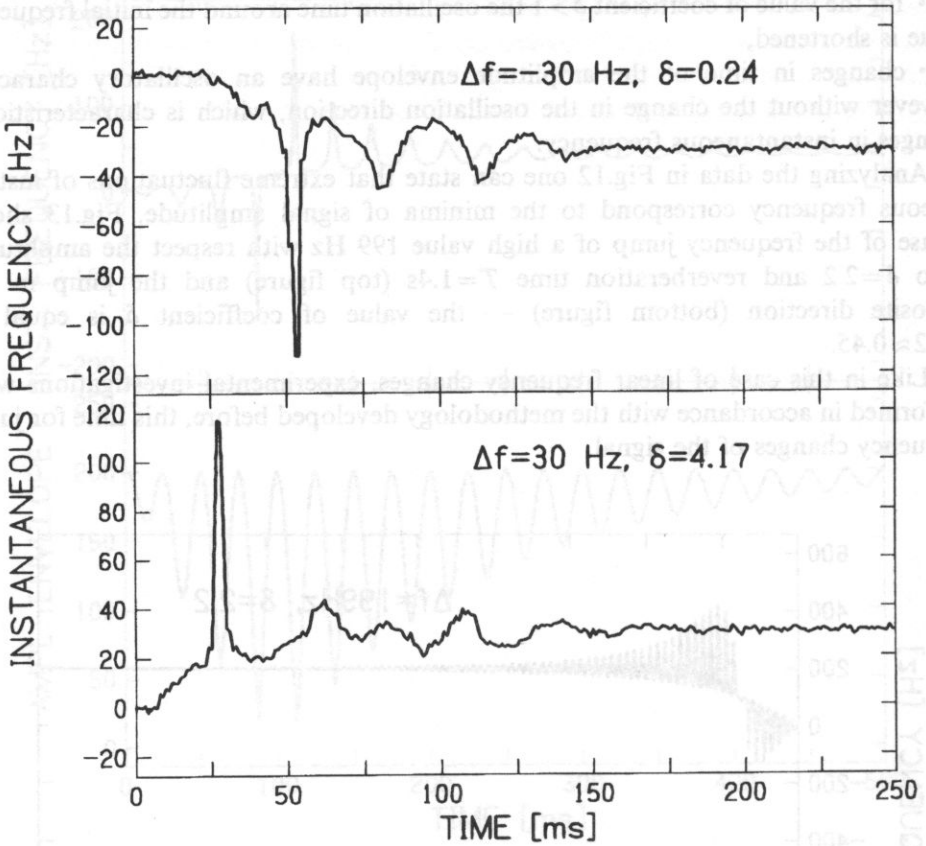

Fig. 14. Changes in instantaneous frequency, measured in a room after a frequency jump, for jump values $\Delta f = 30$ Hz in the negative and positive directions.

Figure 14 – 16 show exemplary results of instantaneous frequency changes for two measurement points, localized in the sound reverberant field of a room. It should be noted that in the case of a real room the sound growth and decay process is irregular and is only similar to the exponential character. This is seen in the figures where one notices irregular oscillations compared with the oscillations obtained as a result of computer calculations. Generally, one can say that the character of changes of the instantaneous frequency observed for a room is to a large extent similar to that obtained by computer calculations. A comparison of the data in Fig.13 and 16 gives us the extent to which the results of experimental investigations and computer simulation results are comparable.

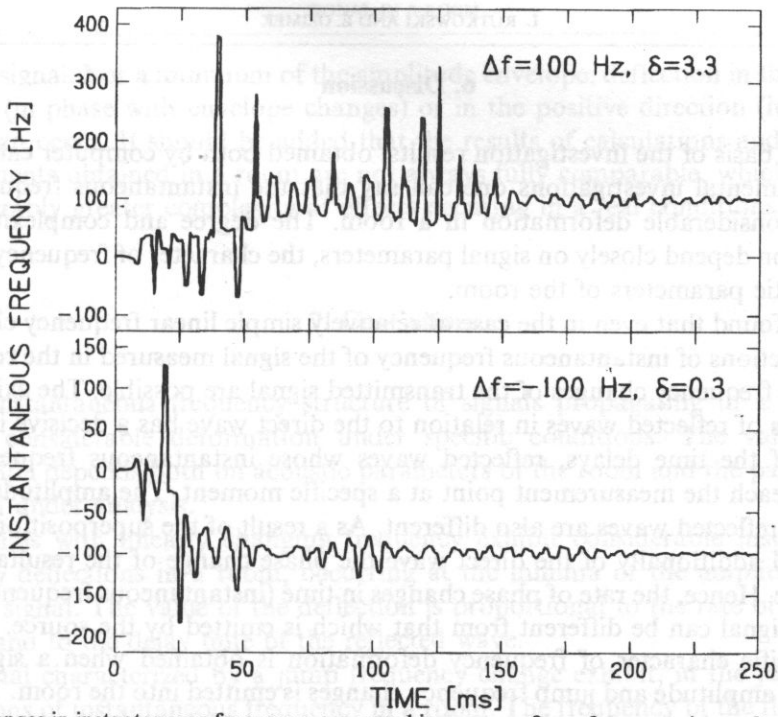

Fig. 15. Changes in instantaneous frequency, measured in a room after a frequency jump, for jump values $\Delta f = 100$ Hz in the positive and negative directions

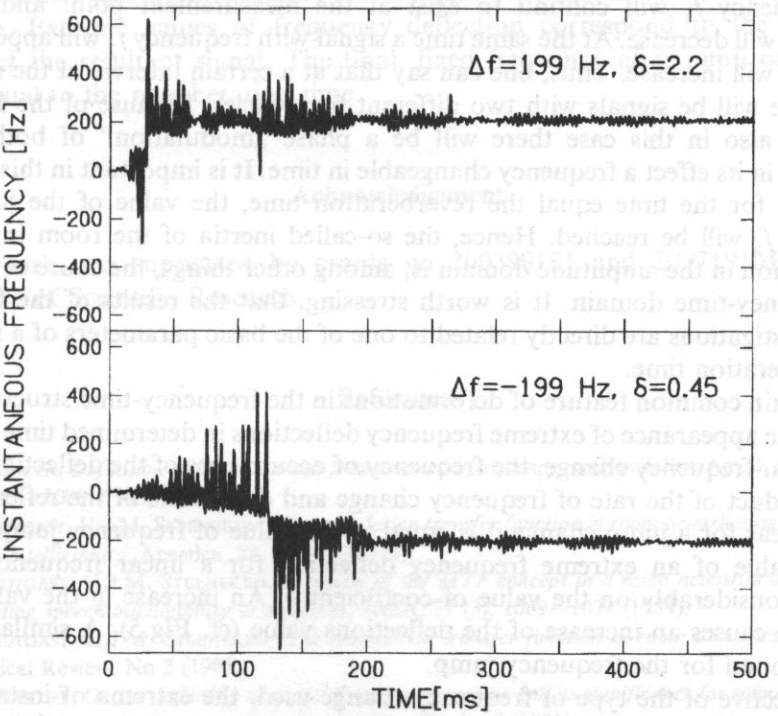

Fig. 16. Changes in instantaneous frequency, measured in a room after a frequency jump values $\Delta f = 199$ Hz in the positive and negative directions.

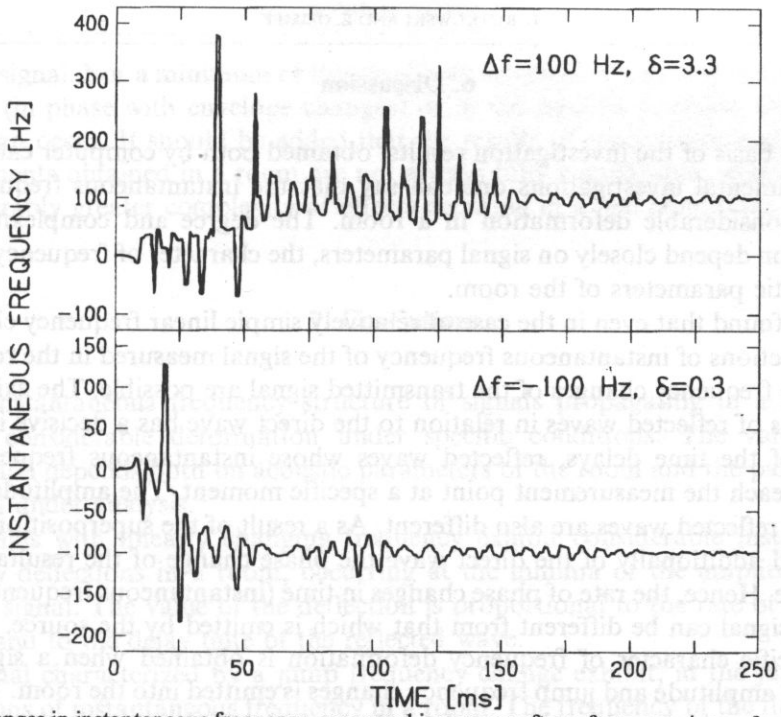

Fig. 15. Changes in instantaneous frequency, measured in a room after a frequency jump, for jump values $\Delta f = 100$ Hz in the positive and negative directions

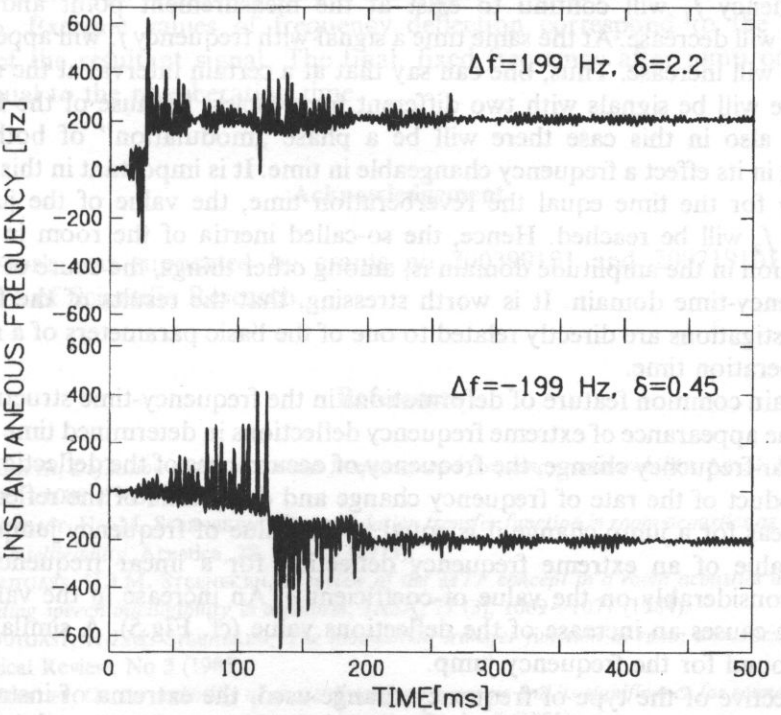

Fig. 16. Changes in instantaneous frequency, measured in a room after a frequency jump values $\Delta f = 199$ Hz in the positive and negative directions.

6. Discussion

On the basis of the investigation results, obtained both by computer calculations and experimental investigations one can say that the instantaneous frequency can undergo considerable deformation in a room. The degree and complexity of the deformation depend closely on signal parameters, the character of frequency changes and acoustic parameters of the room.

It was found that even in the case of relatively simple linear frequency changes in time, deflections of instantaneous frequency of the signal measured in the room with relation to frequency changes of the transmitted signal are possible. The existence of time delays of reflected waves in relation to the direct wave has a decisive influence. Because of the time delays, reflected waves whose instantaneous frequencies are different reach the measurement point at a specific moment. The amplitude ratio of successive reflected waves are also different. As a result of the superposition of these waves, and additionally of the direct wave the phase change of the resultant signal takes place. Hence, the rate of phase changes in time (instantaneous frequency) of the resultant signal can be different from that which is emitted by the source.

A specific character of frequency deformation is obtained when a signal with a constant amplitude and jump frequency changes is emitted into the room. The basic role in this case is played by the reverberant properties of the room in the amplitude domain. Because of these properties after the frequency jump from f_1 to f_2 a signal with frequency f_1 will continu to exist at the measurement point and only its amplitude will decrease. At the same time a signal with frequency f_2 will appear whose amplitude will increase. Thus, one can say that at a certain interval at the measured point there will be signals with two different frequencies. Because of the frequency difference also in this case there will be a phase „modulation" of both signals, producing in its effect a frequency changeable in time. It is important in this case that practically for the time equal the reverberation time, the value of the jump final frequency f_2 will be reached. Hence, the so-called inertia of the room in terms of reverberation in the amplitude domain is, among other things, the cause of inertia in the frequency-time domain. It is worth stressing, that the results of the frequency jump investigations are directly related to one of the basic parameters of a room, i.e. the reverberation time.

A certain common feature of deformations in the frequency-time structure of the signal is the appearance of extreme frequency deflections in determined time intervals. For a linear frequency change, the frequency of occurrences of the deflection is equal to the product of the rate of frequency change and delay time of the reflected wave $\alpha\Delta t$, whereas for a jump change it is equal to the value of frequency jump Δf.

The value of an extreme frequency deflection for a linear frequency change depends considerably on the value of coefficient δ. An increase in the value of the coefficient causes an increase of the deflections value (cf. Fig.5). A similar relation was not found for the frequency jump.

Irrespective of the type of frequency change used, the extrema of instantaneous frequency deflection correspond to the minima of the amplitude envelope of the

resultant signal. For a minimum of the amplitude envelope, deflection in the negative direction (in phase with envelope changes) or in the positive direction (in opposite phases) can occur. It should be added that the results of calculations and results of measurements obtained in a room are not always fully comparable, which indicates a considerably greater complexity of effects occuring in a real conditions.

7. Conclusions

The instantaneous frequency structure of signals propagating in a room can undergo considerable deformation under specific conditions. The value of the deformation depends both on acoustic parameters of the room and the paramters of the signal under analysis.

- Signals with linearly changing frequency exhibit considerable instantaneous frequency deflections in a room, occurring at the minima of the amplitude of the resultant signal. The value of the deflection is proportional to the rate of frequency changes and to the delay time of the reflected wave.
- Signal characterized by a jump frequency change exhibit, in the jump range, fluctuations of instantaneous frequency in a room. The frequency of the fluctuations increases with an increase in the jump value. Their character, on the other hand, depends on the ratio of the amplitudes of a signal with final and initial frequencies of the jump. Extreme values of frequency deflection correspond to the amplitude minima of the resultant signal. The final, fixed frequency after jump occurs after a time equal to the reverberation time.

Acknowledgement

The work was supported by grants no 200399101 and 200719101 from the Committee of Scientific Research.

References

[1] M.S. GUPTA, *Definition of instantaneous frequency and frequency measurability*, Am. J. Phys., **43**, No 12, 1087–1088 (1975)

[2] T. HOUTGAST, H.J.M. STEENEKEN, *The modulation transfer function in room acoustics as a predictor of speech intelligibility*, Acustica, **28**, 66–73 (1973).

[3] T. HOUTGAST, H.J.M. STEENEKEN, *A review of the MTF concept in a room acoustics and its use for estimating speech intelligibility in auditoria*, JASA, **77** (3), 1069–1077 (1984).

[4] T. HOUTGAST, H.J.M. STEENEKEN, *The modulation transfer function in room acoustics*, Bruel-Kjaer Technical Review, No **3** (1985).

[5] H. KUTTRUFF, *On the audibility of phase distortions in rooms and its significance for sound reproduction and digital simulation in room acoustics*, Acustica **74**, 3–7 (1991).

[6] H.N.H. MIYATA, T. HOUTGAST, *Speech intelligibility and modulation transfer function in non-exponential decay fileds*, Acustica, **69**, 151–155 (1989).

[7] E. OZIMEK, *Investigations into the change in the spectral structure of sound propagating in a room* (in Polish with a summary and figure captions in English) Wydawnictwo Naukowe UAM — Poznań 1977, p. 248.

[8] E. OZIMEK, *Problem of the sound spectral changes propagating in a room in the aspect multidimensional space*, Archives of Acoustics, **12**, 251–272 (1987).

[9] E. OZIMEK, *Transformation of the space of room acoustic states into space of sound deformation*, Journal of Sound and Vibration, **113**, 417–423 (1987).

[10] E. OZIMEK, L. JUGOWAR, L. RUTKOWSKI, *Problem of the instantaneous sound frequency measurement*, Archives of Acoustics, **9**, 325–339 (1984).

[11] E. OZIMEK, A. SĘK, *Perception of irregular frequency changes of sinusoidal signal*, Acustica, **66**, 146–152 (1988).

[12] E. OZIMEK, L. RUTKOWSKI, *Deformation of frequency modulated signals (FM) propagating in a room*, Applied Acoustics, **26**, 217–230 (1989).

[13] S.O. RICE, *Mathematical analysis of random noise*, Bell System Tech. J., **23**, 24 (1944/45).

[14] L. RUTKOWSKI, E. OZIMEK, *Changes of the deviation of FM signals in a room*, Proceedings of the International Symposium on „Architectural Acoustics" (**2**). Strbske Pleso, 202–205 (1985)

[15] T. TOHIJAMA, R. LYON, T. KOIKE, *Reverberent phase in a room and zeros in the complex frequency plane*, JASA, **89**, 1701–1707 (1991).

ARCHIVES OF ACOUSTICS
20, 2, 139–150(1995)

SURFACE ACOUSTIC WAVE SPECTROSCOPY INVESTIGATION OF ELECTRICAL PROPERTIES OF THE NEAR-SURFACE REGION GaAs CRYSTALS

T. PUSTELNY

Institute of Physics Silesian University of Technology
(44–100 Gliwice ul. Krzywoustego 2)

The possibility of the appyling the surface acoustic wave of Rayleigh type to semiconductor investigations is described. The transverse acoustoelectric effect has been used to study the real surfaces of GaAs:Cd (111) and GaAs:Si (110) single crystals. The semiconductor surface in the layered structure: piezoelectric wave guide-semiconductor were performed. These investigations for different surface acoustic wave (SAW) frequencies were carried out. The values of the electric surface potentional Φ_s the carrier density n_S as well as the effective life time τ_e of the minority carriers were obtained. The investigations were performed in a $50 \div 200$ MHz frequence range. The dynamic values of these semiconductor surface parameters in a high frequency acoustic wave range were presented. The results have shown that the electrical and electron surface parameters may be various for different frequencies.

PACS: 43.35, 73.20, 72.50
KEY WORDS: acoustoelectric effects, semiconductor surface potential

1. Introduction

The electrical and electronic properties of the near-surface semiconductors region are completely different then its volumetric ones. Very often this region decides about the possibility of semiconductor crystal applications in technology of electronic devices and of their applications as the sensing elements for variety sensors techniques [1,2].

The semiconductor surface properties may be determined by means of the electrical sufrace potential Φ_S carrier density n_S and life time τ_e of minority carriers in the near surface region [1].

For the technology of electronic devices more and more often the III–V group semiconductors are used. In this group the GaAs crystal is a very important target material, first of all for its interesting optical properties. This semiconductor is used among other things technology of laser diodes and non coherent light sources, as well as for very high frequency amplifiers and for different senors construction [3].

The maximum of the work temperature for GaAs is twice as large as for Si and it is about 200 °C. The maximum of the work frequency of electronic GaAs devices may be even five times as large as of Si ones.

The development of the solid state spectroscopy causes the interest of using the acoustic methods in the semiconductor surface investigations. The surface acoustic wave methods seem to be a good tool for the semiconductor surface experimental investigations in high and very high frequency ranges.

When the surface acoustic wave (SAW) propagates in the piezoelectric-semiconductor structure, then the electric field, which accompanies this wave, penetrates the near-surface region of this semiconductor. (The penetration depth of the electric field inside the semiconductor is of the order of the extrinsic Debye lenght or the acoustic wavelenght, whichever is shorter). This electric field changes the free carrier concentration in the semiconductor near-surface region and causes drift of these carriers. There are plenty of aspects of the interaction between surface acoustic wave and charge carriers [4]. Among others, the difference of electrical potentional between the semiconductor surface and its bulk (i.e. transverse acoustoelectric voltage TAV) may be observed [5].

The transverse acoustoelectric method is very useful and attractive one for determination of semiconductor surface parameters. This method is non destructive one, it does not require ohmic contacts and give the dynamic values of investigated parameters.

The influence of the electron and electrical surface parameters on the character of transverse acoustoelectric effect (the amplitude of TAV and its time shape) were already earlier observed. In [6] it was shown that the monitoring of the acoustoelectric voltage or SAW attenuation while varying the conductivity by external means (e.g by temperature) can yield information about the density of the surface and impurity states in the semiconductor. By observing the optical wavelength dependence of the acoustoelectric voltage developed across the semiconductor one may have the information about energy profile of the states in the band gap. The transverse acoustoelectric voltage has been measured as a function of incident photon energy in InAs on $LiNbO_3$ SAW delay line structure in [7]. From the experimental results the energy band gap in InAs was determined. In [8] the transverse acoustoelectric voltage spectroscopy for the GaAs:Cr samples was performed. The samples were illuminated by two monochromatic beams. The characteristic exciton peak was observed at temperature below 200 K. Using two beam light illumination of the investigated semiconductor sample, one could determine the presence of donor and acceptor levels in the band gap of the GaAs:Cr sample. The similar technique of TAV used together with the illumination and temperature changes of GaP and InAs samples was presented in [9]. The deep levels in band gap of the investigated semiconductor samples were presented. This kind of investigations of the energy levels in the near-surface region in a semiinsulating GaAs was also reported in [10]. The acustoelectric measurements allow a precise determination of surface trap level distribution in the silicon band gap at the Si/SiO_2 interfaces [16]. Two kinds of experiments were presented there: the effect of an uniaxial compression and the effect of

HCl annealing are monitored by transverse acoustoelectric voltage versus voltage. The results indicate the presence of three energy levels in the energy midgap.

In the paper [11] we applied the longitudinal and transverse acoustoelectric effects to determine the surface potential in Si nad GaAs crystals. The results of the theoretical analysis of both acoustoelectric effects were described. The new acoustoelectric method of the surface potential determination was also presented. For the high resistivity GaAs: Te samples the values of surface potential were nearly — 0.4 [V]. The experimental results have shown that the acoustoelectric effects, particulary the transverse acoustoelectric effect, may be used for investigations of semiconductor surface properties. In [12, 13] the transverse acoustoelectric effect and the surface photo-voltage effect have been applied to the study of the GaP real surfaces. The values of the effective life time of minority carriers after different surface and their diffusion length have been presented.

The works mentioned above are not the only ones of these kind, of course. We think that the cited papers are important in the domain of application of surface acoustic waves and transverse acoustoelectric effect to semiconductor surface investigations.

In this paper the transverse acoustoelectric effect has been used to study the real GaAs:Cd (111) and GaAs:Si (110) surfaces. The real surface of a semiconductor means the surface obtained after cutting, polishing and standard chemical etching of the crystal. Such surfaces appear at different steps of the semiconductor surface preparation for devices technology. In this paper the investigations of the surface potential Φ_S, the carriers density n_S as well as the effective life time τ_e of the minority carriers in the near-surface GaAs regions have been presented.

2. Theoretical model

The transverse acoustoelectric voltage has been described by the following theoretical formulas [11,13]

$$U_{AE} = K \frac{\mu_p^2 p_b - \mu_n^2 n_b + n_i \frac{L_i}{L}(\mu_n^2 G_n - \mu_p^2 G_p)}{\mu_p p_b + \mu_n n_b + n_i \frac{L_i}{L}(\mu_p G_p - \mu_n G_n)} R. \tag{2.1}$$

$$R = \frac{\omega(\mu_n n_b + \mu_p n_b) + n_i \frac{L_i}{L}(\mu_p G_p - \mu_n G_n)}{\varepsilon_0^2(\varepsilon_S + \varepsilon_p)^2 \ \omega^2 + q^2 \left[\mu_p p_b + \mu_n n_b + n_i \frac{L_i}{L}(\mu_p G_p - \mu_n G_n) \right]^2}. \tag{2.2}$$

$$u = \frac{q\Phi}{k_B T}, \quad u_S = \frac{q\Phi_S}{k_b T}, \quad u_b = \frac{q\Phi_b}{k_b T}. \tag{2.3}$$

where: μ_n, μ_p mobilities of electrons and holes, respectively, in the near surface region

n_b, p_p concentrations of electrons and holes in the bulk of the semiconductor,
n_i electron concentration in the intrinsic semiconductor,
n, p concentrations of electrons and holes ($n=n_b e^{V}$; $p=p_b e^{-V}$)
L_i, L intrinsic and effective Debye lenght, respectively
G_n, G_p Kingston functions of the second type for electrons and holes [15]
Φ electric potential in semiconductor [1, 2, 15]
Φ_S electric surface potential (at the sufrace $\Phi=\Phi_S$)
Φ_b electric potential inside the semiconductor (in the bulk $\Phi=\Phi_b$,)
ε_p, ε dielectric constants of the piezoelectric and semiconductor
ω acoustic wave circular frequency
q electron charge

The Kingston Functions G_n, G_p, carrier mobilities μ_n, μ_p, as well as concentrations of electrons and holes n, p, are complicated functions of the surface potential Φ_S and electron concentration n_S in the near-surface region. (The nonelementar Kingston functions: G_n, G_p may be numerically calculated: they are presented in the graph and in the graph and in the tables [1, 15].)

The theoretical analysis of the acoustoelectric effects were presented in [11, 13]. The teoretical results of this analysis are used for the determination of the electron concentration n_S and the surface potential Φ_S in the next part of this paper.

The surface theoretical and experimental investigation results presented here were obtained for the samples with the following bulk parameters:

i) GaAs:Si (110)

- n-type electrical conductivity
- carrier mobilities:$\mu_n=8200$ [cm^2/V*s], $\mu_p=410$ [cm^2/V*s]
- permittivity: $\varepsilon=10.4$
- band gap: $E_g=1.48$ eV
- electron concentration: n$=1.2*10^{14}$[cm^{-3}]
- resistivity: $\rho=3.6*10^6$ [Ωcm]

ii) GaAs:Cd (111)

- n-type electrical conductivity
- carrier mobilities: $\mu_n=8600$[cm^2/V*s], $\mu_p=400$[cm^2/V*s]
- permittivity: $\varepsilon=9.8$
- band gap: $E_g=1.44$ eV
- electron concentration: $n=1.2*10^{15}$[cm^{-3}]
- resistivity: $\rho=3.0*10^5$[Ωcm]

In Fig. 1. the theoretical function of the amplitude U_{AE} versus carrier density n_S in the surface region for GaAs:Si (110) is presented. This function was calculated using the theoretical results which we presented in [15]. For the GaAs:Cd (111) sample, the theoretical function $U_{AE}=f(n_s)$ was very similar to this one presented in Fig. 1.

For very high carrier concentrations, near the intrinsic region, the interactions between the electric field (from SAW in piezoelectric) and carriers in the near surface region are very small. The TAV voltage, as the results of this interactions, are very

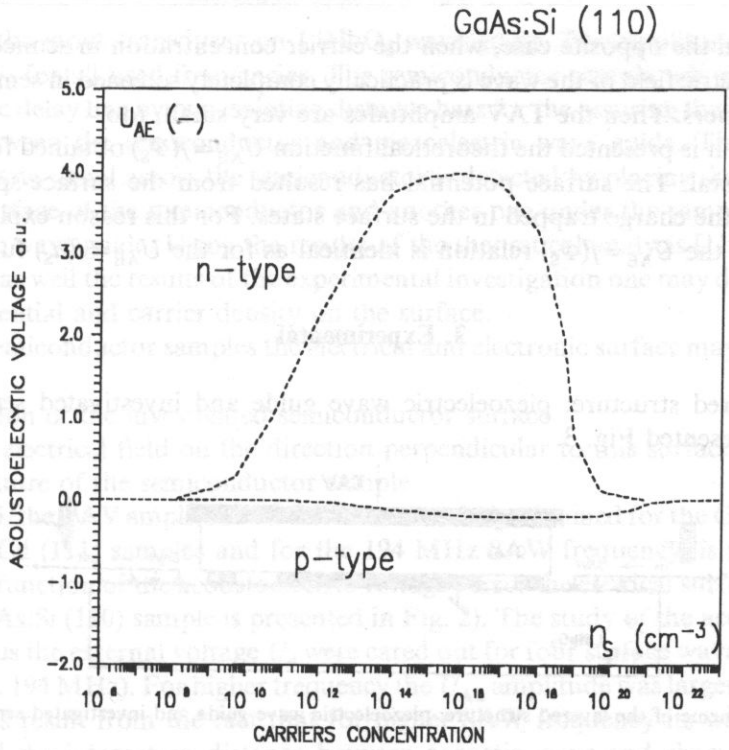

Fig. 1. The transverse acoustoelectric voltage as the theoretical function of the carrier concentration in near-surface region.

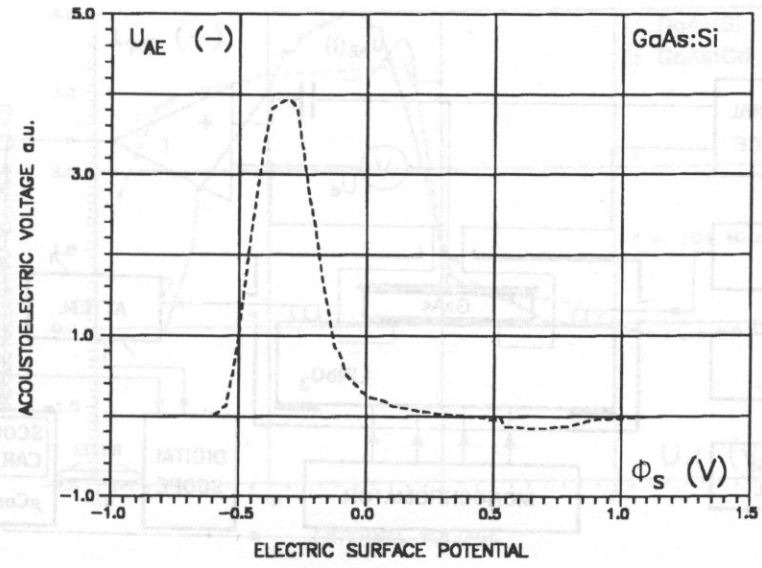

Fig.2. The theoretical relation $U_{AE}=f(\Phi_S)$ for GaAs:Si (110).

small, too. In the opposite case, when the carrier concentration in semiconductor is large, the electric field of the wave is practically completely screened in semiconductor by these carriers. Then the TAV amplitudes are very small, too.

In Fig. 2. it is presented the theoretical function $U_{AE}=f(\Phi_S)$ obtained for the same GaAs:Si crystal. The surface potential has resulted from the surface-space charge neutralising the charge trapped in the surface states. For this reason explantation of the shape of the $U_{AE}=f(\Phi_S)$ relation is identical as for the $U_{AE}=f(n_S)$ function.

3. Experimental

The layered structure: piezoelectric wave guide and investigated semicoductor sample is presented Fig. 3.

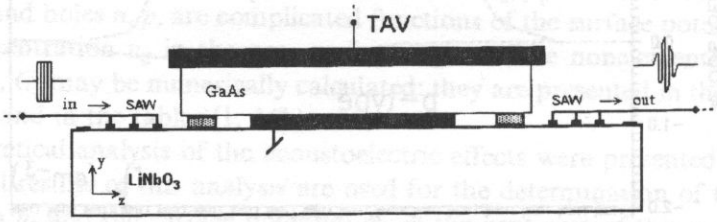

Fig. 3. The scheme of the layered structure: piezoelectric wave guide and investigated semiconductor.

The set-up for the surface semiconductor investigation by means of the transverse acoustoelectric method is shown in Fig. 4. The investigations were performed for the four frequencies: 52, 74, 132, and 194 MHz. The about 2 μs duration r.f. pulse was

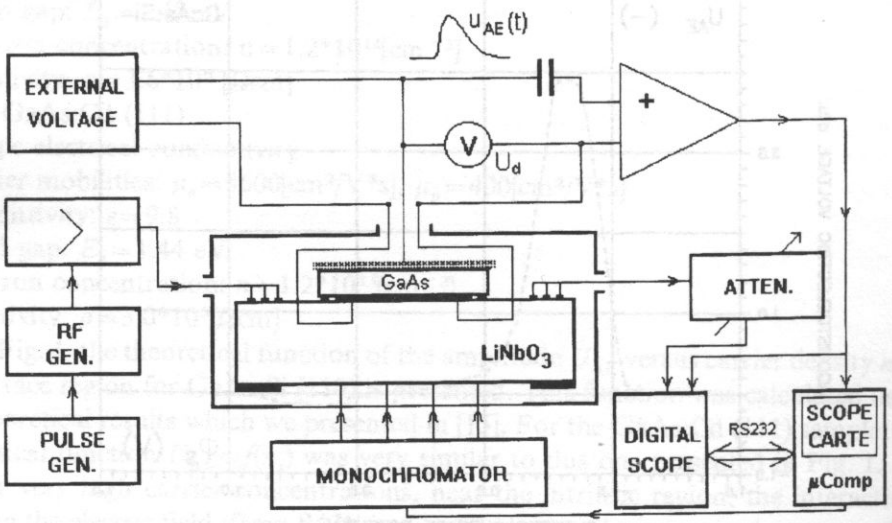

Fig.4. The experimental set-up for the semiconductor surface investigation by TAV method.

applied to the input transducer on $LiNbO_0$ wave guide. The amplitudes of the r.f. pulse 3.5 [V] for all used frequencies. The semiconductor sample was placed at the piezoelectric delay line by two isolating distance bars for the assuring the non acoustic contact between the semiconductor and piezoelectric wave guide. The transverse acoustoelectric signal across the semiconductor is detected by placing the Al plate on the back surface of the semiconductor and another one under the sample placed on the acoustic wave guide. Using the results of the theoretical analysis [11], Eqs. (2.1), (2.2), (2.3), as well the results of the experimental investigation one may determine the surface potential and carrier density on the surface.

In the semiconductor samples the electrical and electronic surface may be changed by [11]:

i) illumination of the investigated semiconductor surface
ii) external electrical field on the direction perpendicular to this surface
iii) temperature of the semiconductor sample

In Fig. 5. the TAV amplitude versus the external U_d, obtained for the GaAs:Si (110) and GaAs:Cd (111) samples and for the 194 MHz SAW frequency, is shown. (The theoretical function of the acoustoelectric voltage versus the eletrical surface potential for this GaAs:Si (110) sample is presented in Fig. 2). The study of the acoustoelectric effects versus the external voltage U_d were cared out for four surface wave frequencies (52, 74, 132, 194 MHz). For higher frequency the U_{AE} amplitude was larger. Frist of all, these effects result from the fact that for higher SAW frequency its wave length is smaller and the interaction distance between acoustic wave and charge carriers in semiconductor is effectively longer. The same semiconductor length contains larger number of the acoustic wave length for a higher frequency. For this reason we relate the transverse acoustoelectric voltage to the length of the acoustic wave.

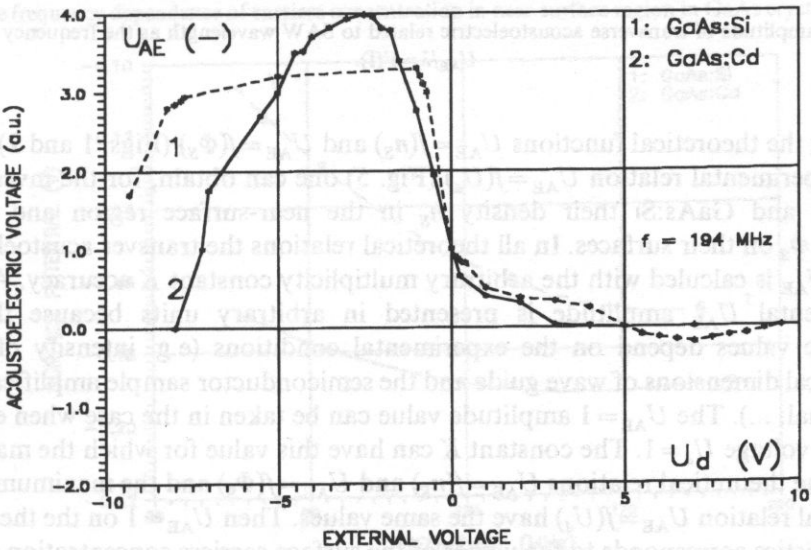

Fig.5. The experimental dependencies of U_{AE} on external U_d for GaAs:Si (110) and GaAs:Cd (111).

In Fig.6 we present the dependence of the TAV amplitude referred to the wave length wersus the SAW frequency: $U_{AE}/\lambda = F(\omega)$. The values of U_{AE}/λ are presented in arbitrary units and the value $U_{AE}/\lambda = 1$ is related to the 52 MHz frequency. This relation seems to proof that higher frequency the trapping of carries by energetic surface states are strong — plenty of carriers interact with these states, there are located in band gap and smaller part of carriers interact with SAW and TAV amplitude U_{AE}/λ are smaller for higher frequency.

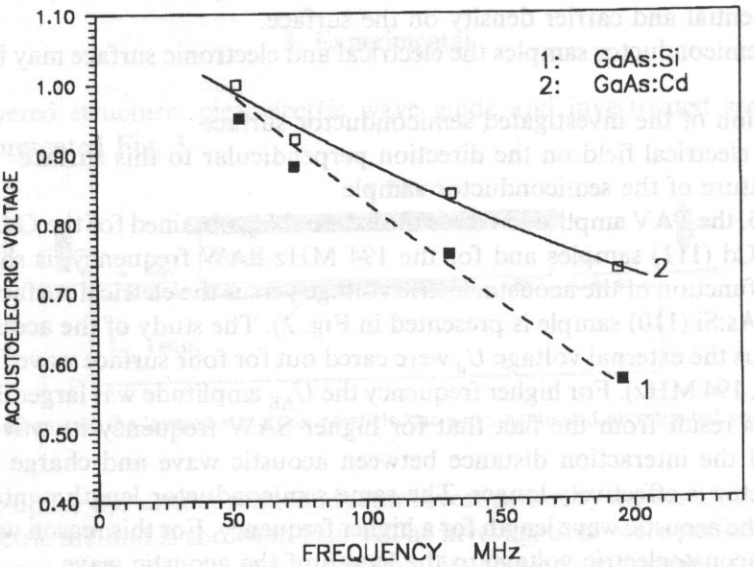

Fig.6. The amplitude of transverse acoustoelectric related to SAW wavelength as the frequency function: $U_{AE}/\lambda = F(f)$.

Using the theoretical functions $U_{AE} = f(n_S)$ and $U_{AE} = f(\Phi_S)$ (Figs. 1 and 2) as well as the experimental relation $U_{AE} = f(U_d)$ (Fig. 5) one can obtain, for the investigated GaAs:Cd and GaAs:Si their density n_S in the near-surface region and electric potential Φ_S on their surfaces. In all theoretical relations the transver acustoelectrical voltage U_{AE} is calculed with the arbitrary multiplicity constant K accuracy. Also the experimeental U_{AE} amplitude is presented in arbitrary units because the U_{AE} amplitude values depend on the experimental conditions (e.g. intensity of SAW, geometrical dimensions of wave guide and the semiconductor sample amplification of TAV signal, ...). The $U_{AE} = 1$ amplitude value can be taken in the case when external electrical voltage $U_d = 1$. The constant K can have this value for which the maximum U_{AE} on the theoretical relations $U_{AE} = f(n_S)$ and $U_{AE} = f(\Phi_S)$ and the maximum on the theoretical relation $U_{AE} = f(U_d)$ have the same values. Then $U_{AE} = 1$ on the theoretical characteristics corresponds to the values of the surface carriers concentration and the surface potential in the investigated semiconductor.

For the higher frequency the surface potential have the smaller values. The frequency dependencies of the carrier concentration in the near surface region for GaAs:Si (110) and GaAs:Cd (111) are show in Fig.7. In Fig. 8 the surface potential versus frequency is presented. One may see that electric field from SAW in piezoelectric wave guide changes the carrier concentration in the conducting band.

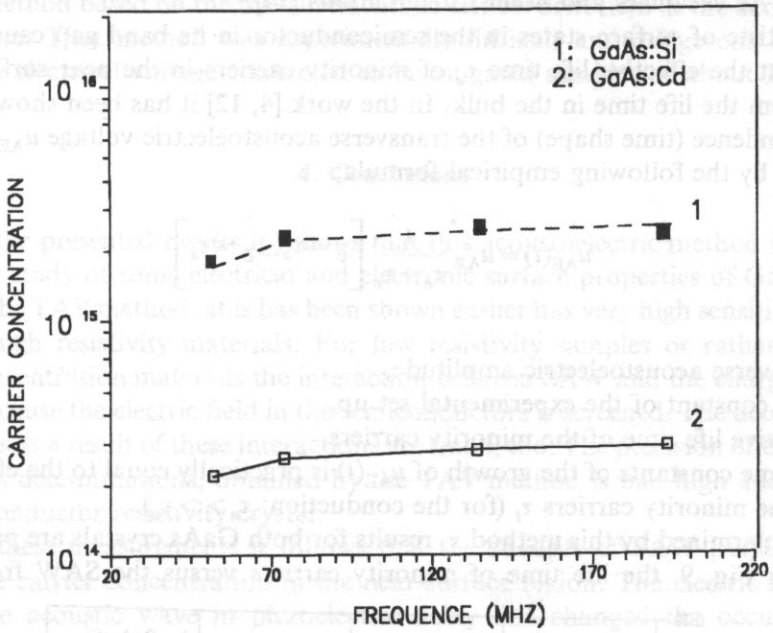

Fig.7. The frequency dependence of carriers concentration in near surface region in GaAs crystal $n_S = F(f)$.

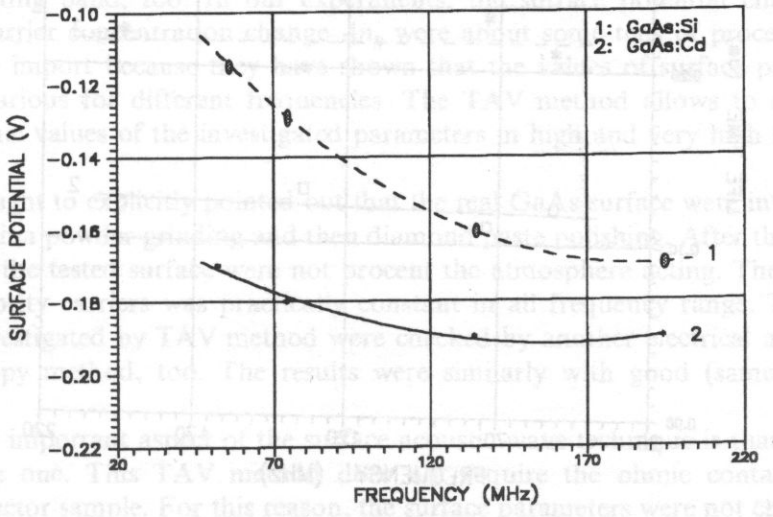

Fig.8. The frequency dependence of the surface potential by TAV method: $\Phi_S = F(f)$.

For our high resistivity GaAs:Cd and GaAs:Si samples with higher frequency the carrier concentration n_S was lower.

The surface states acting as recombination centres or as traps evoking the surface potential barriers can be produced by lattice defects, chemical contaminations (e.g. oxygen, carbon dioxide and hydrogen adsorption), oxidation or complexes formed from Ga, As vacancies and other foreign atoms [19].

The existe of surface states in the semiconductor in its band gap causes among others that the effective life time τ_e of minority carriers in the near surface region differs from the life time in the bulk. In the work [4, 12] it has been shown that the time dependence (time shape) of the transverse acoustoelectric voltage $u_{AE}(t)$ may be described by the following empirical formula:

$$u_{AE}(t) = u_{AE} \frac{t}{\tau_a - \tau_e} \left[e^{-t/\tau_a} - e^{-t/\tau_e} \right]$$

where

U_{AE} transverse acoustoelectric amplitude,

τ_a time constant of the experimental set up,

τ_e effective life time of the minority carriers.

The time constants of the growth of $u_{AE}(t)$ is practically equal to the effective life time of the minority carriers τ_t (for the conduction: $\tau_a >> \tau_e$).

The determined by this method τ_e results for both GaAs crystals are presented in Fig. 9. In Fig. 9. the life time of minority carriers versus the SAW frequency is

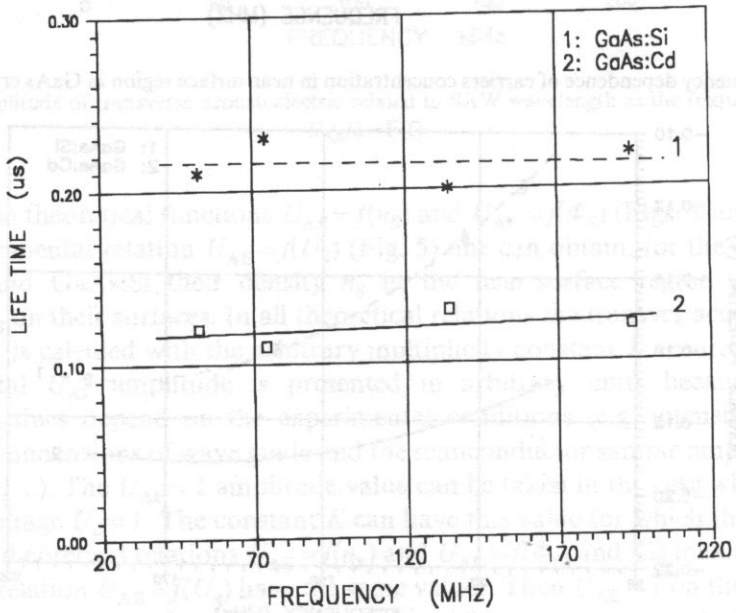

Fig.9. The life time of minority carriers versus of frequency: $\tau_e = F(f)$.

presented. In [12] it was used this τ_e determination method for GaP samples. The values of effective life time of minority carriers τ_e obtained TAV method were verified by the surface photo-voltage method. The results of τ_e determined by both these methods (TAV and photo-voltage) were similar with good accuracy (about ten procent). In the work [19], the life time τ_e for Si samples was obtained by means acoustic method based on the measurements of critical drift field in the acoustoelectric structure. That method was experimentally difficult and dangerous because it needed the electrical voltage connected to investigated samples of about $2 \div 3$ kV.

4. Conclusions

From the presented results it follows that this acoustoelectric method is a useful tool in the study of some electrical and electronic surface properties of GaAs single crystals. The TAV method, at is has been shown earlier has very high sensitivity in the study of high resistivity materials. For low resistivity samples or rather for high carrier concentration materials the interaction between SAW and the charge carriers is weak because the electric field in the semiconductors is screened. The acoustoelectric voltages as a result of these interactions are small, too. The precision of the surface parameters determinations, obtained by the TAV method is bad high and for very low semiconductor resistivity crystal.

From these measurements it follows that the changes of SAW frequency may change the carrier concentration in the near-surface region. The electric field from the surface acoustic wave in piezoelectric delay line changed the occupation of surface energetic states by electric carriers and it caused, as a result, the change in the surface potential. The electric field changes the concentration of free carriers in conducting band, too. In our experiments, the surface potential change $\Delta\Phi_S$ and the carrier concentration change Δn_S were about some tens of procent. These results are import because they have shown that the values of surface parameters may be various for different frequencies. The TAV method allows to determine the dynamic values of the investigated parameters in high and very high frequency ranges.

One ought to explicitly pointed out that the real GaAs surface were investigated after alumina powder grinding and then diamond paste polishing. After this surface treatment the tested surface were not procent the atmosphere acting. The life time τ_e of minority carriers was practically constant in all frequency range. The parameters investigated by TAV method were checked by another electrical and photo spectroscopy method, too. The results were similarly with good (same procent) accuracy.

A very important aspect of the surface acoustic wave technique is that it is non destructive one. This TAV method does not require the ohmic contacs to the semiconductor sample. For this reason, the surface parameters were not changed by difficult technology procces of the ohmic contact preparation.

Acknowledgement

Author wish to thank Prof. A. Opilski from Institute of Physics Silesian Technical University in Gliwice for helpful discussions and mgr. L. Wegierska for help in numerical calculations. Author wish to thank Prof. J. Bobitskij from University of Technology in Lviv (Ukraine Republic) for preparing the semiconductor materials for investigations.

The work was sponsored by Institute of Physics, Silesian Technical University within research project BW/95

References

[1] S. PEKA, *Semiconductor surface physics*, Nauka, kiev 1991.

[2] S.M. SZE, *Physics of semiconductor devices*, Willey, New York 1989.

[3] J. SOLE, *et. al., Multiwavelenght semiconductor laser advance rapidely*, Laser Focus World, **6**, 59–66 (1994).

[4] J.H. GILBOA, M. MOTAMEDI and P. DAS, *Semiconductor surface study by transverse acoustoelectric voltage*, Proc. 1986 IEEE Ultrasonic Symp., pp. 663–667.

[5] Yu. GULAYEV, *Physical acoustoelectronics: Interaction of acoustic wave with free electrons in semiconductors*, Summer Schol on Acoustic Sicily, 95–140 (1989).

[6] R.T. WABSTER *et al., Constacless semiconductor surface characterization using surface acoustic wave*, Surface Science **86**, 848–857 (1979).

[7] M. AYUB and P. DAS, *Spectroscopy of InAs using SAW generated transverse acoustoelectric voltage*, J. Appl. Phys., **51**, 1, 433–436 (1980).

[8] B. DAVARI and P. DAS, *Quenching and enhacement of the excitation and subbandgap absorption in GaAs:Cr using two-beam transverse acoustoelectric voltage spectroscopy*, Appl. Phys. Leet., **40**, 9, 807–809 (1982).

[9] P. DAS, *Transverse acoustoelectric voltage TAV spectroscopy of gallium phosphide and indum arsenide*, J. Vac. Sci. Technical., **48**, 5, 1379–1382 (1989).

[10] M. TABIB-AZIR, *Characterisation of electrical properties of semi-insulating GaAs using acoustoelectric voltage spectroscopy between* 83 K and 300 K *with surface wave power as an additional parameter*, Solid State Electronics, **31**, 7, 1193–1204 (1988)

[11] T. PUSTELNY and Z. KUBIK, *Investigation of surface potentional of GaAs surface by means of acoustic effects*, Archives of Acoustics, **19**, 2, 271–280 (1994).

[12] T. PUSTELNY and B. ADAMOWICZ, *Determination of some electronic and optical parameters by means photoelectric methods*, J. Tech. Phys., **34**, 3, 299–309 (1993).

[13] T. PUSTELNY, *Surface potential investigation of transverse acoustoelectric method*, Ultrasonic, (1994) in press.

[14] T. PUSTELNY and B. ADAMOWICZ, *Transverse acoustoelectric effect and surface photovoltage method in surface study of GaP and InP*, J. Tech. Phys., 3, 211–219 (1994).

[15] A. MANY, Y. GOLDSTEIN and N. GROVER, *Semiconductor surface*, North Holland, Amsterdam 1976.

[16] A. ABBATE and F. PALMA, *Study of* Si/SiO_2 *interface by transverse acoustoelectric voltage measurements*, Appl. Phys. Leet., **55**, 13, 25, 1306–1310 (1989).

[17] I. YAKOVKIN and V. VYUN, *Using of acoustoelectric interaction in studies of semiconductor surface*, Proc. Intern. Symp., „Surface Waves in Solid and Layered Structures", Novosibirsk (1986) v. 1. 183–200.

[18] H. WOHLTJEN, *Chemical sensors and microinstrumentation*, American Chemical Society, Washington, USA 1989.

[19] A. OPILSKI and T. PUSTELNY, *Investigations concerning fast surface states of semiconductors by means of acoustics methods*, Archives of Acoustics, **14**, 3, 253–260 (1989).

ARCHIVES OF ACOUSTICS
20, 2, 151–169(1995)

GENERATION AND DETECTION OF ACOUSTIC WAVES IN MICROWAVE CAVITIES

M. ALEKSIEJUK AND W. PAJEWSKI

Laboratory of Acoustoelectronic
Institute of Fundamental Technological Research
Polish Academy of Sciences
(00–049 Warszawa, Świętokrzyska 21)

This paper containes a detailed analysis of the conditions of acoustic wave excitation in retrant-type, microwave cavities, obtained by means of the methods field. Dependence of the resonance frequency on the resonator parameters and the material constants of a piezoelectric sample placed in the resonator is given. Construction of the resonators investigated and the experimental data concerning their parameters in the 0.210 GHz frequency range are presented. Results of attenuation measurements of waves in lithium niobate and bismuth-germanium oxide crystals obtained by applying the resonators described are also shown.

1. Introduction

Present ultrasonic technology and physics need acoustic sources with higher frequencies. Piezoelectric plate transducers traditionally used for the ultrasound generation become useless, first — from technological reasons (breaking of thin plates), and moreover troublesome because efficiency of transformation of the electric energy into the acoustic one (for harmonic frequencies) is low (losses are proportional to the square of frequency). Therofore, at the end of the fifties BARAŃSKI [1] and BÖMMEL and DRANSFLED [2, 3] proposed the method of existing the acoustic wave in a piezoelectric rod (quartz), one end of which was placed in a microwave resonator. Detection of the generated acoustic waves was done by the Bragg-type light diffraction measurement. Those methods were applied in solid body investigations at frequencies of 0.3–3 GHz. Investigations of the liquids were initiated by LEZHNEV [4]. Measurements in a higher frequency range were also made [5, 6]. In this paper the results of investigations, which represent an extension of the above mentioned method, togehter with a precise analysis of generation and detection conditions of hypersonic waves in the gigacycle frequency range, are presented. Dependence of the resonance frequency on the cavity parameters is determined. The resonators and the measurement setup made in IFTR for acoustic measurements in the gigacycle frequency range are described.

2. Excitation of hypersonic vibrations in resonator cavity

Generation of hypersounds by means of a cavity consists in the non-resonance surface layer excitation of vibrations of a pizoelectric rod, which is placed in a strong electric field of a microwave resonator. The excited hypersonic pulse on the surface layer of this rod, propagates as a consequence of the piezoelectric effect, along the rod, is reflected and returns to the origin of this rod. As a result of the inverse piezoelectric effect, it produces a new electromagnetic pulse, recorded by a microwave detection setup. In the rod with low acoustic losses, this pulse can be reflected many times and produces the subsequent echoes (Fig. 1).

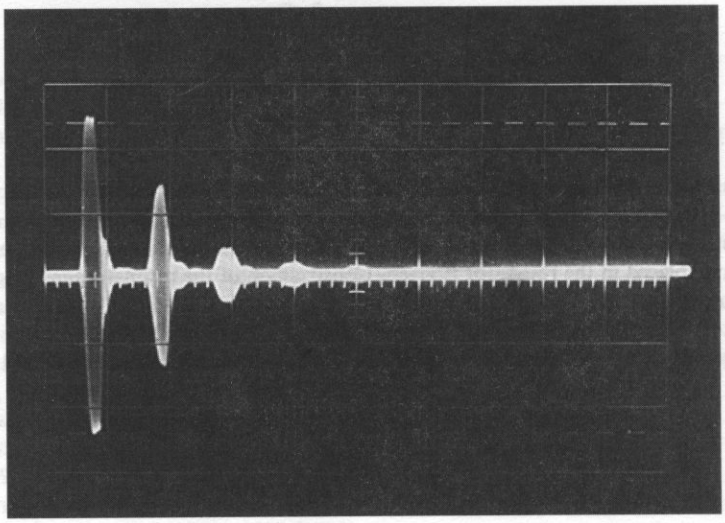

Fig.1. Sequence of electric echoes produced in the resonator as a result of repeated reflections of the hypersonic pulse in piezoelectric rod (frequency 600 MHz, room temperature).

In order to describe the generation phenomenon more precisely, the following assumptions are made: the piezoelectric rod is X-out, the one surfaces of it is placed at $x_1=0$, and the hypersonic wave propagates along the x_1 — axis of the rod (Fig. 2)

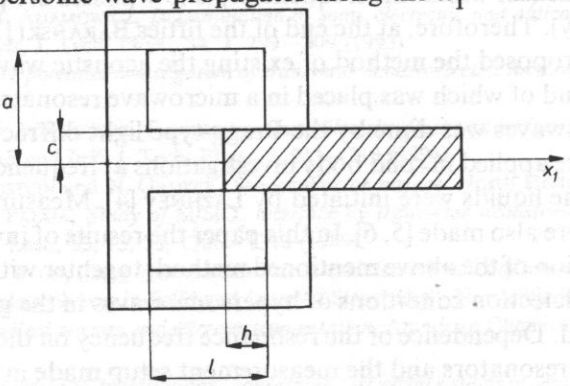

Fig.2. Parameters of the coaxial resonator.

A high-frequency electric filed $E_1(t)$ is also applied in this direction. In quartz with the density ρ, the mechanical stress σ_1 is determined by the expression:

$$\sigma_1 = c_{11}\varepsilon_1 - e_{11}E_1(t), \tag{2.1}$$

where c_{11} and e_n are the elasticity and piezoelectric constants, respectivelly, and ε_1 is the relative deformation. The equation for the displaced is obtained from the equation of motion

$$\rho = \frac{\partial^2 u_1}{\partial t^2} = \frac{\partial \sigma_1}{\partial x_1} = e_{11}\frac{\partial \varepsilon_1}{\partial x_1} - \frac{\partial}{\partial x_1}(e_{11}E_1), \tag{2.2}$$

or

$$\frac{\partial^2 u_1}{\partial x_1^2} = \frac{1}{V_t^2}\frac{\partial^2 u_1}{\partial t^2} = \frac{\partial}{\partial x_1}\left(\frac{e_{11}}{c_{11}}E_1\right), \tag{2.3}$$

where $(c_{11}/\rho)^{1/2}$ is the velocity of lingitudional wave propagation along x-axis the quartz. From Eq. (2.3) one can see that gradient of the electric field is the source of hypersonic waves. This gradient is large only on the surface of the piezoelectric rod, because inside the rod the electric filed gradully decreases with the distance.

Supposing the solutions of that equation to have the harmonic form:

$$E_1 = E_1^0 e^{-i\omega t}, \quad u_1 = u_1^0 e^{-i\omega t}, \tag{2.4}$$

Eq. (2.3) becomes

$$\frac{\partial^2 u}{\partial x_1^2} + k^2 u_1^0 = \frac{\partial}{\partial x_1}\left(\frac{e_{11}}{c_{11}}E_1^0\right), \tag{2.5}$$

where $k^2 = \varepsilon^2/v_1^2$.
Since the Green functions

$$G(x_1.x_1') = i/2k \exp(\mathrm{ik} \mid x\text{-}x' \mid) \tag{2.6}$$

are the solution of a homogenous equation

$$\partial^2 G/\partial x_1^2 + k^2 G + \delta(x_1 - x_1) \tag{2.7}$$

one can obtain

$$u_1^0(x_1) = \int \frac{l}{2k} \exp\left(ik \mid x_1 - x_1' \mid \frac{\partial}{\partial x_1'}\left(\frac{e_{11}}{c_{11}}E_1^0\right)\right) dx_1. \tag{2.8}$$

The largest spatial changes of the electric field occur at the boundary, therefore one can approximate the term corresponding to the source by a δ — function. The vaves which propagate in the x — direction are reflected from the free boundary. The boundary condition can be fulfilled by introducing the second apparent source at

$x_1 = x_0$, and by extending the rod to infinity. Next, two sources are transformed to a single one by passing to the limit for $x_0 = 0$. This gives

$$u_1^0(x_1) = \lim_{x_0 \to 0} \frac{iE_1^0 c_{11}}{2kc_{11}} \int \exp(ik \mid x_1 - x_1' \mid \delta(x_1' - x_0) + \delta(x_i + x_o)] dx_1' = \frac{iE_i^0 e_{11}}{kc_{11}} \exp(ikx_1) \tag{2.9}$$

for $x > 0$

Since the displacement is a real quantity, one takes only the real part of this expression,

$$u_1 = \frac{e_{11} E_1^0}{kc_{11}} \sin(\omega t - kx_1). \tag{2.10}$$

Now it is possible to find the acoustic energy flux and the efficiency of transformation. The density of the acoustic energy R in the rod equals

$$R = 1/2 \; c_{11} (\varepsilon_1^0)^2. \tag{2.11}$$

This energy propagates with velocity v_1 from the surface A. According to (2.10), the deformation equals

$$\varepsilon_1 = \frac{\partial u_1}{\partial x_1} = -\frac{e_{11}}{c_{11}} E_1^0 \cos(\omega t - kx_1), \tag{2.12}$$

and consequently, the amplitude of deformation is equal to $e_{11} E_1^0 / c_{11}$. In this case, the acoustic power obtained is given by

$$S = 1/2 \; e_{11}^2 (E_1^0) A v_l / c_{11}. \tag{2.13}$$

To determine the efficiency coefficient, this power must be compared with the electric power P deliveerd to the cavity. This power equals

$$P = \frac{\omega}{Q} 1/2 \; \varkappa \; (E_1^0) V, \tag{2.14}$$

where Q, V and $\varkappa$ are the quality factor of the resonator, its volume and the dielectric permeability of the rod, respectively.
Then

$$S/P = \frac{e_{11}^2}{\varkappa c_{11}} \frac{A v_l Q}{\omega V} = k_{11}^2 \, A v_l / \omega V, \tag{2.15}$$

where $k_{11} = (e_{11}^2 / \varkappa c_{11})^{1/2}$ is the electromechanical coupling coefficient.

The resonance frequency of the resonator, presented in literature [7], is described by following formula:

$$f_r = \frac{c'}{2\pi}\left[\frac{\varepsilon l c^2}{2h}\, lg\,(a/c)\right]^{-1/2} \tag{2.16}$$

where c' is the light velocity and ε is the dielectric constant. The dependence of frequency f_r, on the resonator parameters, calculated from this formula, is shown in Fig. 3. The dependence was obtained on the assumption that the piezoelectric rod was in contact with the resonator pivot. The case of a gap between the rod and pivot was examined by CARR [8] and, for different resonator shapes, by FUISAVA[9]. However, the theoretical results obtained by them did not coincide with the experiments in a satisfactory manner. Furthermore, our experimental investigations showed that in some cases, particulary the case of samples with large dielectric constants, it was not possible to tune the cavity resonator up. Different unexpected effects were observed which made it imposible to tune the resonator described below indicates the reasons for these difficulties and enables us to make the resonator possess the required features.

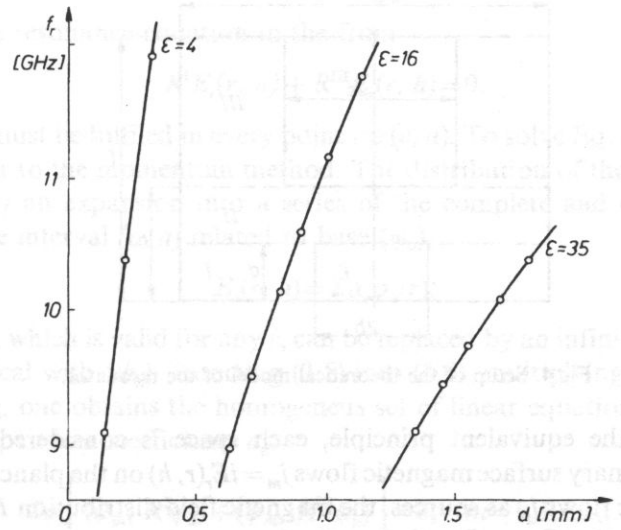

Fig.3. Resonance frequencies for the resonator with parameters 2a=11 mm, 2b=2.5 mm and l=3 mm, calculated from Eq. (16).

The Eq. (2.16) was obtained by means of the circuit methods. Namely, the resonator has been described as a set consisting of both an inductance created by the short section of the concentric line, and a capacitance between the central line and the internal surface of the resonator. The coaxial resonator described is the so-called capacitance shortened resonator [10, 11]. This resonator is made from an ordinary resonator by forming an air gap in the inner line of the resonator. In this manner, a new space with a homogeneus electric field is created and that produces the additional capacitance.

Introduction of the dielectric sample with a high value of the dielectric constant (for instance lithium niobate) to the describe by the circuit methods. Another difficulty in applying these method is due to fact that the part of the resonator in which the sample is placed, has not a strictly capacitive character, because in this space the magnetic filed energy is also accumulated. In particular the value of permeability of the sample, it is possible to obtain the resonance at the distance which corresponds to the depth of the sample immersed in the resonator in the considered space. The field distrribution in this resonator is, of course, unfavourable for the excitation of the hypersonic wave in the sample. These considerations concern the case when the resonance frequency in constant. This case corresponds to the situation in our experiment, when the magnetron generator (from radar emitter) is applied. For these reasons, it is necessary to use the methods for the description of the resonator in our configuration.

In this case the resonance state is obtained in the following manner [11, 12]:

a) The inside of the resonator is divied into space by planes (Fig. 4), in which the Helmholtz solution can be found analytically.

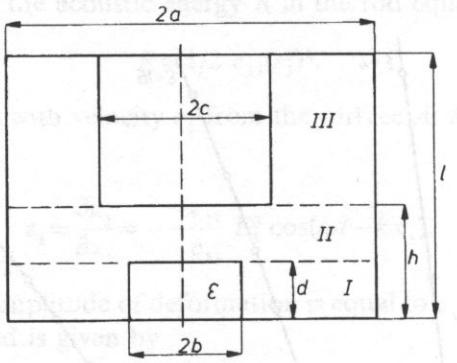

Fig.4. Setup of the theoretical model of the resonator.

b) Appyling the equivalent principle, each space is considered separately by introducing imaginary surface magnetic flows $j_m = iE_r(r, h)$ on the planes of separation.

c) Treating the flows j_m as sources, the magnetic field distribution H in the divided space is found by the Green function method.

d) Imposing the condition of continuity of the field H on the separation boundaries, the resonance condition is found in the form of the equation, which combines the resonance frequency with the material parameters of the sample and the dimensions of the resonator.

3. Model of an ideal resonator and parameters of the real one

First, according to the aformetioned procedure, one considers the particular case $h=d$, i.e. the situation when the dielectric contacts with the central line of the resonator. This case has an accurate solution.

The resonance condition has the form of a condition of continuity on the boundary $z=h$

$$H^{\mathrm{I}}(r, H)—H^{000}(r, h)=0, \tag{3.1}$$

where the magnetic fields in all spaces are expressed by the flows j_m and the proper Green functions

$$\begin{aligned} H^{\mathrm{I}}(r, z)&=i\omega\varepsilon\int G^{\mathrm{I}}(r, r', z, h)E_r(r', h)dr', \\ H^{\mathrm{III}}(r, z)&=—i\omega\varepsilon\int G^{\mathrm{III}}(r, r', z, h)E_r(r', h)dr. \end{aligned} \tag{3.2}$$

Functions G^{I} and G^{III} can be found by the methods described by FRIEDMAN [12] and JAWORSKI [13].

Introducing the symbol of integral operator

$$R_{\Psi}(r, h)=i\omega\varepsilon\int G(r, r', z, h)\Psi(r', h)dr, \tag{3.3}$$

one obtains the resonance equation in the from

$$R^{\mathrm{I}}E_r(r, h)+R^{\mathrm{III}}E_r(r, h)=0, \tag{3.4}$$

This equation must be fulfiled in every point $r\in(c, a)$. To solve Eq. (3.4), one uses the methods similar to the momentum method. The distribution of the field $E_r(r, h)$ can be expressed by an expansion into a series of the complete and orthogonal set of functions in the interval (c, a) related to base (φ_n),

$$E_r(r, h)=\Sigma a_n\varphi_n(r). \tag{3.5}$$

Next, Eq. (3.4), which is valid for any r, can be replaced by an infinite series, where φ_n is a base identical with $\{\psi_n\}$. Inserting (3.5) into (3.4), multiplying the results by ψ_n and integrating, one obtains the homogeneus set of linear equations with respect to the unknow expansion coefficients a_n:

$$\Sigma a_n\left[(\psi_m, R^{\mathrm{I}}\varphi_n)+(\psi_m, R^{\mathrm{III}}\varphi_n)\right]=0, \quad m=0,1,2,3,... \tag{3.6}$$

where $(\psi, R\varphi)$ denotes the scalar product $\int\psi R\varphi\ \mathrm{d}r$.

The set of equations (3.7) has a solution, when its characteristic determinant equals zero.

$$\det\left\{(\psi_m, R^{\mathrm{I}}\varphi_n)+\psi_m, R^{\mathrm{III}}\varphi_n\right\}=0. \tag{3.7}$$

Since both base sets, $\{\varphi_n\}$ and $\{\psi_m\}$, are infinite, the exact solution can be only obtained as a limiting case when $m, n\to\infty$. In practice, finite values $m, n\leqslant M$ are assumed but the approximate solution converges to the exact one when M is assumed to be sufficiently large. First of all, the rate of convergence to the exact solution depends on the choice the base functions φ_m and ψ_m. It will assumed below that

$$\varphi_0=\psi_0=1/ln(a/c)r, \quad n=0;$$
$$\varphi_n=\psi_n=Z_1(\alpha_n r) \,\|\, N \,\| \quad n=1,2,3..., \tag{3.8}$$

where N denotes the normalization factor, α_n are the subsequent solutions of the equation $Z_0(\alpha_n c)=0$, nad I_p and N_n denote the Bessel and Neumann functions of order p respectively. Set $\{\varphi_n\}=\{\varphi_m\}$ is complete and orthonormal with r in the interval (c, a).

It appears that function $\varphi_0=\psi_0=1/\ln(a, c)r$ reproduces quite well the distribution of the field $E_r(r, h)$ and, due to that, further calculations may be confined to the zero-order approximation of Eq. (3.7). Inserting φ_0, ψ_0 to (3.7) and integrating, one obtains the equation for the resonance frequency in the from:

$$\frac{1}{k\,\mathrm{tg}\,k(l-h)}+\frac{1}{k\,\mathrm{tg}\,(kh)}-\frac{\pi}{2h\ln(a/c)}$$
$$\sum_{n=0}^{\infty}\frac{\left[vbJ_1(ub)Z_0(vb)-\dfrac{ub}{\varepsilon}J_0(ub)Z_1(vb)Z_0(vc)\right]}{v^2\left[vbJ_1(ub)Z_0(vb)-\dfrac{ub}{\varepsilon}J_0(ub)J_1(vb)\right]}=0, \tag{3.9}$$

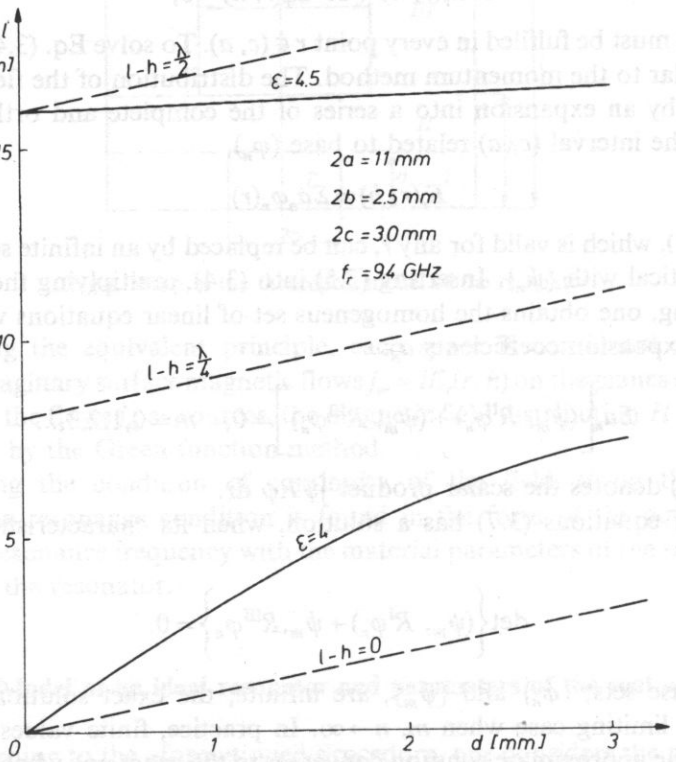

Fig.5. Dependence of the resonator length on the heigth of the piezoelectric rod from parameters 2a=11 mm, 2b=2.5 mm, 2c=3.0 mm, f=9.4 GHz.

where:

$$Z_p(vr)=N(vc)J_p(vr)-J(vc)N_p(vr), \quad p=1,2,$$

$u^2=k^2-(n\pi/h)^2$
$v=k^2-(n\pi/h)^2, \quad n=0,1,2,...,$
$k=2\pi/\lambda$

u denotes the so-called Hankel coefficient: $u=1$ 1 for $n=0$, and $u=2$, for $n=1,2,...$.

If u^2 or v^2 have negative values, then the function J_p and N_p must be replaced by the modified Bessel functions. Examples of the results of calculations for $\varepsilon_w=4$ and $\varepsilon_w=45$ are presented in Fig. 5. These calculation were carried out to determine l as a function of h for the following parameters: $a=5.5$ mm, $b=1.25$ mm, $c=1.5$ mm, $f_r=9.4$ GHz. It should be noticed that for $\varepsilon_w=45$ the lenght of the coaxial part of the resonator is $\lambda/4<1-h<\lambda/2$. This means that space l lies above the self-resonance and has an inducative character. As it has been mentioned before, this effect indicates that the space l can be replaced by a supplementary capacitance. This means that the circuit methods are useless in the description of such resonators.

Generalization of the applied method to the case of three spaces, i.e. $h>d$ (Fig. 4), is connected with considerable calculation difficulties. One of the possible methods of solution of this problem is based on the assumption of two unknown distributions of the field $E_r(r)$ on the boundaries $z=d$ and $z=h$, calculation of the field H_φ in a manner similar to that described above, and next, on the introduction of two conditions of continuity at the boundaries of the spaces. As a results, one obtains a double set of linear equations with respect to the unkown coefficients of the expansion of fields $E_r(r, d)$ and $E_r(r, h)$ into the series of phase functions. As before, vanishing of the characteristic determinant of the set of equations is the resonance conditions. Application of this method gives potentially very accurate results, but it requires the solution of a large set of equations. Confining the considerations to the zero-order approximation, we observe that the results, in the limiting case $d=h$, lead to errors larger then before. Another possibility is to treat the space I and II toghether and adjust the solutions is to the boundary $z=h$. This approch is simpler because it consist in adjusting the solutions in two, not three, spaces. However, it decreases the accuracy of the analysis.

In such a case the aproximate resonance equation has the following form:

$$1/[k\,\mathrm{tg}\,k(l-h)]+A/(k_{10}^2-k^2)+B=0. \tag{3.10}$$

At the zero approximation the coefficients A and B can be considered as constants. They can be determined from two resonance states, $d=0$ and $d=h$, calculated by means of the described method. In turn, k_{10}^2 can be calculated by an analysis of the homogeneus space $I+II$ or estimated by interpelation between the resonance frequencies of the space $I+II$, calculated $d=0$ and $d=h$. In Fig. 6 some results of calculations of k_{10} are presented, corresponnding to the linear interpolation and the case when $d<h$. The calculations were carried out for $\varepsilon_w=4$ and $\varepsilon_w=45$ to determine

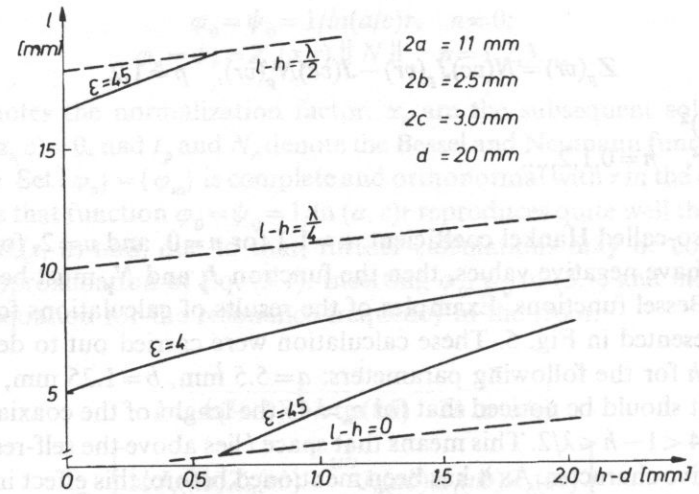

Fig.6. Dependence of the resonator length on the width of the gap.

l as a function of the width of the air gap $(h-p)$, other parameters being constant: $a=5.5$ mm, $b=1.25$ mm, $c=1.5$ mm, $d=2$ mm, $f_r=9.4$ GHz. For $\varepsilon_w=4$ one can observe the monotonic dependence of l on $(h-d)$. When the width of the gap increase, then the resultant capacitance of the space $I+II$ decreases, and so the length of the coaxial part $(l=h)$ increase. The dependence for $\varepsilon_w=45$ is more interesting when the space $I+II$ is of an inductive character for a small width of the gap and, as in the previous case, the length of coaxial part lies in the range $\lambda/4<l-h<\lambda/2$. For $h-d=0.6$ the selft-resonance of the space $I-II$ is obtained. It corresponds to the short-circuit in the plane $z=h$ i.e. $l-h=0$ or $l-h=\lambda/2$. Further increase of the gap width leads to the situation similar to the case $\varepsilon_w=4$, i.e. the space $I+II$ is of a capacitive character and the length of the coaxial part lies in the range $0<l-h<\lambda/4$.

Comparison of the results of the presented above with experimental data necessitates to account for the following facts:

- the resonator presented in Fig.2 is an idealized model of the real system, in which many simplifying assumptions have been made,
- in the nature of things, the method of calculation applied is an approximate one.

In what follows, these two factors will be discused. One of the fundamental simplifications consists in the assumption that the resonator has no hole in the place, where the dielectric sample should be put. Thus the sample is placed directly on the bottom of the resonator. This simplification resulted from numerical estimation of the lowest frequency of propagation of cylindrical modes in the dielectric sample with the largest assumed permeability $\varepsilon_w=45$.These calculations indicated that the resonance frequency was higher than the assumed 9.4 GHz, at which the resonator would be excited. Consequently, the cylindrical modes would be attenuated in the dielectric very quickly and the microwave energy would not be emitted outside the

resonator. For this reason it could be expected that the error caused by the existence of a hole in the real resonator would not have any significant influence on the value of the calculated resonance frequency. The experimental measurements have supported this assumption. Changes of the resonance frequency were unnoticeable after elimination of the hole. Influence of the hole on the quality factor of that resonator is more difficult to estimate, because the depth of the penetration depends on the sample.

The analyzed resonator is a system which is lossless and isolated from surroudings, but in the reality the system is coupled with the surroundings and energy losses occur in the walls and the dielectric material. The influence of the elements, which are coupled with the wave-guide line, is difficult to estimate. It is known, however, that this influence on the resonance frequency can be neglected when coupling with the wave-guide is sufficiently small.

The effect of radiation into surroundings from the dielectric rod, transmitted through the hole placed in the bottom of the resonator, is easier to estimate. With the assumptions that the diameter of the rod is equal to 2.5 mm and the frequency $f_r = 9.4$ GHz, this rod becomes a section of the subcritical wave-guide, fulfilled by the dielectric and excited in the TM_{01} type. For instance, the depth of penetration of the electromagnetic field energy along the rod axis is approximately equal to 0.35 mm for $\varepsilon_w = 45$. This means that the field energy, which is accumulated inside the rod below the bottom of the resonator, can be neglected, and replacement of the hole in the resonator bottom by a plane of perfect conductivity is possible for the values of d and h assumed in these considerations.

In relation to the energy losses and the corresponding finite quality factor the losses in the walls and in the coupling elements are small under typical conditions, and they can be estimated by measurements of the quality factor of the resonator without the sample. On the other hand, the energy losses in the piezoelectric sample depend on the dielectric and acoustic (attenuation) parameters and its volume. The calculations have been made under the assumption of a losseless (real) dielectric, but the calculation formulas are vaild also for a complex one. In particular, it is possible to assume that the energy lost in the dielectric depends approximately on the dimension d, the other dimensions of the resonator being fixed. As a result, the quality factor of the resonator is, approximately, inversely proportional to the height of the sample, d and a reasonable compromise is needed between the requirements of effective coupling of the electromagnetic field with the sample (large d), and the large quality factor of the system (small d)

Estimation of the quality of the investigated resonator by means of numerical methods is extremely complicated and it could not be done with a sufficient accuracy. Thus, the measurements of this factor were carried out experimentally for several samples. From these measurements it follows that this factor is not very large and is of the order of several hundred. Moreover, the quality factor depends at least on two factors, which are difficult to control. They are: uncertain contact in the inner line of

the resonator at the entrance to the resonator cavity, and the position of the coupling antenna inside the resonator. Significant differences in the quality factor measurements were observed even for small displacements of these elements. In the case when the measurements were performed in a stable range, the dependence of the quality factor and the resonance frequency upon the position of the samples and the position of the microwave short-circuit element are similar to those presented in Fig.7 and 8.

Independently of that, the calculations performed are of an approximate character.

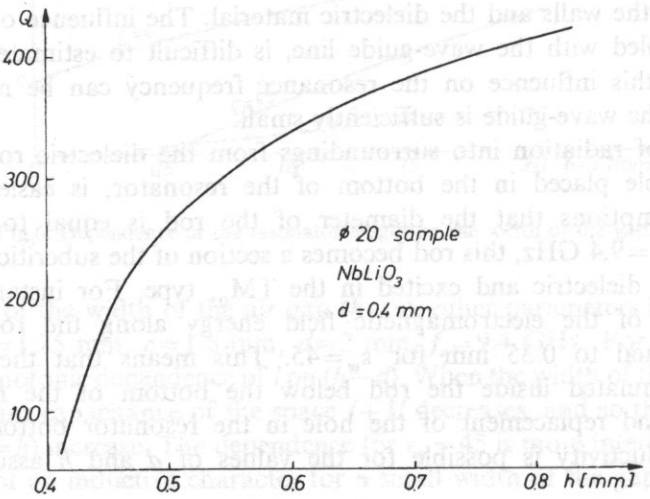

Fig.7. Dependence of the quality factor of the resonator on the inner line position.

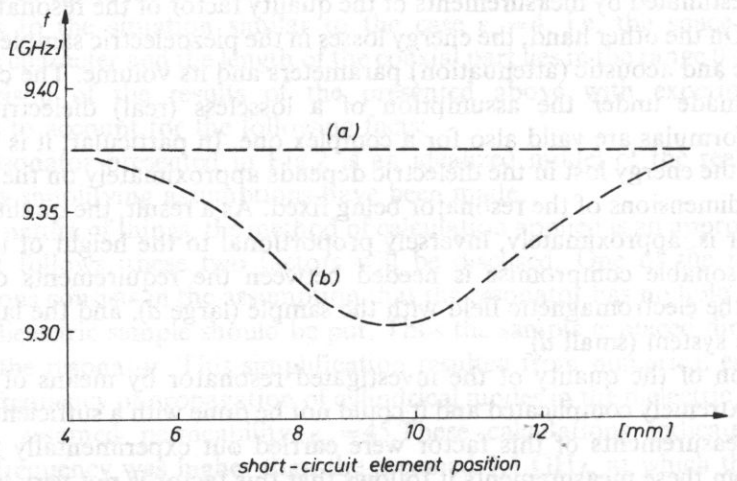

Fig.8. Dependence of the resonance frequency on the position of the microwave short-circuit element (from experiments) a) subcritical coupling b) supercritical coupling.

Typical starting data have been assumed to estimate the dimensions of the construction.

The results of calculations concerning the influence of the sample position and of the gap $h-d$ on the resonator length, are shown in Fig.9 and 10. The discontinuity of the resonator length l is of particular interest for $\varepsilon_w=40$. One can notice that only for the sample with $\varepsilon_w=3.38$ (quartz) it is posible to get the contact of the sample with the

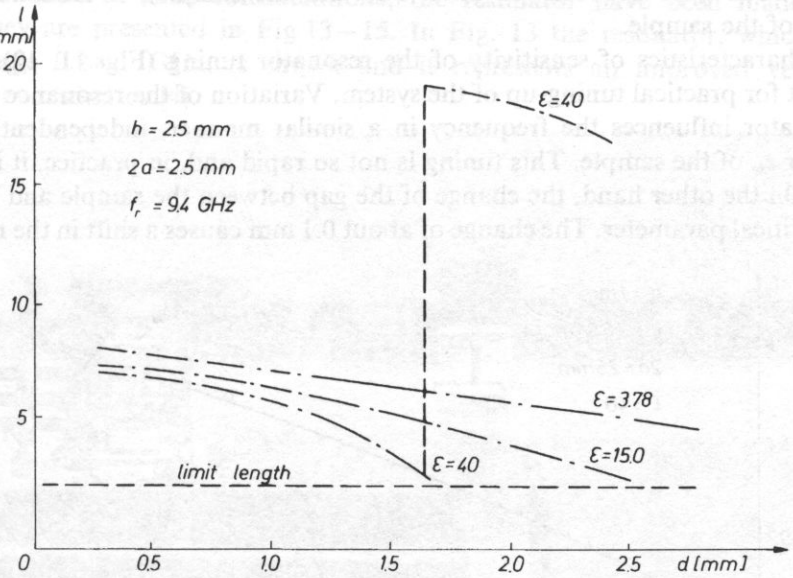

Fig.9. Dependence of the resonator length on the position of the sample.

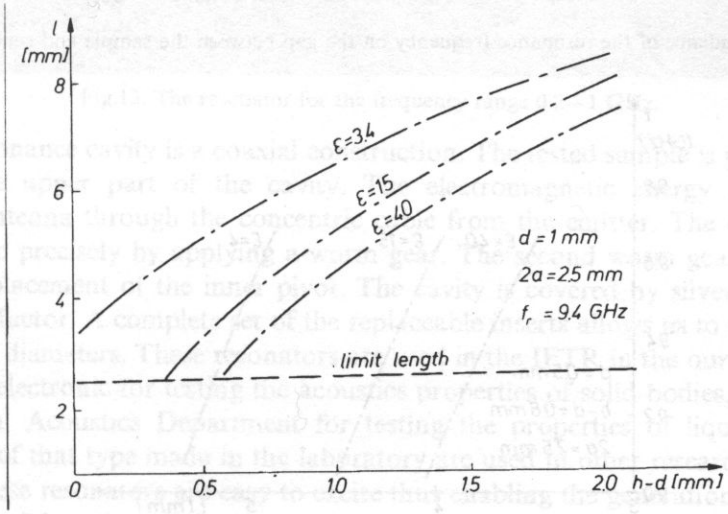

Fig.10. Dependence of the resonator length on the gap between the sample and central line.

inner line of the resonator. For $\varepsilon_w = 15$ and 40 it cannot be done in a continuous manner because of a step change of the resonance length. In both the figures dashed lines mark the actual resonator length of about 2.5 mm. This length from the existence of the exciting antenna in the real resonator. One of the ways to shif the limit, at which the step change of the resonator length occurs, towards smaller values of $h-d$ (this gives, practically, the possibility of getting the tuning continuity in the range of small gaps between the inner line and the sample), is reduction of the diameter of the sample.

The characteristics of sensitivity of the resonator tuning (Figs.11, 12) are very important for practical tuning-up of the system. Variation of the resonance length of the resonator influences the frequency in a similar manner, independently of the parameter ε_w of the sample. This tuning is not so rapid and, in practice, it is easy to control. On the other hand, the change of the gap between the sample and the inner line is a critical parameter. The change of about 0.1 mm causes a shift in the resonator

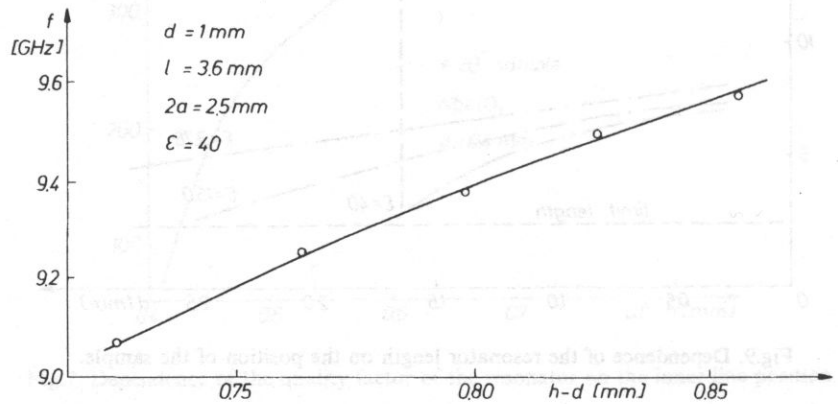

Fig.11. Dependence of the resonance frequency on the gap between the sample and central line.

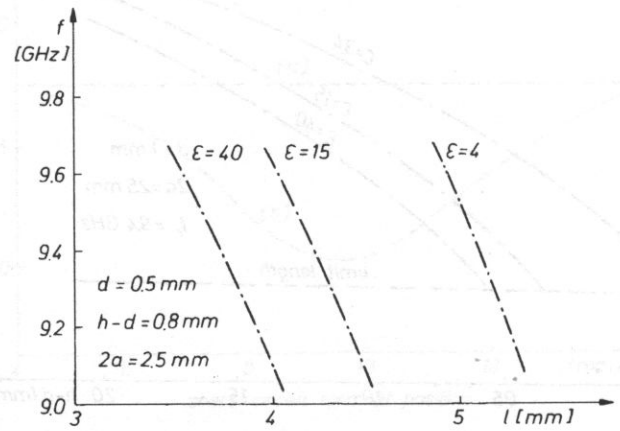

Fig.12. Dependence of the resonance frequency on the resonance length for different samples.

tuning-up frequency by about 500 MHz. For this reason, the micrometric screw was used in the resonator model to displace the inner line.

4. Results of measurements

On the basis of such considerations, the resonator have been made in the IFTR. They are presented in Fig.13–15. In Fig. 13 the resonator, which works in the range 0.2–1 GHz; is shown and it represents an improved version of the LEZHNEV resonator [4].

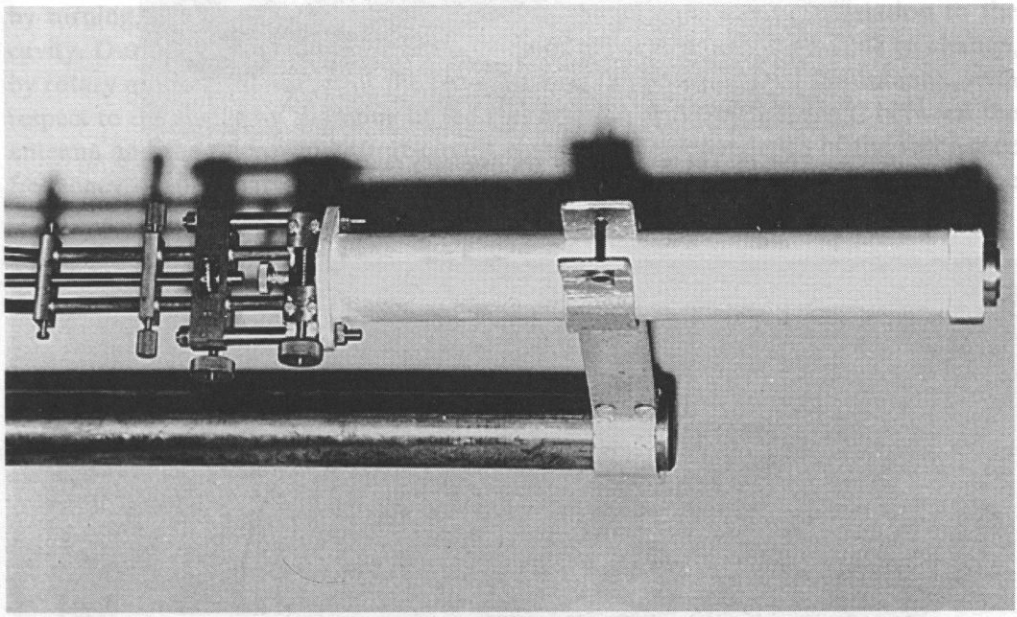

Fig.13. The resonator for the frequency range 0.2–1 GHz.

The resonance cavity is a coaxial construction. The tested sample is placed in the hole in the upper part of the cavity. The electromagnetic energy supplies the coupling antenna through the concentric cable from the emitter. The cavity could be tuned up precisely by applying a worm gear. The second worm gear is used for precise displacement of the inner pivot. The cavity is covered by silver to increase the quality factor. A complete set of the replaceable inserts allows us to test the rods of different diameters. These resonators are used in the IFTR in the our Laboratory of Acoustoelectronic for testing the acoustics properties of solid bodies, and also in the Physical Acoustics Department for testing the properties of liquids. Several resonators of that type made in the laboratory are used in other research centers in Poland. These resonators are easy to excite thus enabling the generation of acoustic waves. The „Matec" setup is especially suitable for cooperation with such resonators.

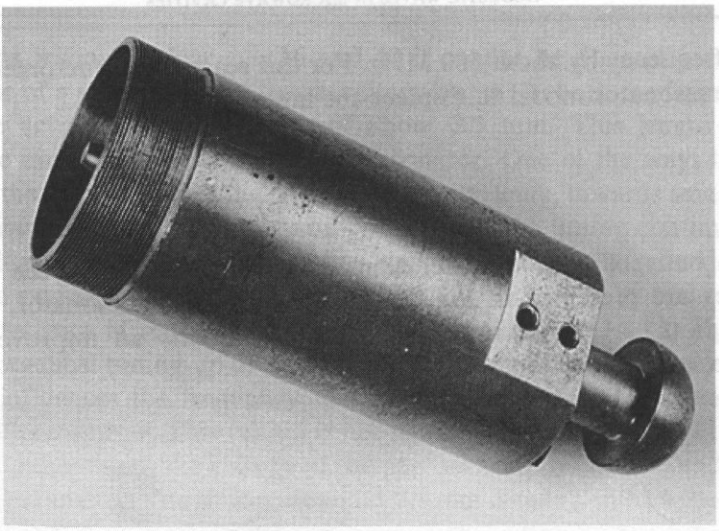

Fig.14. The resonator for the frequency range 3–4 GHz.

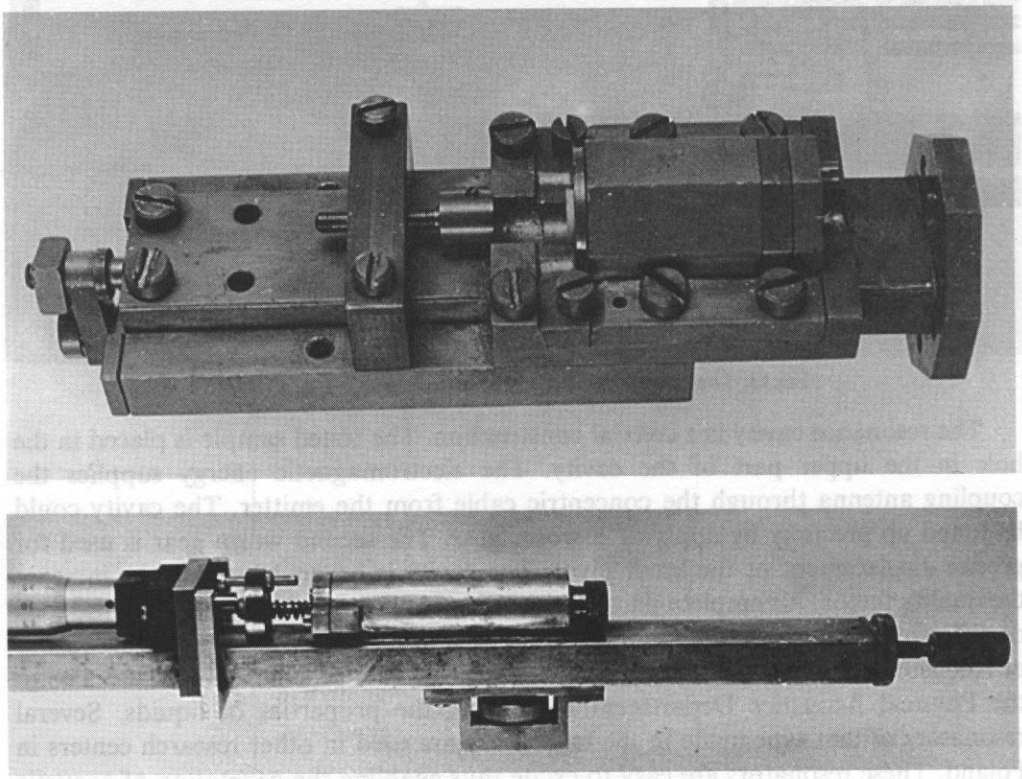

Fig.15. The resonator for the frequency range 9–11 GHz.

The resonator, presented in Fig.14, works in the 3–4 GHz frequency range. Those presented in Fig.15 were made in the IFTR for the 9–11 GHz frequency range. One of them has the displeceable diaphragm *a*, and the second one — an inner pivot which can be displaced by the micrometer screw *b*. These resonators were used in the setup made in the IFTR [14].

Construction of the cavity resonator is schematically presented in Fig.16. The resonator connected to the section of the wave-guide with the microwave short-circuit element (*3*). Copuling of the cavity with the wave-guide occurs by the antenna (*2*). The cavity is tuned by means of the pivot (*5*), attached to the diaphragm (*4*). The piezoelectric rod (*1*) is inserted into the cavity. In the course of tuning one can change, by turning, the piezoelectric rod plunge L in the antenna cavity in relation to the cavity. During the experiment, from outside of the cryostat, it is possible to change, by rotary motion, the values of the plunge L and the position D of the antenna, with respect to the cavity by changing of the rod position and the distance C between the antenna and the microwave short-circuit element. The dependence of the resonance frequency of the cavity on the parameters C, D, and L has been estabilished in the course of experiments.

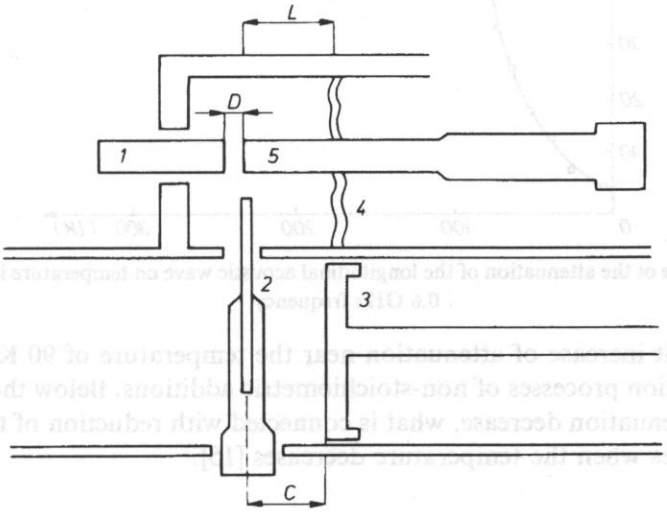

Fig.16. Construction of the reentrant type cavity. *1*-piezoelectric rod, *2*-antenna, *3*-microwave short-circuit element, *4*-diaphragm, *5*-pivot.

In Fig.17 and 18 the results of measurements of the acoustic wave attenuation in crystal, performed by means of the above described resonators, are presented. These measurements were made at cryogenic temperature. The variation of attenuation for the bismuth-germanium oxide (Bi_{19} GeO_{20}) in the 100 direction and the lithium niobate ($NbLiO_3$) crystals, are shown in Fig. 17 and 18, respectively. In the former dependence (Fig.17) one can notice two ranges of temperature, above and below 100 K. In the former one the attenuation of acoustic wave is connected with scattering of the wave on thermic phonones.

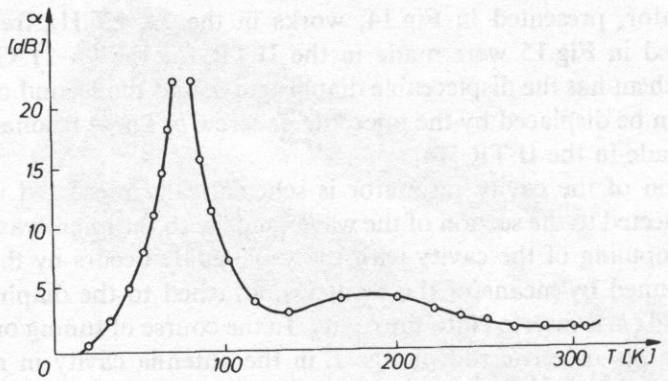

Fig.17. Dependence of the attenuation of the longitudinal acoustic wave on temperature in $Bi_{19}GeO_{20}$ crystal at 0.6 GHz frequency.

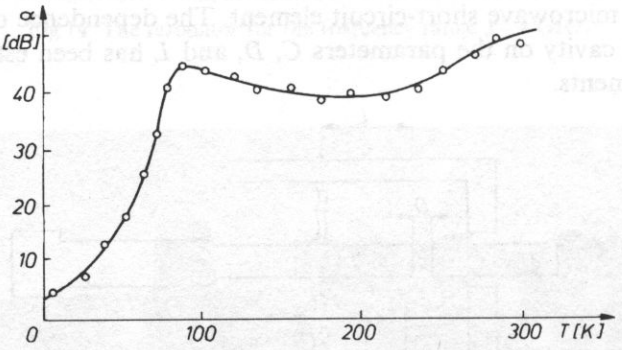

Fig.18. Dependence of the attenuation of the longitudinal acoustic wave on temperature in $NbLiO_3$ crystal 0.6 GHz frequency.

A significant increase of attenuation near the temperature of 90 K is connected with the relaxation processes of non-stoichiometric additions. Below the temperature of 50 K the attenuation decrease, what is connected with reduction of the amount of termic phonones when the temperature decreases [15].

References

[1] K.N. Barański, Kristalografia, 2, 299 (1957).
[2] H.E. Bömmel and K. Dransfeld, Phys. Rev. Lett., 1, 234 (1958).
[3] H.E. Bommel and K. Dransfled, Phys. Rev. Lett., 2, 249 (1959).
[4] N.B. Lezhnev, *Hypersonic methods of investigations in physics of liquide state*, (in Russian), IFTR PAS, Warsaw 1978.
[5] J. Ilukor and E.H. Jacobsen, Science, **153**, 1113 (1966).
[6] J. Ilukor and E.H. Jacobsen, in: Physical acoustics [Ed.] W.P. Mason 1974, vol. VI, ch. 4, p. 1910.
[7] J.W. Tucker and V.W. Rampton, *Microwave ultrasonic in solid state physics*, 1972, Ch. 3, p. 90.
[8] P.H. Carr, J. Acoust. Soc. Am., **41**, 75 (1967).

[9] K. FUISAWA, IRE Trans. MIT, **6** 10 (1958).
[10] T. MORAWSKI, W. GLOGIER and T. MODELSKI, Report of Warsaw University of Technology (in Polish) 330 (1988).
[11] A. MILEWSKI, *Methods of material testing in the range of very high frequencies* (in Polish), WKŁ Warsaw 1983.
[12] B. FREIDMAN, *Principles and techniques of applied mathematics*, New York 1956.
[13] A. JAWORSKI, IEEE Trans. MTT, **26**, 256 (1978).
[14] M. ALEKSIEJUK, Scientific Instrument 1990.
[15] M. ALEKSIEJUK and I. MALECKI, *Electronic and acoustic methods of material testing*, (in Polish), Warsaw 1984. p. 581.

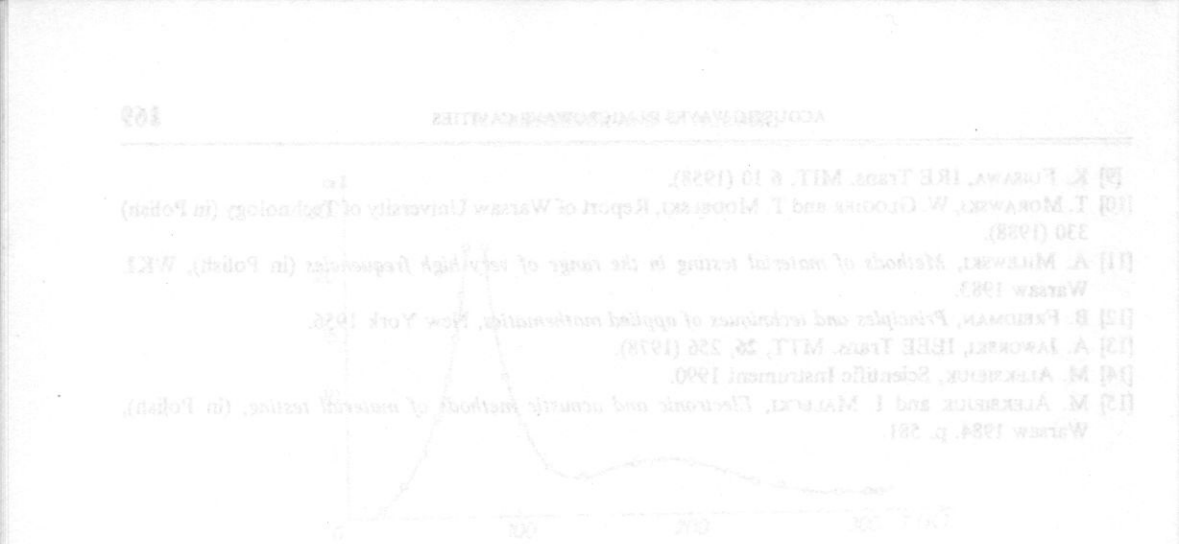

ARCHIVES OF ACOUSTICS
20, 2, 171–175(1995)

ON SPURIOUS BULK WAVE EXCITATION IN SAW GRATING REFLECTORS ON GaAs (001) (110)

E. DANICKI* and W. D. HUNT**

*Institute of Fundamental Technological Research
Polish Academy of Sciences
(00–049 Warszawa, Świętokrzyska 21)
**Georgia Institute of Technology
Atlanta, Georgia, USA

Reflection of SAW from groove gratings on cubic crystal is analyzed numerically on the basis of perturbation theory. It is shown that for certain angles of incidence, the conversion of SAW into bulk waves vanishes. This reduces the SAW reflection loss from grating.

1. Introduction

As known, GaAs is a piezoelectric cubic crystal that posesses also interesting semiconducting properties. This makes possible to place both surface (SAW) devices like SAW resonators, filters and delay lines, and electronic circuitry to drive them (switches, amplifiers and other active elements) on the same chip.

In some applications, for example in filter banks, it is necesary to reflect SAW in perpendicular direction. It happens however, that the reflection losses are high for SAW propagating along (110) direction on (001) cut GaAs, which orientation is prefered in applications. This is because of part conversion of SAW into bulk waves that takes place in such oriented cubic crystal with grooves in it. In this particular direction of SAW propagation, and in its vicinity (and in direction 90^0 degrees from these, due to the crystal symmetry), SAW wave-number is lower than cut-off wave-number of shear wave polarized horizontally. Thus any surface perturbation that results in horizontal surface traction matched to these bulk waves will excite them in expense of the SAW power, thus resulting in the reflection loss.

The idea is to find such reflection angle, that is to determine the groove grating orientation on the crystal, that minimizes the induced surface horizontal traction. In fact this is required for all groove gratings necessary to make SAW circulating on the crystal as discussed above, however with the reflection angles not necessarily being right angles.

This is analyzed in next section, where we propose appyling three subsequent Bragg reflections, as depiced in Fig.1 presenting the SAW propagation path on the

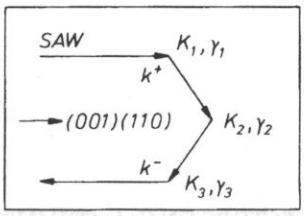

Fig.1. SAW path in the set of three grating reflectors with different grating periods and orientations on the crystal.

crystal. The symetric pattern includes one parameter, angles of the first and the last reflection θ that will be optimized with respect to bulk wave excitation. The Bragg reflective gratings will be characterized by their wave-numbers $K_1 = K_3$ and K_2, and relative reflection coefficients from strip $\gamma_1 = \gamma_3$ and γ_2.

2. Theory of groove-grating reflector

Below, the perturbation theory is applied presented in [1,2]. In the theory, we replace groove grating by sinusoidal corrugation including the lowest Fourier components of the surface profile, that is ($\mathbf{x} = (x_1, x_2)$, $z = x_3$)

$$z = z_S = h \exp(-j\mathbf{K}\mathbf{x}) + cc., \quad K = 2\pi/\Lambda.$$

If grooves width is halft their period Λ, and they are H deep, $h = H/\pi$.

The wave-field on the medium plane $z = 0$ is expanded into

$$[\mathbf{u}, \mathbf{T}]^T(\mathbf{x}) = [u_i^+, T_{3j}^+]^T \exp(-j\mathbf{k}^+\mathbf{x}) + [u_i^-, T_{3j}^-]^T \exp(-j\mathbf{k}^-\mathbf{x}),$$

where time-dependence $\exp(j\omega t)$ has been dropped, and

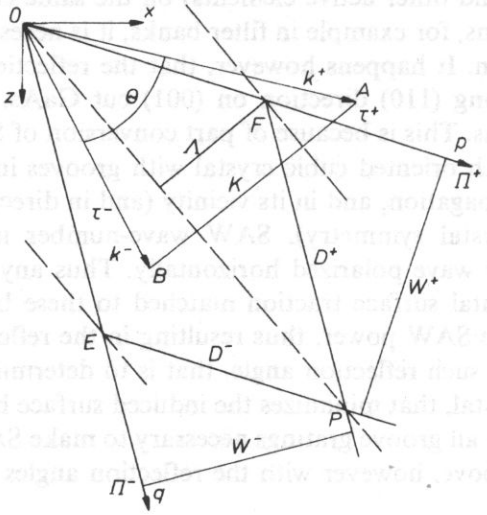

Fig.2. Geometrical relationships between SAW and grating wave vectors, Poynting vectors and SAW beam-widths.

$$\mathbf{k}^+ + \mathbf{k}^- = \mathbf{K} \tag{2.1}$$

is the Bragg condition. Other wave-files components are neglected [1]. The discussed wave-components are shown in Fig. 2, where the beam-steering effects is accounted for (angles $\tau^{\pm}$ between wave-vectors $\mathbf{k}^{\pm}$ and corresponding Poynting vectors $\Pi^{\pm}$); $W^{\pm}$ are the SAW beam-widths.

The theory results in following relations for a tracting arrising on the medium crystal surface when SAW propagates under periodic shallow grooves ($n, m=1, 2$)

$$T_{3n} = -\rho\omega^2(z_S u_n) - (z_S T_{nm})_{,m}, \; T_{33} = -\rho\omega^2 z_S u_3.$$

Expilicitly, for grooved grating reflectors we get

$$\begin{aligned} T^-_{3n} &= -\rho\omega^2 h u^+_n - h(-jk^-_{nm})T^+_{nm}, \\ T^+_{3n} &= -\rho\omega^2 h^* u^-_n - h^*(-jk^+_m)T^-_{nm}, \\ T^-_{33} &= -\rho\omega^2 h u^+_3, \; T^+_{33} = -\rho\omega^2 h^* u^-_3, \end{aligned} \tag{2.2}$$

where ρ is the mass density of the substrate and h characterizes the perturbation introduced by shallow grooves into the system. In the above relations, the left-hand sides represents the response of the grating which is the first-order quantity with respect to h, to the incident wave-field characterized by $\mathbf{u}$ and $\mathbf{T}$ appearing in the right-hand sides (the zero-order quantities, $\mathbf{T}$ can be evaluated as depedent on $\mathbf{u}$ [3]). The perturbation traction is responsible for synchronous generation of SAW in the new direction satisfying the Bragg condition, Eq. (2.1), that is for reflection. As shown in [1], the reflection coefficient can be evaluated with help of reciprocity relationship [4].

3. Bragg reflection at arbitrary angle

Let us consider the case of incident wave having wave-number $\mathbf{k}_1$ (Fig.3), its wave-field includes all particle displacement components, u^-_i on the substrate surface. Let the Bragg reflection structure is chosen with such a wave-vector $\mathbf{K}_1$, that the

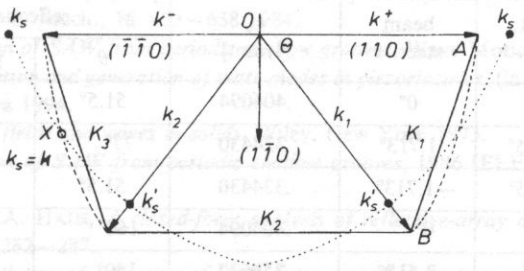

Fig.3. Wave-vectors of SAWs involved in subsequent reflections from gratings, and their relation to cut-off wave-numbers od bulk waves.

reflected SAW wave-number $\mathbf{k}^+=(k,\ 0)$. Thus the reflected SAW propagates in $x_1=(110)$ direction, and its surface wave-motion includes u_3^+ and u_1^+ [4].

One easily notices from Eqs. (2.2) that the traction T_{3i}^+ resulting from the incident SAW includes all three components, which will eventually excite SAW in $\mathbf{k}^+$ direction. But the traction T_{32}^+ is not involved in this SAW excitation because there is not u_2^+ component in the wave-motion of this wave.

The stress T_{32}^+ however, will excite a bulk wave, which cut-off wave vector is higher than k^+. There indeed is the horizontally polarized shear bulk wave with wave-motion u_2 on the crystal surface, which is in synchronism with the traction T_{32}^+. As known [5], the power delivered to this wave by the traction is $\frac{1}{2}\,\mathrm{Re}\{(j\omega u_2)^* T_{32}\}$, the lack of which power in the reflected SAW amounts to the SAW reflection loss.

Numerical evaluation of T_{32}^+ for different incident wave propagation direction θ (Fig.3) shows, that there are two cases where $T_{32}^+=0$: for $\theta\simeq 51.5^0$, and for $\theta\simeq 160^0$, thus there are not bulk wave excitation when SAW is reflected from grooves. The second case however ($\theta\simeq 160^0$), is not convenient for applications because the SAW wave-vector is close to bulk-wave cut-off wave-vector (the point marked by X in Fig.3), and slight missorientation of the substrate can disturb the reflector performance.

4. Properties of a set of Bragg reflectors

To obtain the SAW propagation path shown in Fig.1, another reflections are necessary, involving the grating wave-vector $\mathbf{K}_n$ shown in Fig.3. The reflections $\mathbf{k}^+ \Leftrightarrow \mathbf{k}_1$, and an analogous $\mathbf{k}^- \Leftrightarrow \mathbf{k}_2$ have been discussed above that helped us to evaluate θ.

What concern the reflection $\mathbf{k}_1 \Leftrightarrow \mathbf{k}_2$ involving the grating with wave-vector $\mathbf{K}_2$, this is an ordinary SAW reflection, in which case the corresponding bulk-wave cut-off wave-number k_s' is smaller than the Rayleigh wave-number, and the grating does not excite bulk waves.

In Table 1, one can find parameters describing all three grating reflectors and corresponding SAWs involved in Bragg reflections (the last rows concern the case of

Table 1. Characterization of SAWs and gratings involved in reflection shown in Fig. 3, and resulting relative reflection coeffcients from strips.

k[1/mm]	orient. (110)+	beam steer. τ	k_s [1/mm]	reflection parameters		
				θ	γ [H/Λ]	Λ [mm]
$k^+=.349407$	0°	0°	.404094	51.5°	4.21	20.161
$k_1=.367020$	51.5°	1.713°	.324430	77°	1.19	13.750
$k_2=.367020$	128.5°	−1.713°	.324430	51.5°	4.21	20.161
$k^-=.349707$	180°	0°	.404094	160°	.55	8.953
$k_2'=.363252$	20°	8.513°	.356637	140°	.51	9.204
$k_1'=.363252$	160°	−8.513°	.356637	$\omega=10^6 s^{-1}$		

$\theta \simeq 160^0$). Note that some SAWs are subjected to beam steering. Each grating reflector should have shape of parallelogram *OFPE* shown in Fig.2, with grooves in direction *OP* and period Λ, Because of different velocities of incident and reflected SAWs, the incident and the reflected SAW beam-widths ($W^{\pm}$) are generally different.

The SAW reflection per strip evaluated by interpretation of SAW decaying coefficient κ on the path $D^{\pm}$ along the propagation direction between subsequent grooves, the decaying taking place doe to the reflection from grooves [1, 2]. The relative reflection coefficient γ (relative to H/Λ, here we consider case of groove width $\Lambda/2$), is evaluated as square-root of the ratio of the reflected SAW transmitted through aperture width W^-, to the input SAW power flowing through W^+.

5. Conclusion

Let us stress that we applied perturbation theory that neglects higher field harmonics induced in the gratings. This can bring certain discrepancies in evalution of optimal θ. Experimental investigations are recommended to get its correct value, and lowest SAW reflection loss possible in the proposed tripple grating reflector structure.

It should also be noted that the reflected SAW is no langer plane SAW, even if the incident SAW is plane [6, 7], and the subsequently reflected SAWs will also be nonplanar. In conclusion, we must not attempt to obtain full reflection to avoid seriously nonplaner SAW at the output of the set of reflectors discussed above. That is, some reflection losses are not avoidable, depending on admitted loss of uniformity of the SAW beam, SAW diffraction etc.

Acknowledgments

This work was partly supported by KBN under Grant 3 1212 9101.

References

[1] E. Danicki, *Perturbation theory of surface acoustic wave reflection from a periodic grating with arbitrary angle of incidence*, Arch. Mech., **36**, 623–638 1984.

[2] E. Danicki, *Reflection of SAW from periodic shallow grooves*, Wave Motion, **9**, 445–453 (1987).

[3] D. Bogucki, *Propagation and generation of plate modes in piezoelectrics*, (in Polish) dissertation Ph.D. IFTR-PAS, Warszawa 1994.

[4] B.A. Auld, *Acoustic fields and waves in solids*, Wiley, New York 1973.

[5] E. Danicki, *Reflection of SAW from periodic shallow grooves*, 1986 IEEE Ultras. Symp. Proc., pp. 205–208.

[6] P.V. Wright and H.A. Haus, *A closed-form analysis of reflective-array devices*, 1980 IEEE Symp. Ultras. Symp. Proc., 282–287.

[7] E. Danicki, *General theory of reflection of SAW from periodic metal strips*, Proc. Gdańsk School on Acoustooptics, 380–389, 1983.

ARCHIVES OF ACOUSTICS
20, 2, 177–189(1995)

GENERATION OF ELASTIC WAVES IN A PIEZOELECTRIC PLATE BY INTERDIGITAL TRANSDUCERS

D. BOGUCKI and E. DANICKI

Institute of Fundamental Technological Research
Polish Academy of Sciences
(00–049 Warszawa, Świętokrzyska 21)

Piezoelectric plate with periodic metal strips on both sides is considered. Propagation and Bragg scattering of plate modes and associated made conversion are analyzed. Excitation of acoustic plate modes by interdigital transducers is investigated and results are compared with experimental data.

1. Introduction

Excitation of surface acoustic waves (SAWs) in the piezoelectric halfspace by interdigital transducers (IDTs) was analysed in details in numerous papers [1–4]. In recent years, there is growing interest in applying of acoustic plate modes (APMs) instead of SAW in piezoelectric sensor and filters [5–8]. Theory of APM generation by IDT can be considered more difficult than that of Rayleigh waves [9]. It is caused mainly by

- multimodal propagation of APM, a number of different modes can propagate at the same frequency with different velocities,
- Bragg reflection of APM from transducers fingers can be accompanied with modes conversion,
- generation of APMs by a pair of IDts deposited on both surfaces of piezoelectric plate is unique problem for plates.

In this paper, a theory of generation of APM by such pair of IDTs is devoloped, using Bløtekjaer's method of analysis of waves propagating in the periodic system of metal strips [10].

In next section, we analyze electric properties of piezoelectric plate, with electric charge applied to its both surfaces. The immitance relation is derived which is the planar Green's function for piezelectric plate in spectral domain [9, 12]. The relation is a generalization of effective surafce permittivity, introduced in [12], to the case of piezoelectric plate.

In the following section, propagation of APM in the piezoelectric plate with electrodes deposited on both sides of plate is analyzed. Dispersion relations for most important cases, open and short-circuited strips on both sides of plate are discussed. Numerical results are presented for plates made of some known piezoelectric materials (quartz and $LiNbO_3$)

In Section 3, a theory of APM excitation by IDTs deposited on both sides of plate is presented. The corresponding inhomogenous problem is solved using method proposed in [2, 3, 10]. Numerical results are compared with experimental data presented in [13].

2. Immitance relations

Let us consider an infinite piezoelectric plate bounded by planes $x_2 = \pm d/2$ (Fig.1) and made of material characterized by mass density ρ and material constants ε_{ij}, e_{qij}, c_{ijpq}. Vacuum (ε_0) is outside the plate. We consider harmonic waves propagating along x_3, that is $\exp(j\omega t - jkx_3)$, where k is wavenumber and ω is angular frequency.

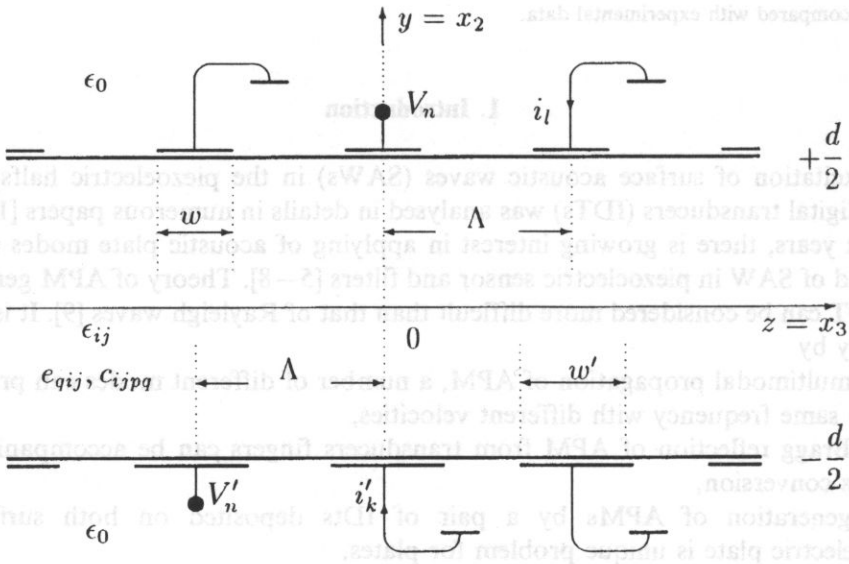

Fig. 1. Piezoelectric plate covered by periodic metal strips.

In the piezoelectric material, the coupled acoustic wave equations are

$$-\rho\omega^2 u_i = c_{ijpq} u_{p,jq} + e_{qij}\varphi_{,ji}$$
$$0 = e_{jpq} u_{p,jq} - \varepsilon_{jq}\varphi_{,jq}, \tag{2.1}$$

where u_n is particle displacement component and φ is electric potential, both inside the plate. Electric potential outside the plate (in vacuum, $D_i'' = -\varepsilon_0 \varphi_{,i}''$) satisfy Laplace equation

$$D_{i,i}''=0. \tag{2.2}$$

Certain electric and mechanical conditions must be satisfied on both surfaces

$$T_{2i}=0 \quad at \quad x_2=\pm d/2, \tag{2.3}$$

and

$$\varphi=\varphi'', \quad D_2-D_2''=\Delta D_\perp, \text{ at } x_2=d/2, \tag{2.4}$$

$$\varphi=\varphi'', \quad D_2-D_2''=\Delta D_\perp', \text{ at } x_2=-d/2,$$

where $\Delta D_\perp$ and $\Delta D_\perp'$ are electric charges induced on uper and bottom surfaces of the plate, respectivelly. Solving the corresponding boundary problem in the way presented in {14], we obtain a set of immitance relations for piezoelectric plate. This set is a generalization to effective electric surface permittivity introduced in [12] that involves that electric charges, and electric fields at both sides of the plate $E_\parallel = jk\varphi(x_2=d/2)$, and $E_\parallel' = jk\varphi(x_2=-d/2)$

$$E_\parallel = jS_k X \Delta D_\perp + jS_k X' \Delta D_\perp' \text{ (for } x_2=d/2),$$

$$E_\parallel' = -jS_k X' \Delta D_\perp - jS_k X \Delta D_\perp' \text{ (for } x_2=-d/2), \tag{2.5}$$

where X and X' are functions of k, and

$$S_k=\begin{cases} 1 \text{ for } k\geqslant 0, \\ -1 \text{ for } k<0. \end{cases} \tag{2.6}$$

In the above equations, we accounted for the symmetry relations {14, 15] (rotation of a plate by 180° does not change its equations, but note that $\Delta D_\perp$ and $\Delta D_\perp'$ include vector components differently oriented with respect to the plate). Generally, the matrix elements of immitance relations (2.5) which can also be considered as a surface Green's matrix function in spectral domain k, can be evaluated only numerically. The matrix elements are singular at k being the wave numbers of plate modes.

An asymptotic behaviour of $X(|k|)$ and $X'(|k)$ for $|k| \to \infty$ are following

$$X \to X_\infty, \; X' \to 0, \tag{2.7}$$

which shows that the system of Eqs. (2.5) separates at large $|k|$. This is because of fast decaying of the wave-field in depth of the plate if the applied electric charge to the plate has large $|k|$.

3. A plate covered by periodic electrodes

3.1. Eigenvalue boundary problem

We consider infinite piezoelectric plate of thickness d. The plate surfaces are covered by periodic systems of weightless, ideally conducting metal strips (Fig. 1) which period Λ is the same on both plate sides but the electrode widths can be different, w and w' at $x_2=y=d/2$ and $-d/2$, correspondingly (in what follows, all quantities at $y=-d/2$ will be marked by 'prime'). The considered problem is 2-dimensional, waves in the system are assumed propagating in $z=x_3$ direction perpendicular to strips.

There are mixed electric boundary conditions on both surfaces

$$\begin{aligned} &E_{\parallel}=0, \quad E'_{\parallel}=0, \quad \text{on electrodes,} \\ &\Delta D_{\perp}=0, \quad \Delta D'_{\perp}=0, \quad \text{between electodes,} \end{aligned} \tag{3.1}$$

where $E_{\parallel}$ and $\Delta D_{\perp}$ are defined as in previous Section.

Accordingly to the Floquet theorem [17], a solution to the eigenvalue boundary problem stated by Eqs. (2.5), (3.1) is searched in form ($K=2\pi/\Lambda$ is the wave-number of periodic strips)

$$\begin{aligned} E_{\parallel} &= \sum_{n=-\infty}^{\infty} E_n e^{-j(s+nK)z}, \\ \Delta D_{\perp} &= \sum_{n=-\infty}^{\infty} D_n e^{-j(s+nK)z}, \end{aligned} \tag{3.2}$$

at the upper plate surface, and similarly at the bottom surface, where $E_{\parallel}$, E_n and $\Delta D_{\perp}$, D_n should be replaced by corresponding 'primed' quantities. The time dependence $\exp(j\omega t)$ is dropped thoughout the paper. There is certain ambiguity concerning spectral parameter s, in what follows we will assume its value in the domain $(0,K)$.

Taking into account Eqs. (2.5) we obtain following relations for amplitudes of Bloch waves included in the above solution

$$\begin{aligned} E_n &= jS_nX_nD_n + jS_nX'_nD'_n, \\ E'_n &= -jS_nX'_nD_n + jS_nX_nD'_n, \end{aligned} \tag{3.3}$$

where $X_n=X(s+nK)$, and $X'_n=X'(s+nK)$, similarly $S_n=S_{s+nK}$.

Asymptotic properties of X and X' (Eqs. (7)) allow us to find such integer numbers N_1 i N_2, that Eqs. (3.3) become separated if $n\notin[N_1,N_2]$

$$E_n=jS_nX_{\infty}D_n, \quad E'_n=-jS_nX_{\infty}D'_n. \tag{3.4}$$

This will be exploited below in expanding the Bloch amplitudes into another series which, according to the method presented in [10], make the solution (3.2) to satisfy the boundary conditions (3.1). The expansion is following

$$E_n = \sum_{m=M_1}^{M_2} \alpha_m S_{n-m} P_{n-m}(\cos\Delta),$$
$$D_n = \sum_{m=M_1}^{M_2} \beta_m P_{n-m}(\cos\Delta), \tag{3.5}$$

and similarly for 'primed' amplitudes in which relations α' and b' substitute α and β, and $\Delta' = \pi\omega'/\Lambda$ substitutes $\Delta = \pi\omega/\Lambda$ in corresponding arguments of Legendre polynomials P_k. Taking into account Eqs. (3.4), we obtain that

$$\alpha_m = jX_\infty \beta_m, \quad \alpha'_m = -jX_\infty \beta'_m. \tag{3.6}$$

Following the method [10], we apply sufficiently large summation limits in expansions (3.5), $M_1 = M_3 = N_1$, and $M_2 = M_4 = N_2 + 1$. The solution given in Eqs. (3.2), (3.5) satisfies the boundary conditions (3.1) and Eqs. (3.3), but only at $n \notin [N_1, N_2]$ so that we must still consider Eqs. (3.3) which are explicitly

$$\alpha_m(S_{n-m} - S_n Z_n) P_{n-m}(\cos\Delta) - \alpha'_m S_n Z'_n P_{n-m}(\cos\Delta') = 0,$$
$$-\alpha_m S_n Z'_n P_{n-m}(\cos\Delta) + \alpha'_m(S_{n-m} - S_n Z_n) P_{n-m}(\cos\Delta') = 0, \tag{3.7}$$

at $n \in [N_1, N_2]$, in order to satisfy Eqs. (3.3) for any $n \in (-\infty, \infty)$. The above set of equations, where $Z_n = X_n/X_\infty$ and $Z'_n = X'_n/X_\infty$ including $2N$ linear equations for $2N+2$ unknowns α_m, α'_m, $N = N_2 - N_1 + 1$, can be solved for any given α_0 and α'_0

$$\alpha_m = a_m \alpha_0 + b_m \alpha'_0, \quad \alpha'_m = a'_m \alpha_0 + b'_m \alpha'_0, \tag{3.8}$$

where $a_0 = 1$, $b_0 = 0$ and $a'_0 = 0$, $b'_0 = 1$. The efficients a_m, b_m, a'_m, b'_m are evaluated numerically from Eq. (3.7).

Integrating electric field $E_\parallel$ and $E'_\parallel$, represented by Eqs. (3.2), (3.5), over the domain between strips, we obtain relations for electric potential of electrodes on the upper ($\hat{V}(s)$), and bottom ($\hat{V}'(s)$) sides of the plate at $z = 0$

$$\hat{V}(s) = \frac{-j\pi}{K \sin\pi s/K}(\alpha_0 A_{11} + \alpha'_0 A_{12}),$$
$$\hat{V}'(s) = \frac{-j\pi}{K \sin\pi s/K}(\alpha_0 A_{21} + \alpha'_0 A_{22}). \tag{3.9}$$

Analogously, integrating electric charge over strips placed on the plate surfaces at $z = 0$, we obtain currents flowing to strips on upper ($\hat{I}(s)$) and bottom ($\hat{I}'(s)$) sides

$$\hat{I}(s)=2\pi\frac{\omega}{KX_\infty}(\alpha_0 B_{11}+\alpha_0' B_{12}),$$
$$\hat{I}'(s)=-2\pi\frac{\omega}{KX_\infty}(\alpha_0 B_{21}+\alpha_0' B_{22}), \tag{3.10}$$

where A_{ij} and B_{ij} are defined as follows ($v=s/K$, summation sumbols over m dropped to shorten notations)

$$\begin{aligned}
A_{11}&=(-1)^m a_m P_{m+v-1}(-\cos\Delta), & B_{11}&=a_m P_{m+v-1}(\cos\Delta),\\
A_{12}&=(-1)^m b_m P_{m+v-1}(-\cos\Delta), & B_{12}&=b_m P_{m+v-1}(\cos\Delta),\\
A_{21}&=(-1)^m a_m' P_{m+v-1}(-\cos\Delta'), & B_{21}&=a_m' P_{m+v-1}(\cos\Delta'),\\
A_{22}&=(-1)^m b_m' P_{m+v-1}(-\cos\Delta'), & B_{22}&=b_m' P_{m+v-1}(\cos\Delta'),
\end{aligned} \tag{3.11}$$

3.2. Dispersion relations

Equations (3.9), (3.10) are sufficient for analysis of propagation of APM in piezoelectric plate covered by strips on both sides. Generally, there are four possibilities

- all electrodes connected to ground, $\hat{V}=0$ and $\hat{V}'=0$,
- open electrodes on both surfaces, $\hat{I}=0$ and $\hat{I}'=0$,
- short-circuited strips on one side, and open strips on the other side of the plate, $\hat{V}=0$ and $\hat{I}'=0$,
- and vice-versa, $\hat{I}=0$ and $\hat{V}'=0$.

Corresponding dispersive relations resulting from Eqs. (3.9), (3.10) are

$$\begin{aligned}
A_{11}A_{22}-A_{12}A_{21}&=0,\\
B_{11}B_{22}-B_{12}B_{21}&=0,\\
B_{11}A_{22}-B_{12}A_{21}&=0,\\
A_{11}B_{22}-A_{12}B_{21}&=0,
\end{aligned} \tag{3.12}$$

which should be solved for s at given ω. Generally, it can be done only numerically. The most interesting feature of the solution for s is the existence, at certain frequency domain called a stopband, of complex s. The imaginary value of s makes the wave-field decaying along its propagation path. The reason of this decaying, which is generally faster for stronger piezoelectrics, is the Bragg reflection of APMs from strips which bring periodic electric perturbation into the elastic waveguide. Similar phenomenon, but caused by mechanical perturbation of plate by shallow grooves, was discussed in [16], for instance.

4. Excitation of APM by a pair of IDTs

4.1. Imhomogeneous problem for metal strips

In Eqs. (3.9) and (3.10), there are two arbitrary constants, α_0 and α'_0 which are, in fact, functions of spectral variable s. Evaluation of these functions is the subject of inhomogeneous problem considered below.

In the considered inhomogeneous problem (Fig. 1), two electrodes, one on upper and the second on the bottom side of plate, have given voltages V_n and V'_m correspondingly, and the others are grounded. We will evaluate the transadmittance relations for strips,

$$\begin{aligned} i_l &= y^u_{lm} V_m + v^u_{lm} V'_m, \\ i'_l &= v^b_{lm} V_m + y^b_{lm} V'_m, \end{aligned} \tag{4.1}$$

which describe signal transmission between strips by both means of electric interaction [11], and APMs. The evaluation of transadmittance will be carried out on the way similar to that applied in [2–4] for Rayleigh waves.

The given strip voltages V_n and V'_m are following inverse Fourier transforms defined for discrete functions over periodic strips

$$V_n = \frac{1}{K}\int_0^K \hat{V}(s) e^{-jns\Lambda}\, ds, \quad V'_m = \frac{1}{K}\int_0^K \hat{V}'(s) e^{-jms\Lambda}\, ds, \tag{4.2}$$

where $\hat{V}(s)$ and $\hat{V}'(s)$ are as given in Eqs. (3.9). To satisfy the above relations, we must apply that

$$\begin{aligned} V_n e^{jsn\Lambda} &= \frac{-j\pi}{K \sin \pi s/K} (\alpha_0(s) A_{11} + \alpha'_0(s) A_{12}), \\ V'_m e^{jsm\Lambda} &= \frac{-j\pi}{K \sin \pi s/K} (\alpha_0(s) A_{21} + \alpha'_0(s) A_{22}), \end{aligned} \tag{4.3}$$

which can be solved for unknown $\alpha_0(s)$ and $\alpha'_0(s)$

$$\begin{aligned} \alpha_0(s) &= j\frac{K}{\pi} \sin \pi v \frac{V_m A_{22} - V'_m A_{12}}{A_{11}A_{22} - A_{12}A_{21}} e^{jsm\Lambda}, \\ \alpha'_0(s) &= j\frac{K}{\pi} \sin \pi v \frac{V'_m A_{11} - V_m A_{21}}{A_{11}A_{22} - A_{12}A_{21}} e^{jsm\Lambda}. \end{aligned} \tag{4.4}$$

The currents I flowing to upper electrodes, and I' flowing to bottom ones can be evaluated by applying similar inverse Fourier transforms to Eqs. (3.10)

$$I_l=\frac{1}{K}\int_0^K \hat{I}(s)e^{-jlsA}\,ds, \quad I'_l=\frac{1}{K}\int_0^K \hat{I}'(s)e^{-jlsA}\,ds, \tag{4.5}$$

which, applying solutions (4.4) yield ($v_{lm}=v^u_{lm}=-v^b_{lm}$ on the principle of virtual works)

$$y^u_{lm}=\frac{j2\omega}{KX_\infty}\int_0^K \frac{B_{11}A_{22}-B_{12}A_{12}}{A_{11}A_{22}-A_{12}A_{21}}\sin\pi\nu e^{-js(l-m)A}\,ds,$$

$$v_{lm}=\frac{j2\omega}{KX_\infty}\int_0^K \frac{B_{12}A_{11}-B_{11}A_{12}}{A_{11}A_{22}-A_{12}A_{21}}\sin\pi\nu e^{-js(l-m)A}\,ds= \tag{4.6}$$

$$\frac{j2\omega}{KX_\infty}\int_0^K \frac{B_{21}A_{22}-B_{22}A_{12}}{A_{11}A_{22}-A_{12}A_{21}}\sin\pi\nu e^{-js(l-m)A}\,ds,$$

$$y^b_{lm}=-\frac{j2\omega}{KX_\infty}\int_0^K \frac{B_{22}A_{11}-B_{21}A_{12}}{A_{11}A_{22}-A_{12}A_{21}}\sin\pi\nu e^{-js(l-m)A}\,ds$$

4.2. Radiation admittances

Integrals in Eqs. (4.6) have following general form

$$Y_{lm}=\frac{j2\omega}{KX_\infty}\int_0^K R(s)\sin\pi s/Ke^{-js(l-m)A}ds \tag{4.7}$$

where function $R(s)$ which is different for different y^x_{lm}, but in all cases the denominator is the same in Eqs. (4.6), as singular at single poles for s being the solutions of dispersion equation for short-circuited strips. $R(s)$, and Y can be decomposed as follows

$$R(s)=R^c(s)+R^r(s), \quad Y_{lm}=Y^c_{lm}+Y^r_{lm}, \tag{4.8}$$

where $R^c(s)=R(s)-R^r(s)$ is assumed regular function of s, thus the corresponding integral for Y^c can be easily evaluated numerically. It describes mutual capacitance of electrodes l and m, placed on the same or different sides of the plate [11].

The function $R^r(s)$ that includes all singularities, is defined as follows

$$R^r(s)=\sum_i\frac{b_i}{s-s_i}+\sum_i\frac{\bar{b}_i}{s-K+s_i}, \tag{4.9}$$

where we accounted for that both s_i and $K-s_i$ are solutions to dispersion equations in the considered system, s_i-K being the wave-number of APM propagating backward. Corresponding integrals can be evaluated approximately by expanding the integration path to infinity on the complex plane s, and thus applying Jordan's lemma and residual theorem (see [3], for instance). We obtain

$$Y_{ll}^{r}=j2\frac{\omega\Lambda}{X_{\infty}}\sum_{i}b_{i}e^{-js_{i}\Lambda/2},$$

$$Y_{lm}^{r}=2\frac{\omega\Lambda}{x_{\infty}}\sum_{i}b_{i}e^{-js_{i}|l-m|\Lambda}\sin\pi s_{i}/K,\quad\text{for}\quad l\neq m. \tag{4.10}$$

This is similar equation to that presented in [2, 3] for Rayleigh waves. The main difference is in the number of propagating modes generated in plate which contribute to the strip radiation admittance.

5. Some numerical and experimental results

Typical interdigital transducers are composed of a number of metal strips connected to transducers bar-buses [1], which buses are connected to external voltage sources, in generating IDT, or to loading impedance, in receiving IDT. In piezoelectric plate covered by strips on both its sides, there is interesting possibility of APM excitation by a pair of transducers having their fingers on different sides of the plate.

In [13], an experiment is described where a pair of IDTs were placed face-to face on two sides of YX quartz, 64 μm thick plate. Both IDTs had 40 pairs of split A1 fingers (strip period $\Lambda=40$ μm and $w=w'=20$ μm). There are measurements presented for IDTs connected in parallel and antiparallel, which means that corresponding strips on two sides of plate had the same, or oposite electric potentials. The measurements have not been interpreted as concern waves excited by transducers in the measured frequency band (10 – 100 MHz). This will be provided below, by comparison with numerical results. Let us note that the discussed plate is relatively thick as compared to the strip period, its normalized thickness is $Kd=10.035$, thus several modes can be observed in the measured frequency band. The numerical calculations presented here will include A_0, SH_0, S_0 and SH_1 modes only.

We introduce notations A, B for IDT bus-bars on the upper side, and A', B' — for corresponding bus-bars of IDT on the bottom surface of the plate. The voltages of these bus-bars will be noted V_A, V_B, $V_{A'}=V_A'$, $V_{B'}=V_B'$, and similarly for currents. Eqs. (4.6) results in following relations for the discussed IDTs

$$I_A=W\sum_{m=1}^{80}\sum_{l=1}^{80}w_m w_l y_{lm}^{u}V_A+w_l(1-w_m)y_{lm}^{u}V_B+$$
$$w_m w_l v_{lm}^{u}V_A'+w_l(1-w_m)v_{lm}^{u}V_B', \tag{5.1}$$

$$I_B=W\sum_{m=1}^{80}\sum_{l=1}^{80}(1-w_l)w_m y_{lm}^{u}V_A+(1-w_l)(1-w_m)y_{lm}^{u}V_B+$$

$$(1-w_l)w_m v^u_{lm} V'_A + (1-w_m)(1-w_l)v^u_{lm} V'_B,$$

and similarly for I'_A and I'_B, with w_k defined as follows

$$w_k = \begin{cases} 1 & \text{if electrode } k \text{ is connected to } A \text{ or } A' \text{ bus-bars,} \\ 0 & \text{elsewhere, and } W \text{ is IDT aperture width,} \end{cases} \tag{5.2}$$

In the analyzed configurations, we have

- in symmetric configuration, $I=((I_A+I'_A)-(I_B+I'_B))/2$, and $V_A=V'_B=V/2$, $V_B=V'_B=-V/2$,
- in antisymmetric configuration, $I=((I_A+I'_B)-(I_B+I'_B))/2$, and $V_A=V'_B=V/2$, $V_B=V'_A=-V/2$,

and the measured admitance of transducer pairs is

$$Y=I/V \tag{5.3}$$

Its values are computed in following frequency bands: 13–16 MHz, 32–34 MHz, and 54–58 MHz, and presented in Figs. 2, 3.

In conclusion, we recognize that the measured radiation conductances result from excitation of following APMs

- Lamb A_0 mode for $f\approx 14.5$ MHz, in antisymmetric configuration,
- transvers SH_0 mode for $f\approx 33.4$ MHz, in symmetric configuration,
- Lamb S_0 mode for $f\approx 56$ MHz, in both configurations, but in antisymmetric case more efficiently,
- transverse SH_1 mode for $f\approx 54.5$ MHz, in both configurations but for symmetric case more efficiently, and modes S_0 and SH_1 overlap in this case what makes the measured conductance of IDT highly distorted.

6. Conclusions

An analysis of propagation of plate modes in piezoelectric plate covered by periodic strips is presented. Bragg reflection and mode conversion is discussed. Inhomogeneous problem of generation of plate modes is solved and experimentally verified. Physical interpretation of measurement is provided.

Acknowledgments

This work was partly supported by State Committee for Scientific Research (Grants 8S501 001 07 and 312129101).

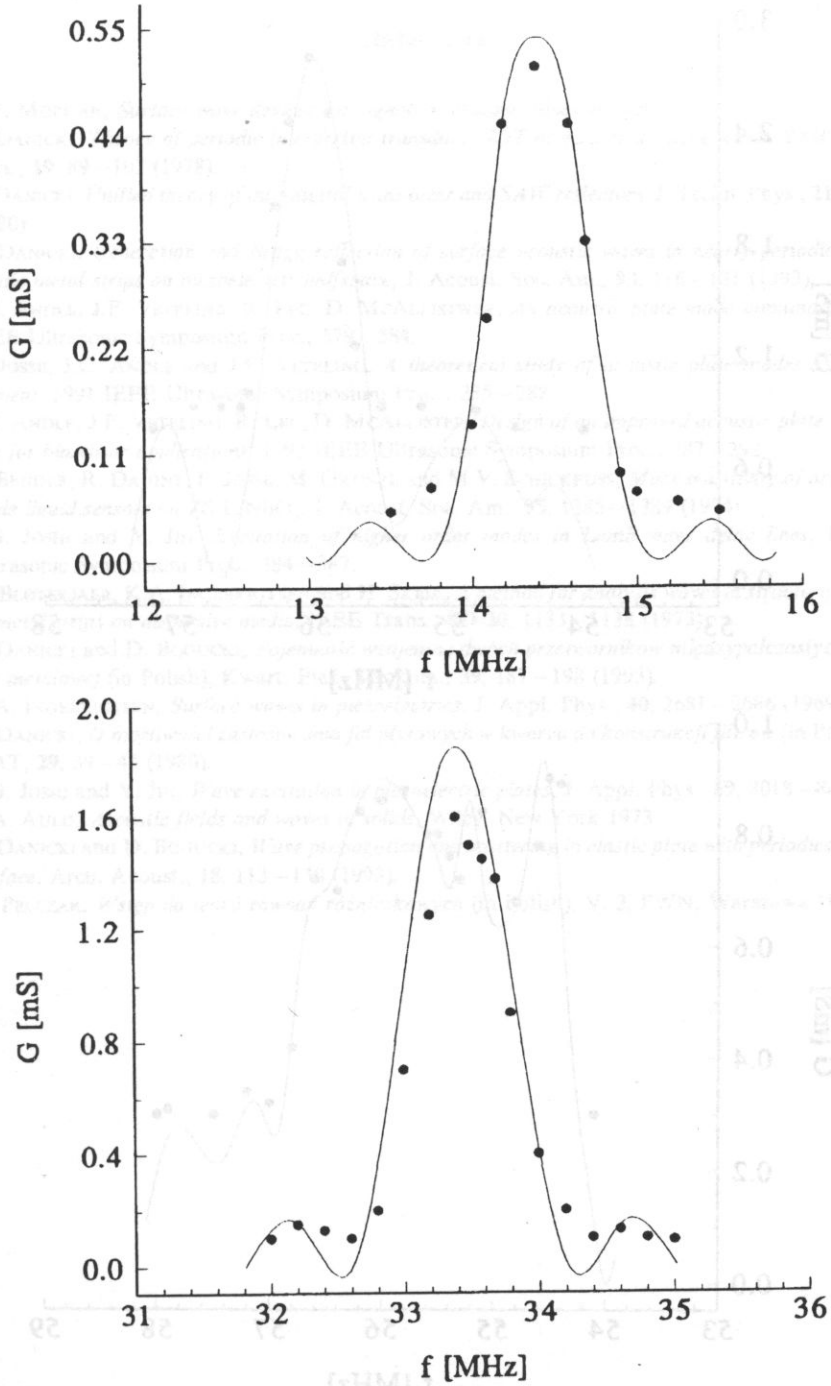

Fig. 2. Comparison of numerical (lines) and experimental values (dots) of radiation conductance of a two-sided pair of IDTs in antisymmetric configuration (upper figure, A_0 mode excited), and in symmetric configuration (below, SH_0 mode excited).

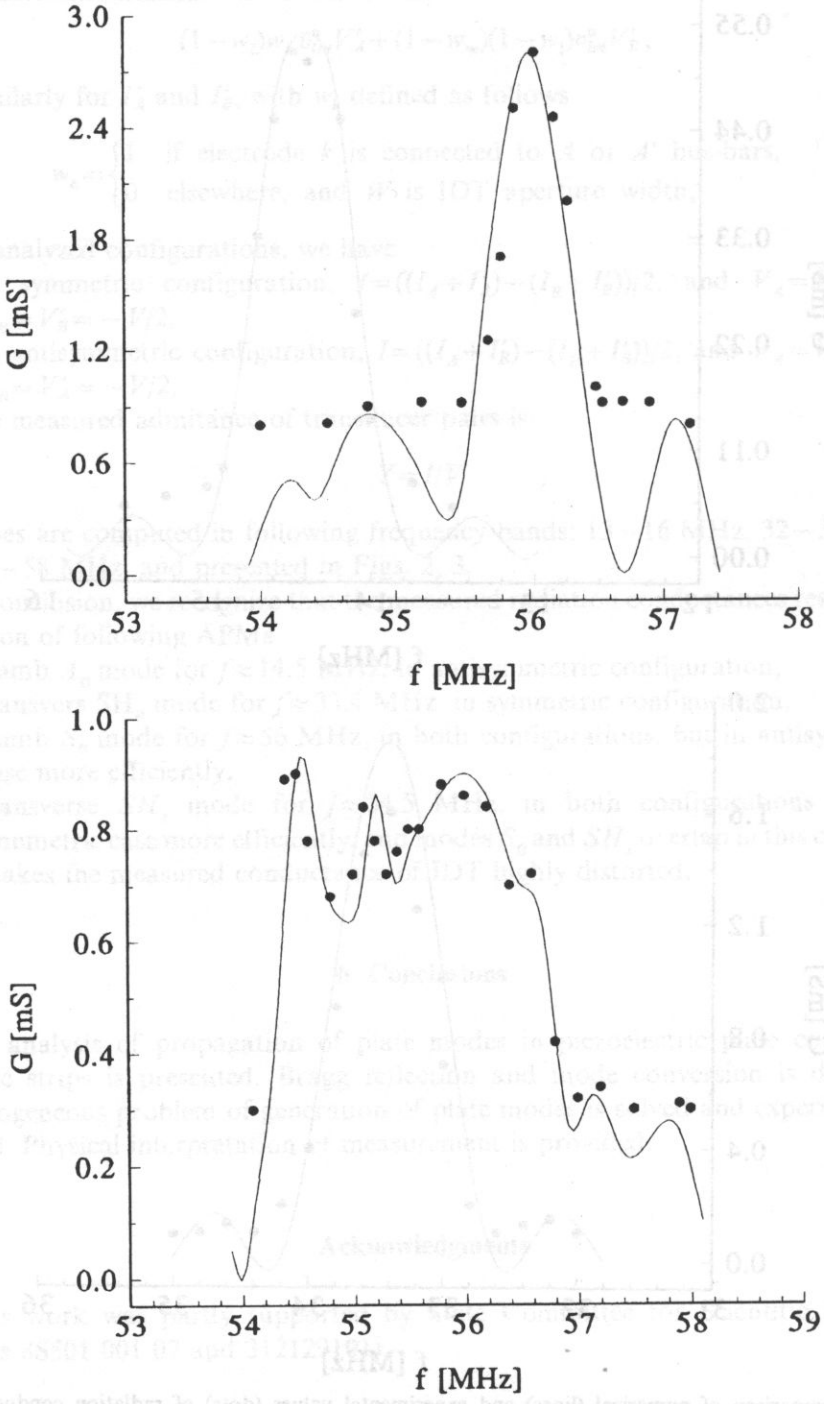

Fig. 3. Radiation conductances for antisymmetrical configuration (upper figure, S_0 mode), and for symmetric configuration of IDTs (below, S_0 and SH_1 modes excited almost at the same frequencies).

References

[1] D.P. MORGAN, *Surface-wave devices for signal processing*, Elsevier, 1985.

[2] E. DANICKI, *Theory of periodic interdigital transducer IDT of surface acoustic waves SAW*, J. Techn. Phys., **19**, 89–102 (1978).

[3] E. DANICKI, *Unified theory of interdigital transducer and SAW reflectors*, J. Techn. Phys., **21**, 387–403 (1980).

[4] E. DANICKI, *Generation and Bragg reflection of surface acoustic waves in nearly periodic system of elastic metal strips on piezoelectric halfspace*, J. Acoust. Soc. Am., **93**, 116–131 (1993).

[5] J.C. ANDLE, J.F. VETELINO, R. LEC, D. MCALLISTWER, *An acoustic plate mode immunosensor*, 1989 IEEE Ultrasonic Symposium Proc., 579–584.

[6] F. JOSSE, J.C. ANDLE and J.F. VETELINO, *A theoretical study of acoustic plate modes as biosensing element*, 1991 IEEE Ultrasonic Symposium Proc., 285–288.

[7] J.C. ANDLE, J.F. VETELINO, R. LEC, D. MCALLISTER, *Design of an improved acoustic plate mode delay line for biosensor applications*, 1992 IEEE Ultrasonic Symposium Proc., 287–292.

[8] F. BENDER, R. DAHINT, F. JOSSE, M. GRUNZE and M.V. SCHICKFUSS, *Mass sensitivity of acoustic plate mode liquid sensors on* ZS-$LiNbO_3$, J. Acoust. Soc. Am., **95**, 1385–1389 (1994).

[9] S.G. JOSHI and Y. JIN, *Excitation of higher order modes in Lamb wave delay lines*, 1922 IEEE Ultrasonic Symposium Proc., 384–387.

[10] K. BLØTEKJAER, K.A. INGEBRIGTSEN and H. SKEIE, *A method for analysis waves in structures consisting of metal strips on dispersive media*, IEEE Trans., **ED-20**, 1133–1138 (1973).

[11] E. DANICKI and D. BOGUCKI, *Pojemność wzajemna dwóch przetwornikow międzypalczastych w obudowie metalowej* (in Polish), Kwart. Elek. Telekom., **39**, 187–198 (1993).

[12] K.A. INGEBRIGTSEN, *Surface waves in piezoelectrics*, J. Appl. Phys., **40**, 2681–2686 (1969).

[13] E. DANICKI, *O możliwości zastosowania fal płytowych w kwarcu do konstrukcji filtrów* (in Polish), Biul. WAT, **29**, 39–46 (1980).

[14] S.G. JOSHI and Y. JIN, *Wave excitation in piezoelectric plates*, J. Appl. Phys., **69**, 8018–8024 (1991).

[15] B.A. AULD, *Acoustic fields and waves in solids*, Wiley, New York 1973.

[16] E. DANICKI and D. BOGUCKI, *Wave propagation and scattering in elastic plate with periodically grooved surface*, Arch. Acoust., **18**, 113–130 (1993).

[17] A. PELCZAR, *Wstęp do teorii równań różniczkowych* (in Polish), V. 2, PWN, Warszawa 1991.

ARCHIVES OF ACOUSTICS
20, 2, 191–205(1995)

NUMERICAL MODEL OF MULTIPLE SOUND SCATTERING FROM GAS BUBBLES IN THE SEA

J. SZCZUCKA

Institute of Oceanology
Polish Academy of Science
(81-712 Sopot, ul. Powstańców Warszawy 55)

This paper presents a model of sound scattering on gas bubbles aggregations in water. Coherence and second order scattering effects are taken into account for random and regular 3-dimensional distributions of bubbles with different parameters like bubble size, average separation between scatterers, distance to the receiver, incident sound frequency. Results of calculations for various sets of parameters are compared. Excess attenuation is also considered.

1. Introduction

Different objects enclosed in the sea water can be detected and counted by the sound scattering methods. Gas bubbles floating in the upper sea layer are generated mainly by breaking wind waves and by biological sources (photosynthesis, decaying organic matter). These bubbles play an important role in the ocean-atmosphere gas exchange. On the other hand they strongly influence the conditions of sound propagation in the sea, scattering and absorbing acoustic energy and changing the sound velocity. The intensity of all these processes depends on the concentration of microbubbles, which can be measured by means of acoustic methods, similar to fish counting. The majority of these methods is based on two fundamental assumptions concerning *single scattering* — that is equivalent to the noninteraction between scatterers — and *incoherent scattering* — the total intensity of backscattered sound is treated as a sum of intensities originating from the individual centres. If the discrete scatterers are distributed in space randomly and not too densely, these assumptions can be sufficient for solving the problem of backscattering, but in some circumstances depending on the wavelength, distance between scattering centres, distance between receiver and scatterers, they can oversimplify the real sitaution and lead to significant errors, therefore this problem should be taken into consideration in each individual case.

Most of scattering models applied to marine inhomogeneities ignore the effects of coherence and multiple scattering, but these effects were considered by some authors

using different simplifying assumptions. KURIANOV [3] showed analytically, that coherent scattering of the time-limited acoustic pulse on the set of randomly distributed objects can be neglected. STANTON [5, 6] evaluated the second order effects for scattering on clouds of identical randomly distributed isotropic scatterers under the following assumptions: the average distance between individual objects was much greater than the acoustic wavelength (the short wavelength limit), the swarm of scatterers was located in the plane-wave region of the transceiver and absorption was negligible. Under these conditions, second order scattering was shown to play an important role, especially in the case of using multibeam sonars. BRUNO and NOVARINI [1] considered both coherence and interaction effects, but only for 1-dimensional (linear) distributions of gas-filled bubbles.

In this paper the mathematical model of acoustic backscattering of spherical wave from the aggregation of gas bubbles in water has been considered. The expressions for the coherent and incoherent terms of the first and second order of the backscattered energy have been obtained. The model was used for both random and regular 3-dimensional distributions of gas bubbles with the same radii or with given size spectrum, for various densities and various distances to the receiver, with the attenuation included or not.

2. Scattering and attenuation by a single gas bubble

For the acoustic wave of frequency f the function of backscattering t_j on a gas bubble with the radius a_j is given by [4, 7]:

$$t_j = \frac{a_j}{(f_{Rj}/f)^2 - 1 + i\delta_j}, \tag{2.1}$$

where δ_j is a damping constant of the jth bubble, depending on the bubble size, incident sound frequency and number of physicochemical parameters of the gas and sea water, and f_{Rj} is its resonant frequency

$$f_R = \frac{\sqrt{3\gamma P/\rho}}{2\pi a}, \tag{2.2}$$

where γ — the ratio of specific heats of gas, P — hydrostatic pressure at given depth, ρ — water density. Taking the complex function t_j in the form

$$t_j = \rho_j \exp(i\varphi_j), \tag{2.3}$$

we get

$$\rho_j = \frac{a_j}{\sqrt{[(f_{Rj}/f)^2 - 1]^2 + \delta_j^2}}, \tag{2.4}$$

$$\tan\varphi_j = -\frac{\delta_j}{(f_{Rj}/f)^2 - 1}.$$

There is the following relationship between the backscattering function and backscattering cross-section of a gas bubble [4, 7]:

$$\sigma_{bs} = |f|^2 = \frac{a_j^2}{[(f_{Rj}/f)^2 - 1]^2 + \delta_j^2}. \tag{2.5}$$

Extinction cross-section of a gas bubble looks similar:

$$\sigma_e = \frac{4\pi a_j^2 (\delta_j / k a_j)}{[(f_{Rj}/f)^2 - 1]^2 + \delta_j^2} \tag{2.6}$$

At resonance bubble cross-sections are reduced to:

$$\sigma_{bs,R} = a_j^2/\delta_j^2$$
$$\sigma_{e,R} = 4\pi a_j/k\delta_j \tag{2.7}$$

The dependence of ρ, φ and δ on frequency for air bubble with radius 100 μm is displayed in Fig. 1.

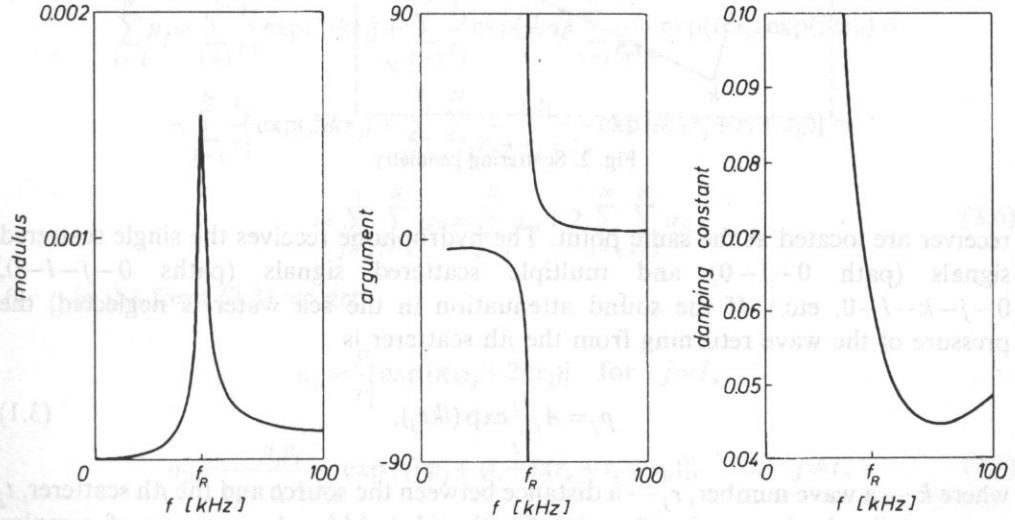

Fig. 1. Dependence of the modulus and argument of backscattering function and damping constant on frequency of incident sound for air bubble with radius $a = 100$ μm located at depth $z_0 = 10$ m.

3. Scattering model without attenuation

Let us consider the problem of backscattering of the spherical sound wave on the aggregation of N gas bubbles enclosed in any volume V with the centre at a depth z_0 related to the source depth (Fig. 2). The geometry is monostatic — source and

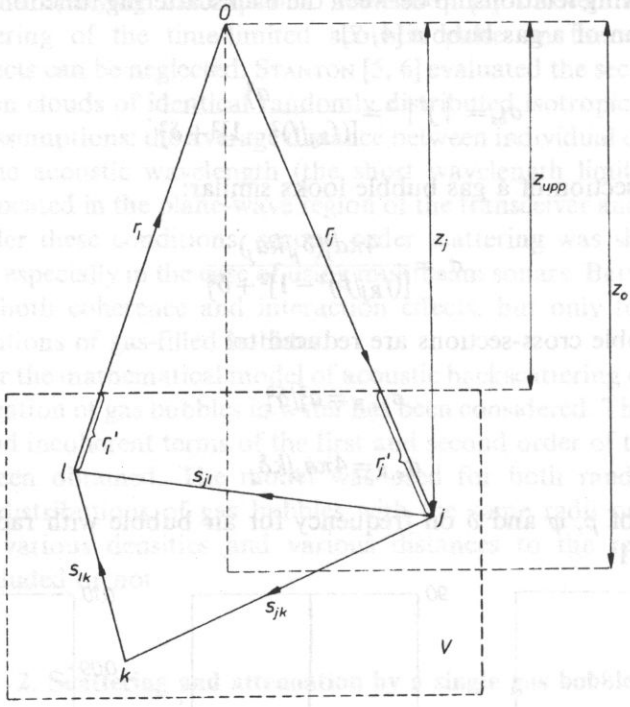

Fig. 2. Scattering geometry

receiver are located at the same point. The hydrophone receives the single scattered signals (path $0-j-0$) and multiple scattered signals (paths $0-j-l-0$, $0-j-k-l-0$, etc.). If the sound attenuation in the sea water is neglected, the pressure of the wave returning from the jth scatterer is

$$p_j = A_j \frac{t_j}{r_j} \exp(ikr_j), \tag{3.1}$$

where k — a wave number, r_j — a distance between the source and the jth scatterer, t_j — a complex backscattering function for the jth bubble, A_j — a sum of complex amplitudes of the spherical waves coming to the jth scatterer from all other bubbles

$$A_j = A_{0j} + \sum_{l \neq j}^{N} A_l \frac{t_l}{s_{jl}} \exp(iks_{jl}). \tag{3.2}$$

In this formula s_{jl} is a distance from the jth to lth scattering object and A_{0j} is an amplitude of the spherical wave coming to the jth scatterer directly from the source

$$A_{0j} = \frac{A_0}{r_j} \exp(ikr_j), \tag{3.3}$$

where A_0 is an amplitude of the wave emitted from the source.

The expression (3.2) is a reccurence formula including scattering effects to all orders. In the presented model it is assumed $A_l = A_{0l}$, what is a consequence of neglecting all the effects over the second order, and for simplicity, $A_0 = 1$. According to the fundamental hypothesis, in practice we measure an incoherent field of single scattered signals:

$$I_{\text{in}} = \sum_{j=1}^{N} | p_j^{(1)} |^2, \tag{3.4}$$

but in fact we measure a total field (including coherent terms) of multiple scattered signals:

$$I_{\text{tot}} = \left| \sum_{j=1}^{N} p_j \right|^2. \tag{3.5}$$

The main goal of calculations is a total intensity with taking phase relations into account, therefore the coherent sum of pressure is needed:

$$\sum_{j=1}^{N} p_j = \sum_{j=1}^{N} \frac{t_j}{r_j^2} \exp(2ikr_j) + \sum_{j=1}^{N} \frac{t_j}{r_j} \exp(ikr_j) \sum_{l \neq j}^{N} \frac{t_l}{r_l s_{jl}} \exp(ikr_l) \exp(iks_{jl}) =$$

$$= \sum_{j=1}^{N} \frac{t_j}{r_j^2} \exp(2ikr_j) + \sum_{j=1}^{N} \sum_{l \neq j}^{N} \frac{t_j t_l}{r_j + r_l + s_{jl}} \exp[ik(r_j + r_l + s_{jl})] =$$

$$= \sum_{j=1}^{N} \sum_{l=1}^{N} a_{jl} = \sum_{j=1}^{N} a_{jj} + 2 \sum_{j=1}^{N} \sum_{l>j}^{N} a_{jl}. \tag{3.6}$$

for t_j in the form (2.3) we get

$$a_{jj} = \frac{\rho_j}{r_j^2} \exp[i(\varphi_j + 2kr_j)] \quad \text{for} \quad j = l,$$

$$a_{jl} = \frac{\rho_j \rho_l}{r_j + r_l + s_{jl}} \exp\{i[\varphi_j + \varphi_l + k(r_k + r_l + s_{jl})]\} \quad \text{for} \quad j \neq l, \tag{3.7}$$

The total scattered field is:

$$I_{\text{tot}} = \left| \sum_{j=1}^{N} p_j \right|^2 = \left(\sum_{j=1}^{N} p_j \right) \cdot \left(\sum_{j=1}^{N} p_j \right)^* = \sum_{j=1}^{N} \sum_{k=1}^{N} a_{jk} \cdot \sum_{l=1}^{N} \sum_{m=1}^{N} a_{lm}^*. \tag{3.8}$$

The product of these two sums comprises $N(N+1)/2$ incoherent terms $a_{jk} a_{jk}^* = | a_{jk} |^2$, where $j = l$, $k = m$, and $N(N+1)[N(N+1)/2 - 1]/4$ coherent terms $a_{jk} a_{lm}^* + a_{jk}^* a_{lm}$ involving phases. As a result w obtain:

$$I_{\text{tot}} = I_{\text{in}}^{(1)} + I_{\text{coh}}^{(1)} + I_{\text{in}}^{(2)} + I_{\text{coh}}^{(2)}, \tag{3.9}$$

where

$$I_{\text{in}}^{(1)} = \sum_{j=1}^{N} | a_{jj} |^2$$

$$I_{\text{coh}}^{(1)} = 2 \sum_{j=1}^{N} \sum_{l>j}^{N} | a_{jj} \| a_{ll} | \cos[\varphi_j - \varphi_l + 2k(r_j - r_l)]$$

$$I_{\text{in}}^{(2)} = 4 \sum_{j=1}^{N} \sum_{k>j}^{N} | a_{jk} |^2$$

$$I_{\text{coh}}^{(2)} = 4 \sum_{j=1}^{N} \sum_{l=1}^{N} \sum_{m>l}^{N} | a_{jj} \| a_{lm} | \cos[\varphi_j - \varphi_l - \varphi_m + k(2r_j - r_l - r_m - s_{lm})] +$$

$$+ 8 \sum_{j=1}^{N} \sum_{k>j}^{N} \sum_{l=1}^{N} \sum_{m>l}^{N} | a_{jk} \| a_{lm} | \cos[\varphi_j + \varphi_k - \varphi_l - \varphi_m + k(r_j + r_k + s_{jk} - r_l - r_m - s_{lm})] .$$

In the case of only coherent scattering of the first order (the phases of echoes from individual scatterers are equal), for identical objects we have $I_{\text{coh}}^{(1)} = (N-1) I_{\text{in}}^{(1)}$ or $I_{\text{tot}} = N I_{\text{in}}^{(1)}$.

As it was mentioned above, $N(N+1)[N(N+1)/2+1]/4$ terms must be calculated to obtain the value of I_{tot}. This gives 1540 components for $N=10$ and 813450 for $N=50$.

Total backscattering intensity can be greater or smaller than its incoherent part because echoes from single centers can interfere constructively or destructively (coherent terms can be positive or negative). For estimation of an error connected with the assumption of the dominant role of incoherent scattering it is useful to introduce the following correction coefficient:

$$c_{\text{cor}} = I_{\text{in}}^{(1)} / I_{\text{tot}} .$$

For purely incoherent scattering its value is 1 and it decreases with rising contribution of coherent effects.

4. Scattering model with attenuation

Attenuation of the running wave takes place only inside the volume V on the way r_j' to the individual scatterer and on the way s_{jl} between two consecutive scatterers (Fig. 2)

$$r_j' = r_j (z_{\text{upp}} - z_j)/z_j ,$$

where r_j — a distance from the source to the jth bubble, z_j — its depth and z_{upp} — a depth of the upper boundary of the swarm of scatterers. Energetic coefficient of sound attenuation in bubbly water is expressed in Np/m and for identical bubbles has a form [7]:

$$\alpha = N\sigma_{e,R}/V,$$

where $\sigma_{e,R}$ is given by the formula (2.7).

Expressions (3.1)–(3.3) and (3.7) change their appearance:

$$p_j = A_j \frac{t_j}{r_j} \exp(ikr_j) \exp(-0.5\alpha r'_j), \tag{3.1}'$$

$$A_j = A_{0j} + \sum_{l \neq j}^{N} A_l \frac{t_l}{s_{jl}} \exp(iks_{jl}) \exp(-0.5\alpha s_{jl}). \tag{3.2}'$$

$$A_{0j} = \frac{A_0}{r_j} \exp(ikr_j) \exp(-0.5\alpha r'_j) \tag{3.3}'$$

$$a_{jj} = \frac{\rho_j}{r_j^2} \exp[i(\varphi_j + 2kr_j)] \exp(-\alpha r'_j) \quad \text{for} \quad j = l \tag{3.7}'$$

$$a_{jl} = \frac{\rho_j \rho_l}{r_j + r_l + s_{jl}} \exp\{i[\varphi_j + \varphi_l + k(r_j + r_l + s_{jl})]\} \exp[-0.5\alpha(r'_j + r'_l + s_{jl})] \quad \text{for } j \neq l$$

The effect of sound wave extinction was introduced to the model according to formulae (3.1)′–(3.7)′.

5. Numerical results

The first stage of calculations concerned N identical scatterers distributed both regularly and randomly in volume V with a given mean distance d between the neighbouring individuals. Sound attenuation was not included. The volume V was chosen as a parallelepiped with edges $n_1 d$, $n_1 d$ and $n_2 d$ ($n_1 * n_1 * n_2 = N$). In regular distributions bubbles were located in the nodes of a network, in random distributions each coordinate (x, y, z) of a scatterer was a random variable from the interval equal to the appropriate edge length determined for the regular case. In the random case the distances s_{jl} between all scatterers were tested and values smaller than diameter of a bubble were eliminated. Obtained values of backscattered field were averaged over 50 realisations.

In the first series of calculations the dependence of the scattered field on swarm density was investigated. For this purpose the value of d was being changed from $d=1$ cm to $d=10$ cm which resulted in change of total volume and, in consequence, in the bubble concentration. Various values of bubble number N (27 or 48), bubble radius a (10, 50, 75 and 100 μm) and swarm depth z_0 (1,5 and 10 m) were taken for each numerical calculation. Resonant frequency of a single bubble was chosen as a frequency of incident sound ($f=f_R$). Incoherent scattering of the first order practically depends neither on bubble

concentration nor on character of a distribution. In the random case it dominates for $d>2$ cm (Fig. 3). Incoherent term of the second order increases with decreasing volume for all kinds of distributions. For the densest packing ($d=1$ cm, i.e. $N/V=10^6/m^3$) this term contributed significantly — for random distribution it is even greater than the first order incoherent part. Regular distributions give the interference picture of I_{tot} with oscillations of order 30 dB which are connected with a vertical network dimension — large maxima occur at half wavelength and smaller — at quarter wavelength distance between horizontal layers of scatterers. It can be clearly seen on the diagram with horizontal axis and scale d/λ (Fig. 4).

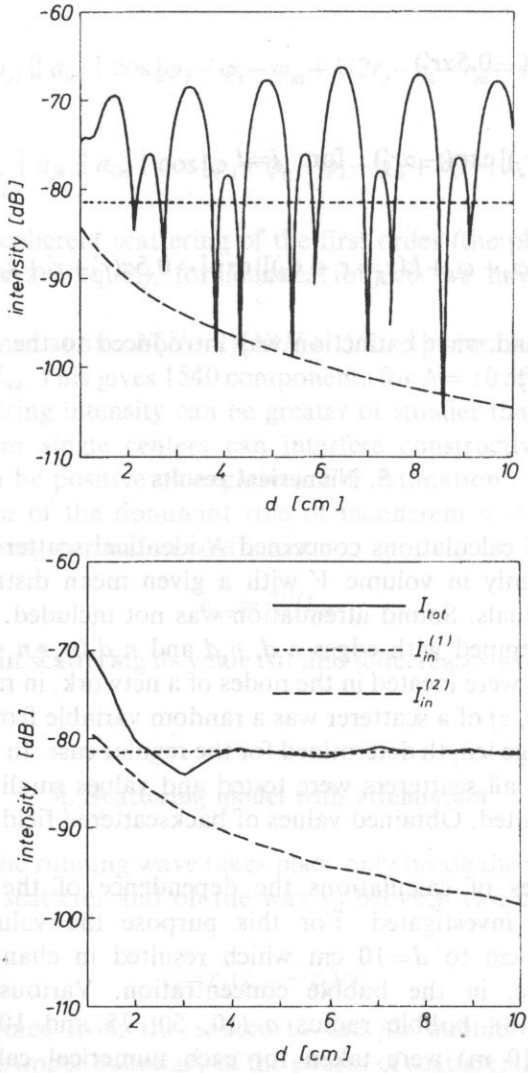

Fig. 3. Comparison of different order scattering effects for regular (upper) and random (lower) bubble distributions. $N=27$, $a=100$ μm, $z_0=10$ m.

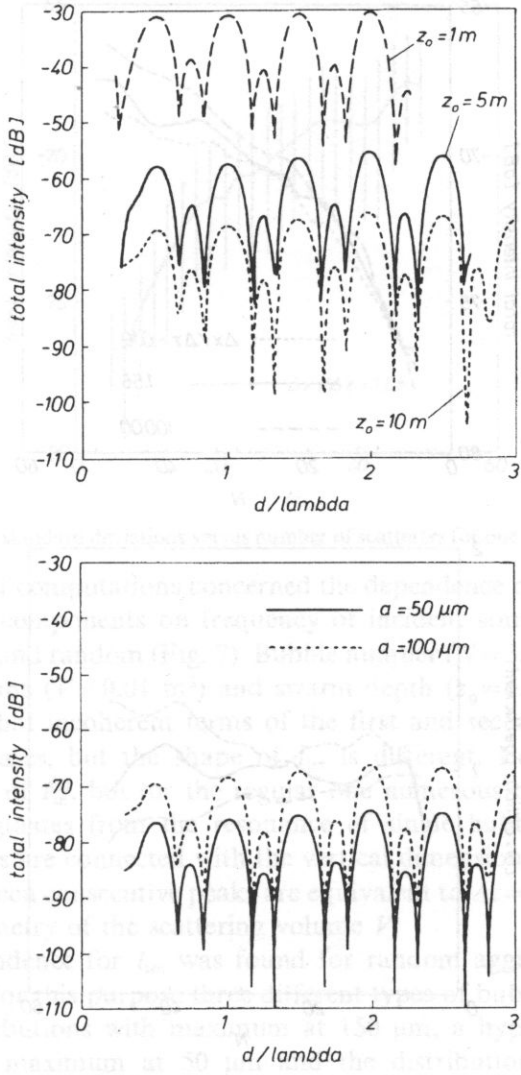

Fig. 4. Total intensity versus d/λ for regular bubble distribution for different swarm depths (upper) and different bubble radius (lower). $N=27$.

The second series of computation concerned the random distributions only. Values of scattering volume ($V=0.01$ m^3), bubble radius ($a=100$ μm) and swarm depth ($z_0=5$ m) were fixed and bubble number N was varied. Calculations were carried out for seven different ratios $\Delta x/\Delta z$ of scattering volume: from $\Delta x/\Delta z=0.1$ — tall and narrow parallelepiped (in practice it is equivalent to narrow beam and long pulse) to $\Delta x/\Delta z=100$ — low and broad (broad beam and short pulse). Fig. 5 shows the dependence of the total intensity and correction coefficient on number of bubbles in given volume for three chosen geometries. Apart from an obvious fact that

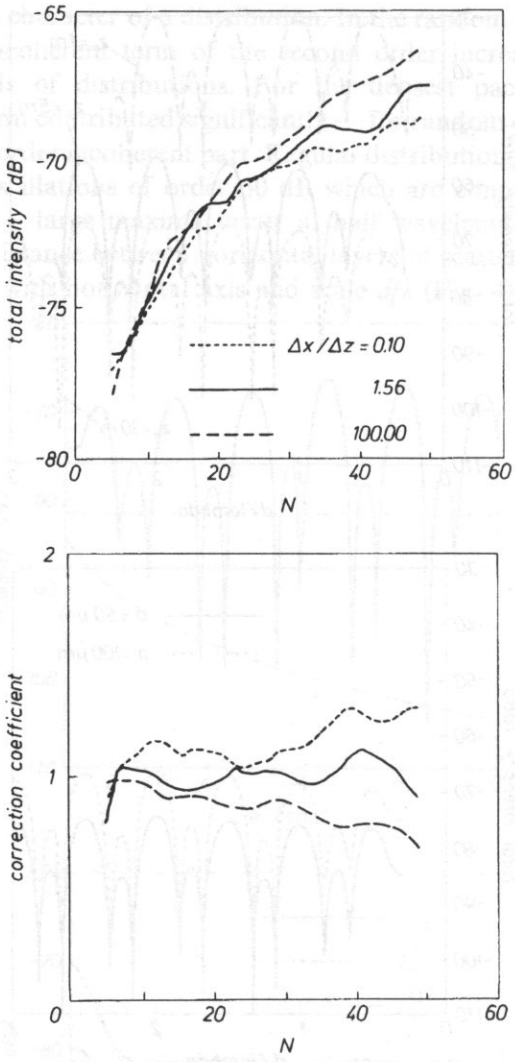

Fig. 5. Dependence of total intensity (upper) and correction coefficient (lower) on number of bubbles enclosed in volume $V=0.01$ m^3 for three geometries. Bubbles distributed randomly, averaging over 100 realisations.

intensity increases with increasing number of scatterers, we can see the tendency that with flattening and broadening of the parallelepiped the total echo rises and correction coefficient falls. It means that coherent scattering becomes more substantial, what is obvious for 2-dimensional (flat) scattering systems. The shape of these curves is very uneven despite increasing the number of averaged realisations to 100, because of large changeability of succesive realisations (see standard deviations in Fig. 6).

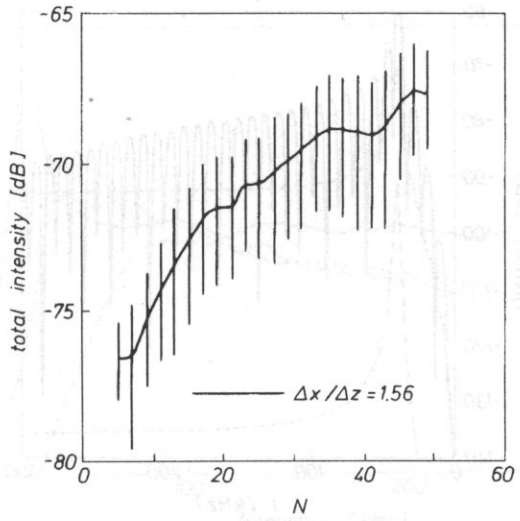

Fig. 6. Total intensity with standard deviations versus number of scatterers for one of geometries from Fig. 5.

The third series of computations concerned the dependence of the total backscattered signal and its components on frequency of incident sound for two types of distribution: regular and random (Fig. 7). Bubble number ($N=32$), its radius ($a=100$ μm), scattering volume ($V=0.01$ m^3) and swarm depth ($z_0=5$ m) were fixed. The comparison shows that incoherent terms of the first and second order are almost identical for both cases, but the shape of I_{tot} is different. For the random case I_{tot} repeats the form of $I_{\text{in}}^{(1)}$, but for the regular one numerous maxima appear. The largest of them originates from the resonance of single bubble f_R (according to formula (2.2)), others are connected with the vertical dimension Δz of the scattering area. Distances between consecutive peaks are equivalent to $\Delta z=\lambda/2$ and they change together with a geometry of the scattering volume V.

Analogous dependence for I_{tot} was found for random aggregations of bubbles with various radii. For this purpose three different types of bubble size spectra were chosen: Gauss distributions with maximum at 150 μm, a hypothetical power law distribution with a maximum at 50 μm and the distribution of KOLOBAEV and DEKTEREV [2] describing natural marine population of gas bubbles:

(1) $n(a)\sim\exp[-(a-\bar{a})^2/2\sigma^2]$ $\bar{a}=150$ μm (Gauss),

(2) $n(a)\sim\begin{cases} a & \text{for } a<50 \text{ μm} \\ a^{-3} & \text{for } a>50 \text{ μm} \end{cases}$ (power law),

(3) $n(a)\sim a^{-3}\exp(-3\bar{a}/a)$ $\bar{a}=15$ μm (KOLOBAEV and DEKTEREV [2]).

All these distributions were normalized to give $N_{\text{tot}}=50$. Fig. 8 illustrates the dependence $I_{\text{tot}}(f)$ (upper part) for particular distributions (lower part). It can be seen that for aggregation of bubbles with different radii the resonant maximum of I_{tot} is

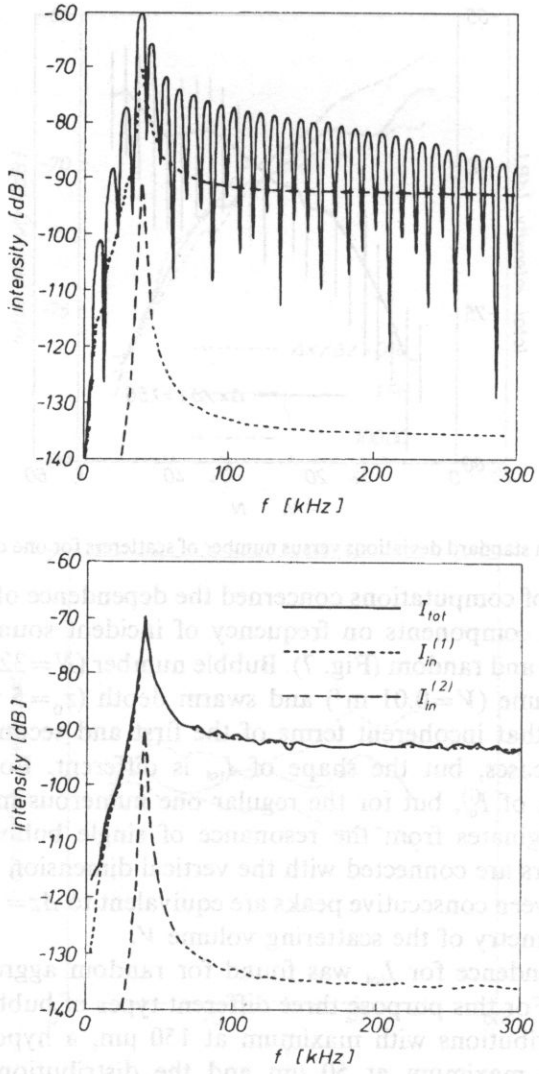

Fig. 7. Frequency dependence of the total backscattering energy and its components for regular (upper) and random (lower) bubble distributions. $N=32$, $a=100$ μm, $z_0=5$ m, $V=0.01$ m^3, $\Delta x/\Delta z=1.56$.

broadened in comparison with the case of bubbles with the same radii (see Fig. 7) and the shift of maximum in size spectrum causes the shift of resonant peak of backscattered intensity according to reverse proportionality of f and a_R. Additionally, the bigger bubbles dominate in the aggregation, the higher is the level of I_{tot} in the nonresonant area (large frequencies).

The dependence of the calculated backscattered intensity without and with attenuation on the linear dimension of swarm is shown in Fig. 9. For very small volumes V (i.e. huge bubble densities N/V) the attenuated field is about tens of dB

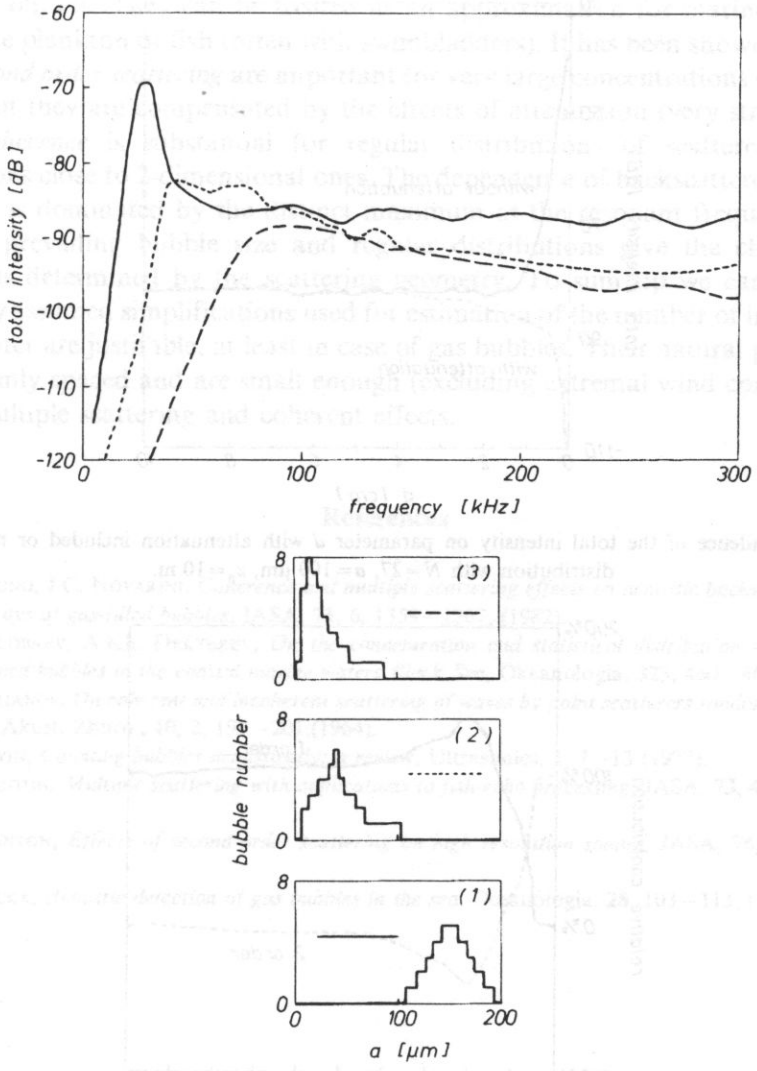

Fig. 8. Frequency dependence of the total backscattering energy (upper) for different kinds of bubble size spectra (lower).

smaller than the unattenuated one. A comparison of this diagram with the dependence of the first and second order terms of backscattered energy on the linear size of aggregation (Fig. 10) shows that the range of large attenuation is the same as the range of domination of the second order scattering. Therefore we can conclude that strong attenuation eliminates the second order effects. On the other hand, in the range of moderate bubble densities (under $10^4/m^3$), the role of both attenuation and interaction diminishes and these effects become negligible.

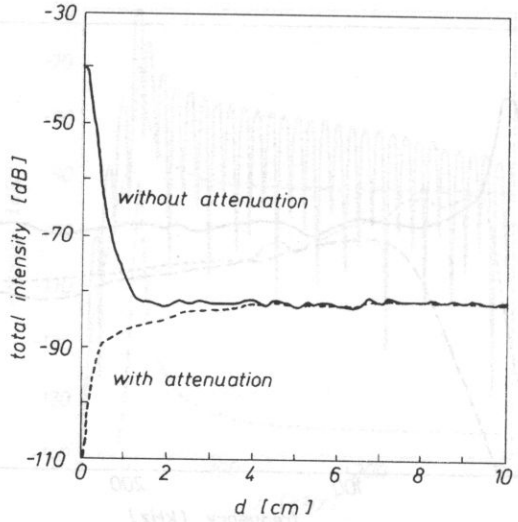

Fig. 9. Dependence of the total intensity on parameter d with attenuation included or not. Random distribution with $N=27$, $a=100$ μm, $z_0=10$ m.

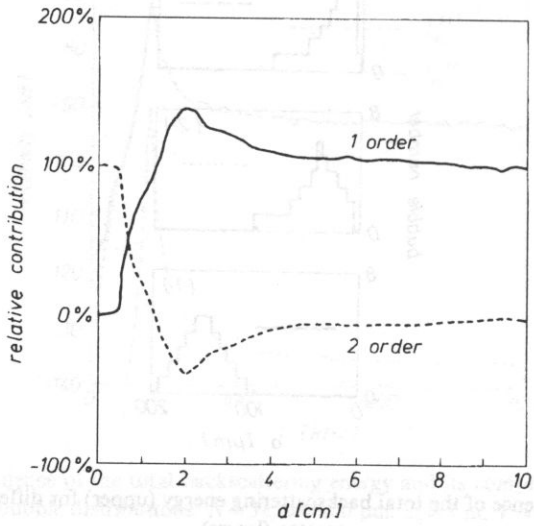

Fig. 10. Relative contribution of the first and second order scattering effects to total intensity for random set of bubbles. $N=27$, $a=100$ μm, $z_0=10$ m.

6. Summary

On the basis of numerical model describing the total field of signals backscattered on the collection of isotropic scatterers an attempt of verification of two fundamental assumptions of echosounding was made. Free gas bubbles were chosen as modelled

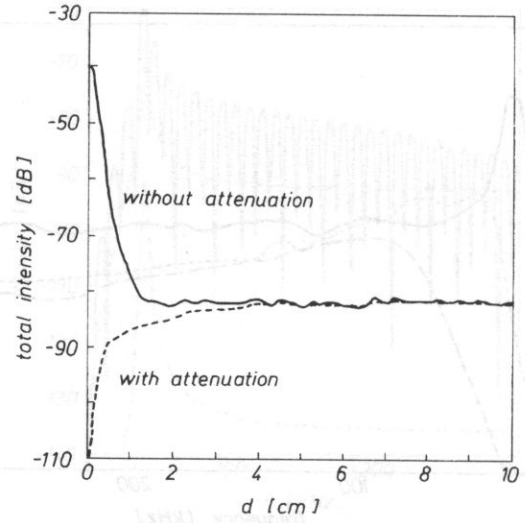

Fig. 9. Dependence of the total intensity on parameter d with attenuation included or not. Random distribution with $N=27$, $a=100$ μm, $z_0=10$ m.

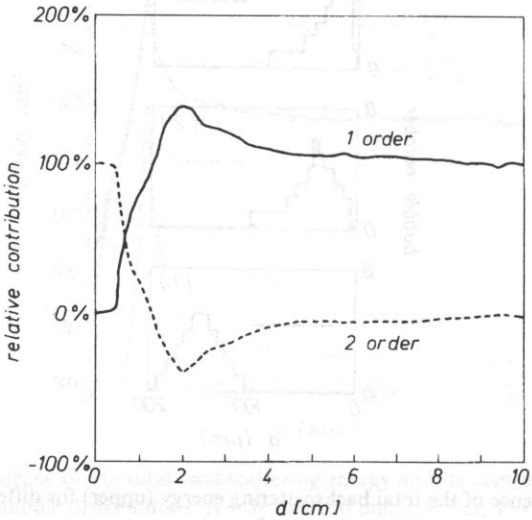

Fig. 10. Relative contribution of the first and second order scattering effects to total intensity for random set of bubbles. $N=27$, $a=100$ μm, $z_0=10$ m.

6. Summary

On the basis of numerical model describing the total field of signals backscattered on the collection of isotropic scatterers an attempt of verification of two fundamental assumptions of echosounding was made. Free gas bubbles were chosen as modelled

scattering objects. They can be treated as an approximation for marine biological objects like plankton or fish (often with swimbladders). It has been shown that terms of the *second order scattering* are important for very large concentrations of the order $10^6/m^3$, but they are compensated by the effects of attenuation (very strong in that area). *Coherence* is substantial for regular distributions of scatterers and for aggregations close to 2-dimensional ones. The dependence of backscattered signal on frequency is dominated by the distinct maximum at the resonant frequency of the single or prevailing bubble size and regular distributions give the characteristic oscillations determined by the scattering geometry. To sum up we can state that commonly assumed simplifications used for estimation of the number of intrusions in the sea water are justifable, at least in case of gas bubbles. Their natural populations are randomly spaced and are small enough (excluding extremal wind conditions) to neglect multiple scattering and coherent effects.

References

[1] D.R. Bruno, J.C. Novarini, *Coherence and multiple scattering effects on acoustic backscattering from linear arrays of gas-filled bubbles*, IASA, **71**, 6, 1359–1367, (1982).

[2] P.A. Kolobaev, A.Kh. Dekterev, *On the concentration and statistical distribution of the sizes of wind-formed bubbles in the coastal marine waters Black Sea*, Okeanologia, **323**, 460–465, (1992).

[3] B.F. Kurianov, *On coherent and incoherent scattering of waves by point scatterers randomly distributed in space*, Akust. Zhurn., **10**, 2, 195–201,(1964).

[4] H. Medwin, *Counting bubbles acoustically: a review*, Ultrasonics, **1**, 7–13 (1977).

[5] T.K. Stanton, *Multiple scattering with applications to fish-echo processing*, JASA, **73**, 4, 1164–1169, (1983).

[6] T.K. Stanton, *Effects of second-order scattering on high resolution sonars*, JASA, **76**, 3, 861–866, (1984).

[7] J. Szczucka, *Acoustic detection of gas bubbles in the sea*, Oceanologia, **28**, 103–113, (1989).

ARCHIVES OF ACOUSTICS
20, 2, 207–211(1995)

C H R O N I C L E

98TH AES CONVENTION — 25–28.02.1995 — PARIS
POLISH AES SECTION REPORT

Audio Engineering Society Conventions became traditional world meeatings of all scientist, engineers, industry managers, producers, dealers and even fanciers interested in the domain of sound and vision system, equipments, facilities, component, hard — and software computer elements etc. Such meetings take place twice a year: Spring in Europe (denoted with consecutive even numbers), and Fall Convention in the USA (denoted with odd ones).

The latest European Conventions: the 94th in Berlin, the 96th in Amsterdam, and the 98th one in Paris, reported herewith, were marked with parcitipation of several newly organized AES Sections from countries of former Eastern socialist block of states. Among te members to those Sections, the most numerous participation was of the Polish Section. Since the Berlin Convention, the Polish AES Section has organized, for the third time already, inexpensive coach expeditions for their members, mostly student-members, to participate in Conventions. Such parcipation is highly valubale, especially for young adepts of acoustics, sound engineering and related topics who otherwise would be unable to cover all costs of participation, accomodation, transport etc. In appreciation of those numerous participations and of other initiatives, as well as assessing the whole scientific activity of the Polish Section, the Vice-President for Europe AES Region, Mr Dan Popescu, during the special Convention meeting in Paris, highly estimated its achievements in 1994, calling the Polish Section „the best of all Europe Sections".

Among Polish participants of the 98th AES Convention, heeld in Paris, at Palais de Congrès, were numerous authors and coauthors who read their papers and took part in discussion during the debates within the scientifical Convention program. The debates were grouped in the sixteen sessions: Audio Data Reduction I & II (A & C), Architectural Acoustics I & II(B & D), Electronic Music and Musical Instrument Acoustics (E), Sound Reinforcement I & II (F & H), Audio Electronics (G), Audio Signal Processing I & II (I & K), Transducers I & II (J & L), Measurement (M), Psychoacoustics I & II (N & P), Networks and Interfacing (O).

All the eighty five Convention papers were supported by a preprint. The Polish presentation included the following ones (in brackets — preprint no. and in parentheses — session no.): A. Czyżewski, B. Kostek, S. Zieliński, *New Approach to*

the Synthesis of Organ Pipe Sound [3957] (E2); B. ŻÓŁTOGÓRSKI, *Inverse Radiation Problem — capabilities and Limitations*, [3981] (J1); D. RUSER, H. RUSER, *An Elementary High Resolution Microphone System for Localization of Sound Source in Air*, [4002] (M1); M. NIEWIAROWICZ, *Directional Proporties of sound Sources During Transients*, [4004] (M3);B. KOSTEK, *Statistical versus Artificial Inteligence Based Processing of Subjective Test Results* [4018] (P3); M. KIN, J. RENOWSKI, *The Influence of Spectrum on Perception of Differential Pitch Sensitivity for Short Waves*, [4020] (P5).

Moreover, Polish AES Section members, in particular the young student-members, have taken an active participation in the, so called, workshop sessions. Those were devoted to the following technical aspects: Preservation of and Access to Audio and Video Carriers; New Digital media Developments; Wave Front Sculpture for Sound Reinforcement; Premastering for the New CD Formats; The Interaction of the Visual and Auditory Senses: „How Does One Measure It"; Current Trends of Research in Musical Instruments Acoustics: Musical nad Non-Musical Application; Digital Audio broadcasting.

Aparat from the scientific activities, the parcipants got an enormous quantity of information concerning the most recent audio systems and equipments presented during a large exhibition, accompanying traditionally the Convention. The exhibition was held inside the Convention site, at the Palais de Congrès, on three levels, however, being easy acessible to all participants. more than three hundred enterprises, from all over the world, displayed their best products in richly outfitted demonstration stands, giving a visitor a unique possibility to keep track of the development trends in the whole domain of audio engineering. Broadly disseminated leaflets, prospects, technical data lists, system descriptions, records, even manuals, etc. will provide valuable information and reference source for participants at their professioanl practice.

Immediate press assessments, which appeared still before closing of the Conventions debates, have stated that the greatest interest of industry representatives concentrated on problems connected with the digital sound processing and the reinforcement systems. The latter ones were often entitled as room acoustics or building acoustics problems, however, only sound reinforcement techniques were treated thereby, withouth any reference to proper desing, measurement and acoustical correction or adaptation of rooms. At any rate, those were discussed during session debates devoted to Architectural Acoustics.

Generally, the scientific part of the Paris Convention was not so largely filled as e.g. the 94^{th} one, held in Berlin. The number of papers was almost halved in comparison to Berlin record. However, may be, it was intended by Paris Convention Committe, which probably dismissed a part of the submmitted papers in order not ot exaggerate the numbers of parallel sessions, necessary otherwise. So, the more important is the number of Polish Section presentations, which amounted 7% of the total number papers.

It may be interesting to compare the share of authors' contribitions from particular countries. The most numerous were twelve papers from the U.S.A. Next in

number were papers from Germany and from the United Kingdom, ten papers from each country. Nine papers were presented by French authors. Eight ones by Dutch authors. Poland and Russia presented six papers each. Denish authors presented four papers. Finnland and Hong-Kong presented three papers each. Two papers came from authors from Greece, Ireland, Portugal and Switzerland. One paper was presented by authors from Australia, Austria, Italy, Japan, Spain and Sweden. Thus, it was a really international contribution to audio engineering scientific progress.

Such yearly repeated contact with the international progress in the audio angineering domain is, without a doubt, a very useful event for the Polish AES Section members and for their entire scientific and professional surrounding. Thus, a continuation of similar contacts in the future seems to bee highly desirable. In this context, it has to be added here, that the 100^{th} AES Convention, the jubilee one, will be held in Copenhagen, at Bella Center, on May 11–14, next year, 1996.

Marianna Sankiewicz
(Chairman of the Polish AES Section)

Information about CIB W–51 Acoustics Metting in Warsaw, 25–27 May 1994

The Information Council for Bilding Research Studies and Documentation is an international organization concerned with studies, research and documentation in the building industry. It unites 70 countries. It has over 500 collective and individual members.

Over 70 International Commitees and Working Groups operate within CIB. One of them is the W–51 Acoustics Committee. The Committee is heated by Prof. A. Cops and Prof. G. Vermieir from the Catholic University in Leuven.

The W–51 Acoustics Committee consists of the representatives of Research Centers, dealing with building acoustics, requiring more in-depth theoretical and experimental examination, are discussed during these meetings. Discussion are held on the chosen scientific issues, study and measurement methods, and the results of studies obtained in the lest several years in the various Institutes are analyzed.

Scientific presentations are prepared for the Committee meetings and these are later presented and discussed at the seminar. Later on these papers are prepared — according to the publisher's requirements — for publication in Applied Acoustics.

A collective publication is prepared from each seminar, which includes the written and presented papers. This publication includes the papers presented at the meeting of the CIB W–51 Acoustics Committee on May 25–27, 1994 in Warsaw.

The seminar in Warsaw was devoted to two very significant groups of topics, namely:

I. Experimental study and modeling of sound insulation in construction building joints in buildings.

II. Sound absorption, shape and indicator of reference curve, measurement and desing.

A total of 21 papers were announced 11 — in Section I, 10 — in Section II; 18 papers were presented. From which 16 were delivered in the from 16 were delivered in the from of xerox-copied publications the remaining 2 due to research being in progress, were only presented, and will published at a later date in Applied Acoustics. Three papers were not sent in their authors were also absent.

A list of the presented papers, according to the program of the meeting, is given.

Participation in the CIB W—51 Acoustics Committee meeting undoubtedly allowed its participants to confront the progress of studies conducted on similar topics in the various countries, as well as facilitated better planning in the area of building acoustics studies to be carrier out in the forthcoming years.

Prof. André Cops
Laboratory for Acoustic and Thermal Physics
Catholic University of Leuven, Belgium

Prof. Gerrit Vermeir
Laboratory for Building Physics
Catholic University of Luven, Belgium

Prof. Jerzy Sadowski
Zakład Akustyki Instytutu Techniki
Budowlanej.

Presented papers

Theme 1 — JUNCTION DAMPING: modeling, experiments

1. Bosmans I., Mees., Vermeir G. (Belgium),
   Structure-borne sound transmission between thin ortotropic plates: analytical solution.
2. Craik R. (England), Osipow A. (Russia),
   The use elastic interlayers at joints to reduce structure-borne sound transmission.
3. Villot M., Jean P. (France),
   Structure-borne sound transmission though a pillar-beam-floor system. Case of bulidings constructed on top of covered raliways.
4. Pedersen D.B. (Denmark),
   Estimation of vibration attenuation trough junctions of building structures.
5. Gerretsen E. (The Netherlands),
   Junction transmission with double-leaf building elements.

Theme 2 — JUNCTION DAMPING: examples, applications

1. Nightingale T. (Canada),

Application of the CEN draft building acoustics prediction model to a lightweight double leaf construction.

2. MARTIN H.J., MOORLACH M.F.C. (The Netherlands),
   Sound transmission and junction damping in sheet steel dwellings.
3. SZUDROWICZ B., IŻEWSKA A. (Poland),
   Simplified evaluation of flanking transmission based on the mean mass and mean area of flanking elements.
4. PIETRZYK A., KROPP W., KIHLMAN T. (Sweden), *Numerical simulation of low frequency air-borne sound transmission in buildings.*

Theme 3 — SOUND ABSORBTION: reference artefacts, measurement, design

1. VORLÄNDER M. (Germany),
   Reverbation room measurements and preparations of round robin tests on the sound absorption coeffcient of reference artefacts.
2. KRISTIANSEN U.R., VIGRAN T.E. (Norway),
   On the design resonant absorbers.
3. CHYLA A., CZYŻEWSKI K., NURZYŃSKI J. (Poland),
   Reverberation time: comparison of measurement results obtained in the laboratory using different methods and instrumentation.
4. MIROWSKA M. (Poland),
   Sound absorption of spatial acoustics absorbers, laboratory measurements, repeatibility, reproducibility.

Theme 4 — SOUND ABSORPTION MEASUREMENT: simulation, experiments, in-situ mesurement

1. MEES P., VERMEIR G. (Belgium),
   Numerical simulation of sound absorption in reverbation rooms.
2. COPS A., VANHAECHT J., LEPPENS K. (Belgium),
   Sound absorbtion in a reverbation room: causes of discrepancies on measurement results.
3. MOMMERTZ E. (Gremany),
   Angle-dependent in situ measurements of the complex reflection coefficient using a subtraction technique.
4. MADALIK L. (Estonia),
   Measurements and computer simulation of sound field of the St. Charles' Church in Tailin.

ARCHIVES OF ACOUSTICS
20, 1, 77–90(1995)

Erratum

ENHANCED BANDWIDTH MULTILAYER TRANSDUCERS FOR IMAGING APPLICATIONS

Q. ZHANG AND P. LEWIN

$$\begin{pmatrix} F_1 \\ U_1 \\ V_1 \\ I_1 \end{pmatrix} = \begin{pmatrix} \cosh(\gamma d) & Z_0\sinh(\gamma d) & 0 & -\dfrac{Z_0\sinh(\frac{\gamma d}{2})}{\Phi} \\ \dfrac{\sinh(\gamma d)}{Z_0} & \cosh(\gamma d) & 0 & \dfrac{\cosh(\frac{\gamma d}{2})}{\Phi} \\ \dfrac{\cosh(\frac{\gamma d}{2})}{\Phi} & \dfrac{Z_0\sinh(\frac{\gamma d}{2})}{\Phi} & 1 & jX_1+\frac{1}{j\omega C_0} \\ 0 & 0 & 0 & 1 \end{pmatrix} \begin{pmatrix} F_2 \\ -U_2 \\ V_2 \\ I_2 \end{pmatrix} \quad (A.11 \text{ p. } 88)$$

$$C_0 = \frac{A\varepsilon_3^{*S}}{d} \quad (A.17 \text{ p. } 88)$$

ARCHIVES OF ACOUSTICS
20, 1, 77–90 (1995)

ERRATUM

ENHANCED BANDWIDTH MULTILAYER TRANSDUCERS FOR IMAGING APPLICATIONS
Q. ZHANG AND P. LEWIN

ACKNOWLEDGEMENT

This work is supported by the National Institute of Health Program Project.